SURFACE ROUGHNESS EFFECTS ON OVERLAND FLOW

A Thesis

Submitted to the Faculty

of

Purdue University

by

Terence Hugh Podmore

In Partial Fulfillment of the

Requirements for the Degree

of

Doctor of Philosophy

December 1975

Grad. School
Form No. 9
Revised

PURDUE UNIVERSITY

Graduate School

This is to certify that the thesis prepared

By Terence Hugh Podmore

Entitled Surface Roughness Effects on Overland Flow

Complies with the University regulations and that it meets the accepted standards of the Graduate School with respect to originality and quality

For the degree of:

Doctor of Philosophy

Signed by the final examining committee:

L. J. Huggins, chairman

Louis J. Bode

J W Delleur

E Monke

Approved by the head of school or department:

Nov 20 1975 J W Delleur

To the librarian:

This thesis is not to be regarded as confidential

L. J. Huggins

Professor in charge of the thesis

"For the Lord is a great God,
and a great King above all gods.
In his hand are the deep places of the earth:
the strength of the hills is His also.
The sea is His, and He made it:
and His hands formed the dry land."

Psalm 95, v 3-5

ACKNOWLEDGMENTS

I wish to thank Dr. Huggins for serving as chairman, and for his continued support and guidance throughout the program. Dr. Huggins' breadth of knowledge and attention to detail have made this study a learning experience.

Thanks are extended to Dr. E. J. Monke, Agricultural Engineering, Dr. J. W. Delleur, Civil Engineering, and L. J. Cote, Statistics, for their valuable contributions and counsel.

I have enjoyed and benefitted from discussions with Dr. George Foster, where many ideas were developed and tested. In addition Fred Hood, David Beasley and other graduate students and staff provided useful contributions. Mr. Don Rhine and the technical staff gave help with equipment construction. Dr. G. W. Isaacs, as Head of Agricultural Engineering, was responsible for a stimulating working environment. To all those above, and to many others not mentioned, appreciation is expressed.

Special gratitude is due to my parents, Mr. and Mrs. Arthur Podmore, and to my parents-in-law, Mr. and Mrs. Carl M. Lipscomb, for their continued guidance and support.

Carol Ann, my wife has provided loving help and encouragement throughout the study, and a home where Alethea and Jonathan can learn love and understanding. Carol's patience, fortitude and sensitivity have enabled this project to be completed. Thank you for your love.

TABLE OF CONTENTS

TABLE OF CONTENTS, cont.

LIST OF TABLES

LIST OF TABLES, cont.

LIST OF FIGURES

LIST OF FIGURES, cont.

LIST OF SYMBOLS

a	Roughness element height (ft.)
a_i	Amplitude band mean value (in.)
A	Flow cross-sectional area ($ft.^2$)
$c(p)$	Unbiased autocovariance estimate of lag number p ($in.^2$)
C	Chezy flow resistance coefficient
CV	Coefficient of variation (%)
$\bar{d}$	Mean particle diameter (in.)
D	Hydraulic depth (ft.)
$D(f)$	Spectral density estimate of frequency f (in.)
D_a	Detention (ft.)
DF	Center-bed detention depth (ft.)
E	Exposure parameter
f	Darcy-Weisbach friction factor
F_o	Normal Froude number
g	Acceleration due to gravity ($ft./sec.^2$)
h	Roughness height for exposure parameter E
H_o	Normal flow depth (ft.)
$H_{1/3}$	Average height of highest one-third of sand waves (ft.)
k	Kinematic number
k_s	Nikuradse sand roughness
l	Prandtl mixing length (ft.)
L_o	Normal flow bed length (ft.)

m	Maximum lag number
M(a)	Amplitude distribution estimate of amplitude a
n	Manning's flow resistance coefficient
n*	Composite Manning's n
N_{ij}	Number of events at amplitude a_i and separation s_j.
p	Lag number
P	Wetted perimeter (ft.)
P(f)	Raw spectral estimate at frequency f ($in.^3$)
q	Discharge/unit width (cfs/ft.)
q_s	Runoff rate/unit width (cfs/ft.)
Q	Discharge (cfs)
QC	Center-bed discharge (iph)
r	Height standard deviation (cm.)
r^2	Correlation coefficient
R	Hydraulic radius (ft.)
R'	Logarithmic surface roughness parameter
R_e	Reynolds number
s_j	Separation band mean value (in.)
S	Slope (ft./ft.)
S_f	Slope of energy grade line (ft./ft.)
S_o	Normal bed slope (ft./ft.)
SP	Slope (percent)
S(f)	Smoothed spectral estimate of frequency f ($in.^3$)
t	Time (sec.)
v	Velocity (ft./sec.)
V_f	Shear velocity (ft./sec.)

V_o	Normal flow velocity (ft./sec.)
x	Distance (ft.)
y	Flow depth (ft.)
$\bar{y}$	Mean flow depth (ft.)
y_n	Normal flow depth (ft.)
z	Raw profile height (in.)
$\hat{z}$	Detrended profile height (in.)
α	Energy coefficient
$\gamma(s)$	Autocovariance function at separation s ($in.^2$)
$\Gamma(f)$	True spectral value at frequency f ($in.^3$)
Δs	Profile data spacing (in.)
κ	Von Karman turbulence coefficient
λ	Particle distribution ($No./in.^2$)
ρ	Mass density of fluid ($lbm./ft.^3$)
σ	Standard deviation (in.)
σ_d	Standard deviation about regression (in.)
σ^2	Variance ($in.^2$)
τ	Shear stress ($lbf./ft.^2$)
τ_o	Tractive force ($lbf./ft.^2$)
ϕ^2	Aliasing function
χ	Prandtl-von Karman roughness coefficient
Ω	Dimensionless roughness geometry parameter

ABSTRACT

Podmore, Terence Hugh. Ph.D., Purdue University, December 1975. Surface Roughness Effects on Overland Flow. Major Professor: Dr. L. F. Huggins.

Watershed response to rainfall inputs is a function of surface roughness conditions. The present study investigated methods of surface roughness estimation, analysis of hydraulic behavior and the development of estimation and prediction techniques for the surface roughness component of overland flow equations. The overland flow depth-discharge equation is a fundamental component of watershed simulation models and design studies for flood and erosion control structures.

A profile meter was constructed to measure linear height profiles at a spacing of 0.00982 in. over a length of 72.65 in. In addition to an existing surface, a stable surface was constructed using a resin application process. The surface had a distinct rilling pattern which became more pronounced with distance down the slope. Profiles were measured across and down the slope on a 2 ft. grid over the surface, avoiding end and edge effects. Two replications of factorial hydraulic tests were performed consisting of 5 slope levels, 4 rainfall levels and

4 upstream inflow levels.

The surface profiles were analysed to identify variations within and between surfaces. Spectral analysis was used to investigate contributions to the total variance across the frequency range 0.027 to 51 cycles per inch. Results indicated that the spectral estimate S(f) could be described by:

$$S(f) = A f^{B}$$

A joint probability distribution of amplitude and frequency was approximated by the amplitude/separation distribution. When collapsed into separate amplitude and separation distributions, the amplitude distribution gave some qualitative information about the surfaces. The separation distributions were similar for both surfaces.

The cross-slope profiles were used to develop area/wetted perimeter curves for the surfaces from which flow pattern development could be discerned. Mean area/wetted perimeter curves were obtained for the two surfaces and also for three plane grain roughened surfaces and two pseudo-natural surfaces for which hydraulic data were available. Down-slope roughness was characterized by the standard deviation of heights relative to a linear regression line through a series of points 0.0982 in. apart over a length of 24 in.

Various hydraulic equations were tested using the hydraulic data, the cross-slope roughness being incorporated

using the area/wetted perimeter relationships. Roughness coefficients were optimized for each flow surface using non-linear regression analysis. For the equations tested the correlation coefficient had a range of 0.68 to 0.99, and a range of coefficients of variation values between 5.3% and 21.3%.

For single parameter equations the roughness coefficient was related to standard deviation, the measure of down-slope roughness, and data trends were observed. An attempt was made to relate laboratory results with field simulation studies.

CHAPTER I

INTRODUCTION

The current awareness of problems concerned with surface runoff together with its associated erosion and subsequent transport of soil particles and chemicals has given impetus to the investigation of overland flow. The use of models in studying watershed responses to rainfall input has pointed out the need for a relationship between quantity of flow, flow depth, slope of the surface, and surface roughness parameters. The determination of various surface roughness parameters and their effect on the depth/discharge relationship has been a major objective of this study.

The study was completed as a natural development starting with the investigation by Huggins (1966) into the development of a distributed parameter watershed model. Huggins indicated in his conclusions that further investigation of the runoff and infiltration functions would provide significant benefits of more precisely establishing the hydrologic component relationships required by the distributed parameter watershed model. It was considered at that time that adequate research into infiltration processes was taking place elsewhere. Accordingly, an investigation into the nature of the runoff component was

undertaken at the Agricultural Engineering Department of Purdue University.

A flow table with the capabilities for simulating rainfall and overland flow was constructed (Das (1970)), and the apparatus has been used by all the succeeding studies. In his study Das tested flow over a smooth plane surface, and two plane sand grain roughened surfaces having different particle size distributions. The flow profile over the smooth surface was compared to the predicted profile using the kinematic wave theory, and close agreement was obtained. For the rough surfaces Manning's "n" and the friction factor f were related to the flow properties.

The following study (Kundu (1971)) added small gravel particles to the last remaining surface used by Das to obtain two rougher surfaces. The surfaces were plane although the combination of particle heights was sufficient to cause projection of the particles through the flow. A Poisson distribution of particles was assumed and consequently the surface roughness in the cross-slope and down-slope directions were identical.

Immediately preceeding the present study Burney (1973) formed two eroded sand surfaces that were stabilized before being tested. Surface roughness measurements were taken using an automatic micro-relief meter and area spectral analyses were performed on the data. Hydraulic tests were

performed as in the previous studies. Relating the spectral analyses of the grain and form roughness to the hydraulic data proved difficult.

After a review of the previous investigations the following conclusions were drawn:

a) It was unfortunate that no surface roughness measurements were taken by Das and Kundu.

b) The Poisson distribution of particles was only approximated by Kundu's first surface, while close agreement was obtained for the second and third surfaces.

c) Considerable effort had already been expended in studying plane grain roughened surfaces.

d) The area spectral analyses obtained by Burney contained a great deal of information which was difficult to utilize meaningfully using currently available techniques.

e) Burney's recommendations for future investigations were to be used as guidelines for the present study.

Objectives

After a review of currently available (1974) research findings, the following objectives were developed:

1. To develop a standard surface roughness measurement method and evaluate surface roughness estimation techniques.

2. To correlate hydraulic response with surface roughness for a range of surface roughness conditions.
3. To test prediction of hydraulic behavior from surface roughness estimation.

CHAPTER II

LITERATURE SURVEY

Overland flow analysis has developed after channel flow analysis, and consequently much of the subject matter developments have their roots in theoretical and experimental investigations of channel flow. Inclusion of a resistance to flow term has long been a topic of interest and much work has been done to establish criteria for measurement or estimation (Task Force Report (1963)). Although a considerable amount of work has been carried out in researching overland flow, a level of estimation and measurement technique similar to that for channel flow has not yet been achieved. Review of the literature covers three broad areas: theoretical analysis including the Saint-Venant equations and the simplification due to the kinematic wave approximation; the empirical approach from the experimental uniform flow equations to the development of the Prandtl-von Karman equation and its applications; and the study of surface roughness, methods of measuring random roughness geometry on actual surfaces, and bed form effects in channel flow. Since the areas frequently overlap, inclusion of material under a particular heading is often arbitrary.

Theoretical Analysis

The theoretical analysis of overland flow had its inception in the formulation of the equations of continuity and momentum for open channel flow which were first developed by Saint-Venant in the 1840's. Chow (1959) states the equations for a prismatic channel as follows:

Continuity equation

$$D\frac{\partial V}{\partial x} + V\frac{\partial y}{\partial x} + \frac{\partial y}{\partial t} = 0 \qquad (2.1)$$

Momentum equation

$$\frac{\partial y}{\partial x} + \frac{\alpha V}{g}\frac{\partial V}{\partial x} + \frac{1}{g}\frac{\partial V}{\partial t} = S_o - S_f \qquad (2.2)$$

where D = hydraulic depth, V = velocity, y = depth of flow at location x and time t, α = energy coefficient (normally approximated as being equal to unity), g = acceleration due to gravity, S_o = bed slope and S_f = slope of the energy grade line. Eagleson (1970) gives the equations in integral form. According to Chow (1959), Massau obtained a trial and error solution using the method of characteristics during the period 1880-1900. Lin (1952) simplified the procedure by using a graphical technique incorporating a constant time step.

The advent of large high speed digital computers has enabled approximate solutions to be found for specific

cases. When applied to overland flow, Chen (1962) developed the general momentum equation from first principles, and, together with the continuity equation, used an implicit difference method to calculate the solutions. Morgali (1963) used a finite difference technique to solve the equations but the results were plagued by stability problems. Chen and Hansen (1966) developed dimensionless forms of the momentum and continuity equations and obtained the characteristics of the flow profile. Liggett and Woolhiser (1967) used the dimensionless representation and compared different procedures for implicit and explicit solutions with the method of characteristics, since the latter had the advantage of being accurate and fast, although involving a tedious interpolation procedure. Explicit methods were found to be unsuitable, while the implicit methods provided stable solutions over a wide range of parameters.

Strelkoff (1969) derived the Saint-Venant equations from the general one-dimensional equations for continuity and either momentum or energy. He also gave the simplifying assumptions for which the transformation is valid. In later work Strelkoff (1970) presented the general one dimensional Saint-Venant equations for a rigid open channel of arbitrary form for which the flow may be spatially varied. The theoretical basis for the method of characteristics is reviewed together with a stability analysis of the various

solution techniques used. Explicit numerical schemes using small time steps were constrasted with implicit schemes enabling numerical solutions over large time steps but requiring solutions of large sets of simultaneous equations at each step.

In one of the most fundamental treatments to date, Yen (1973) used the generalized equations of continuity, energy and momentum formulated over a cross section in integral form and transformed them into one dimensional "unified general open channel flow equations". Based on the equations derived, the assumptions involved in conventionally used open channel flow equations such as the backwater flow equations, and the Saint-Venant equations were examined, and inherent differences between flow equations derived from momentum and energy concepts were compared.

Lighthill and Whitham (1955) first showed that in a case of one dimensional flow when an approximate functional relationship between quantity of flow and concentration or depth of flow replaces the momentum equation, the equation of continuity can be solved more simply. The condition is referred to as the kinematic wave approximation, since dynamic terms of the momentum equation are ignored. Iwagaki (1955) studied unsteady flow in open channels with lateral inflow using the method of characteristics and used the kinematic approximation for flow estimation. The work was applied primarily to steep rivers and streams. Ishihara (1964) used Iwagaki's approach to analyse overland flow

in sub-basins of a watershed. Henderson and Wooding (1964) showed that the kinematic wave approximation can be applied to overland flow and illustrated the rising and falling limbs of a predicted hydrograph. Grace and Eagleson (1966) developed a dimensionless form of the overland flow equations and applied them to the simulation of flow over a parking lot model and prototype. Woolhiser and Liggett (1967) compared solutions using finite difference integration of the characteristic equations with kinematic wave solutions and experimental results. A single dimensionless parameter k, (sometimes called the kinematic number (Foster (1971)), was developed to serve as a choice criterion between the methods employed.

$$k = \frac{S_o L_o}{H_o F_o^2} \tag{2.3}$$

The kinematic number reflects the effects of length L_o and slope S_o of the overland flow plane, as well as the normal flow variables: depth H_o and Froude number F_o

$$F_o = \frac{V_o}{\sqrt{gH_o}} \tag{2.4}$$

and V_o = velocity of flow. For values of k greater than 10, the kinematic wave solutions correspond closely with the characteristic solutions. From experimental results

overland flow was adequately described using the kinematic wave approximation.

Brakensiek (1967) obtained numerical solutions of the kinematic wave equations for overland flow using an implicit differencing scheme. The kinematic wave solution was applied to flow on a converging surface by Woolhiser (1967) using the dimensionless form. A convergence factor was introduced to account for flow concentration, and theoretical hydrographs were derived. Foster, Huggins and Meyer (1968) used the Darcy-Weisbach uniform flow equation and implicit finite difference equations (after Brakensiek (1967)) to model overland flow on erosion plots 35 feet long. Field hydrograph results were modelled and the kinematic number k was always much greater than 10. Foster et al, verified that the kinematic wave approximation gave good reproduction of the overland flow hydrograph provided that the friction coefficient was obtained empirically at the site. Friction coefficients were expressed as Darcy-Weisbach f, Chezy C, Mannings's n and a variable friction factor as a function of Reynold's number. Little difference could be found between the friction coefficients for the short plots studied. It was also noted that the coefficient of friction could not be obtained from a qualitative description of the soil surface.

Brakensiek and Onstad (1968) developed a surface flow model based on the kinematic wave theory for

hydrograph prediction using a distributed parameter model to avoid lumping effects. The model was fitted by adjustment of the Manning's roughness coefficient n. Hill (1969) used the kinematic wave approach for overland flow on a plane surface and also applied the technique to open channel flow, where lateral inflow replaced rainfall excess. For channels, Hill found that the depth-time curve was a function of the cross-sectional geometry.

A detailed treatment of the kinematic wave theory and its applications has been presented by Eagleson (1970). Overland flow is examined using the methods of Iwagaki (1955) and Henderson and Wooding (1964). The effects of infiltration on overland flow were also investigated. Since 1970 the kinematic wave approximation has been widely used in studies of overland flow. Das (1970) obtained good agreement between observed and predicted hydrographs from a laboratory catchment using smooth and grain-roughened plane surfaces. Kundu (1971) also achieved satisfactory agreement for observed and predicted hydrographs obtained from plane surfaces having large grain roughness where roughness elements projected through the flow. Langford (1971) and Langford and Turner (1973) reported the application of the kinematic wave theory to overland flow over a rough uneven surface. The hydraulic resistance for flows under rain was calculated using the rising limb of the runoff hydrograph and recession curves were calculated using

the kinematic wave theory. Close agreement was obtained between observed and calculated recessions. Depression storage was measured and hysteresis was observed in the storage-discharge curves. The hysteresis effect was explained in terms of the kinematic wave theory.

Foster (1971) used the kinematic number k to determine the applicability of the kinematic approximation to overland flow in agricultural and urban situations to determine detention storage and to estimate erosion. Overton (1971) showed that the kinematic approximation was sufficiently accurate to describe overland flow on hill slopes. The extent of the application of kinematic wave theory can be gauged from the following studies. Singh (1975) formulated equations for overland flow on a converging surface using the kinematic wave approximation. Judah, Shanholtz and Contractor (1975) applied the kinematic wave theory to the prediction of flood hydrographs using a finite element approach similar to that used by Huggins and Monke (1968). Fread (1975) used the kinematic wave assumption applied to flood waves in large rivers to develop stage-discharge relationships given cross-sectional properties, channel slope and Manning's n.

Depth-Discharge Relationships

The equations used to describe uniform flow in open channels include a term to account for hydraulic resistance.

According to Chow (1959) the first uniform flow formula was developed by Chezy in 1769, and is usually expressed as

$$V = C\sqrt{RS} \tag{2.5}$$

where V = mean velocity, R = hydraulic radius, S = slope of the energy line and C is a resistance coefficient. The Darcy-Weisbach formula was developed primarily for flow in pipes, but can be modified for flow in open channels (Chow (1959)) as

$$V = \left(\frac{8gRS}{f}\right)^{1/2} \tag{2.6}$$

The other well known formula is attributed to Manning (Chow (1959)) developed in 1889, and expressed as

$$V = \frac{1.486}{n} R^{2/3} S^{1/2} \tag{2.7}$$

where n is the coefficient of roughness known as Manning's n.

The roughness coefficients can be related as follows:

$$C = \sqrt{\frac{8g}{f}} = \frac{1.49}{n} R^{1/6} \tag{2.8}$$

and hence the Chezy and Darcy-Weisbach equations can be considered as equivalent except for a numerical constant. It should be noted that Manning's n is dependent on the hydraulic radius for constant C or f. However, due to the wide usage in open channel flow applications, the uniform

flow equations have been applied to overland flow situations.

Ragan (1965) investigated the errors associated with the selections of incorrect roughness parameters, and showed that analytical water surface profiles are particularly sensitive to roughness parameter values. Huggins and Monke (1966) showed the sensitivity analysis for Manning's n in a distributed parameter model for small agricultural watersheds, and a similar effect was noted by Brakensiek and Onstad (1968) in a separate study. Foster (1968) investigated the selection of roughness coefficients for short erosion plots, and hydrographs were simulated using a coefficient of friction predicted from field hydrograph analysis. Foster et al (1968) discussed the lumping of various effects when a single roughness or friction coefficient was determined or selected. From their study, Foster et al concluded that for overland flow over short distances, a kinematic wave model adequately described the flow process. A constant coefficient of friction, derived from the analysis of hydraulic results, was used in the flow equation. Schreiber and Bender (1972) used optimization of flow regime parameters to obtain overland flow resistance. Hydrographs were simulated using the precipitation number during rainfall and the Weber number during recession. Good agreement between calculated and observed hydrographs was obtained.

In studies such as that of Brakensiek and Onstad (1968) the model was fitted to observed data by adjustment of the roughness parameter, in this case Manning's n. While providing acceptable results for simple hydrographs the method was shown to change the shape of complex predicted hydrographs making fitting difficult (Huggins and Monke (1966)). Becker and Yeh (1972) developed an influence coefficient algorithm for optimum parameter identification from system input and output. It was found that the algorithm depended on stability and convergence features of finite difference solutions which were not readily recognized.

Chow (1959) reviewed the open channel flow formulae, and gave approximate friction factor values. The method of Cowen (1955) for predicting Manning's n from resistance components due to channel bed irregularities, channel shape and size variation, obstructions, vegetation and meandering was noted. The Task Force Report (1963) selected the Darcy-Weisbach-type formula as being most universally applicable for open channel flow and commented that the Manning equation can lead to grave errors if used in unsuitable cases (Closure of Task Force Report (1964)).

For overland flow Horton (1938) proposed a depth-discharge relationship of the form:

$$q_s = KD_a^m \qquad (2.9)$$

where q_s = runoff rate, D_a = detention, and K and m are empirically determined parameters. Assuming that detention is equivalent to uniform flow depth, and applying Manning's equation, m = 5/3 for turbulent flow, m = 3 for laminar flow and m = 1 was proposed for flow over and through surface vegetation. Horton also obtained an overland flow hydrograph equation applied to a 75 percent turbulent condition. Manning's n was also related to slope length and steepness, the rainfall intensity and the parameter K. Horton's depth-discharge equation was widely used in experiments to obtain data for runway and highway design, and for soil conservation studies as reported by Izzard (1942). A preliminary analysis of runoff from simulated rainfall on a smooth paved plot was reported by Izzard and Augustine (1943) and the parameters in Horton's equation were obtained from log-log plots of detention against discharge.

Keulegan (1944) formulated the flow equations for runoff from a plane surface using energy and momentum concepts. The frictional effects of surface resistance and turbulent mixing were separated, the surface resistance component being introduced in terms of shear stress. An approximate solution was derived using an order of magnitude analysis. Izzard (1944) analysed flow profiles of overland flow over rough plane and turf surfaces using Keulegan's approach and showed that the raindrop momentum,

or overpressure, term was negligible except on very flat slopes. Izzard (1946) also developed a dimensionless hydrograph approach for estimating the overland flow hydrograph from the slope length, steepness and roughness. Izzard's data has been used by many investigators, including Morgali and Linsley (1965), Woolhiser and Liggett (1967), and Langford (1971), to verify analytical and numerical solutions.

The effect of rainfall intensity on the friction coefficient was noted by Izzard (1944). Woo (1956) studied the effects of raindrop input on overland flow profiles, and showed that rainfall intensity has a significant effect. Woo related the friction factor modified by rainfall to Reynolds number following a similar approach to Izzard (1944). Yoon and Wenzel (1971) investigated the effects of rainfall on sheet flow over a hydraulically smooth boundary. The laminar flow relationship $f = C/R_e$ described the flow reasonably well up to $R_e = 1000$, where C is a function of rainfall intensity and slope. Kisisel, Rao, Delleur and Meyer (1971) also studied the effects of surface roughness and found that rainfall increased friction factor values on both smooth and rough surfaces. The mean velocity distributions were found to be essentially logarithmic. Shen and Li (1973a) studied rainfall effects on flow over a smooth surface for a wide range of Reynolds numbers. Water surface profiles and boundary shear stresses

were described using a friction coefficient (Darcy-Weisbach f) with an added component due to rainfall. For a flow Reynolds number less than 900 f is a function of Reynolds number and rainfall intensity, while for a flow Reynolds number greater than 2000 f is a function of Reynolds number only. Foster (1975) studied rainfall effects on flow in a rill, and found that rainfall had little effect on average velocity, which could be adequately described by a power relationship of slope and hydraulic radius.

The application of boundary layer theory to flow in pipes and channels is discussed by Schlichting (1951). Prandtl's mixing length hypothesis and von Karman's similarity hypothesis are combined into the Prandtl-von Karman universal velocity distribution law, and is stated as follows:

$$v = \frac{V_f}{\kappa} \ln \left(\frac{y}{y_o}\right) \qquad (2.10)$$

where v = velocity at a distance y from the boundary, y_o is a constant of integration, κ = von Karman's constant (generally 0.4) and V_f = shear velocity given as:

$$V_f = \sqrt{gRS} \qquad (2.11)$$

Schlichting (1951) gives the work of Nikuradse, who studied flow in smooth and rough pipes, and gave experimental verification of the Prandtl-von Karman equation. For rough surfaces Nikuradse obtained the following:

$$v = V_f \left[5.75 \log \left(\frac{y}{k_s}\right) + 8.5\right] \qquad (2.12)$$

where k_s = mean height of roughness elements (otherwise the Nikuradse sand roughness) and incorporating $\kappa = 0.4$.

Keulegan (1938) derived equations for mean velocity of turbulent flow in open channels, and using Bazin's data, the following formula was developed for rough surfaces:

$$v = V_f \left[A_o + 5.75 \log \left(\frac{R}{k_s}\right)\right] \qquad (2.13)$$

where A_o is an experimental constant having a range from 3.23 to 16.92. A mean value of $A_o = 6.25$ was suggested. Keulegan introduced a free surface effect which was used by Iwagaki (1954) to formulate an expression for A_o, which also included the Froude and Reynolds numbers. Chow (1959) showed that A_o has an approximately constant value of 7.5 for F_r less than 1.0.

From equations (2.5), (2.8), and (2.11) it can be seen that

$$\frac{v}{V_f} = \frac{C}{\sqrt{g}} = \sqrt{\frac{8}{f}} \qquad (2.14)$$

For studies of friction coefficients the terms C and f are commonly used. Robinson and Albertson (1952) used baffle plates as artificial roughness elements in a rectangular channel to attempt to formulate roughness standards for open channels. Using Chezy C as the roughness coefficient, they obtained

$$\frac{C}{\sqrt{g}} = 4.7 \log \left(\frac{d}{a}\right) + 1.31 \qquad (2.15)$$

where d = mean depth of flow and a = height of artificial roughness elements.

Since the 1950's a considerable amount of attention has been focused on the study of artificial and natural roughness effects in open channel flow. Sayre and Albertson (1961) used baffles arranged in various patterns and developed the equation

$$\frac{C}{\sqrt{g}} = 6.06 \log \left(\frac{y_n}{\chi}\right) \qquad (2.16)$$

where y_n is the normal depth of flow, χ is a roughness parameter dependent on the size, shape and spacing of the roughness elements, and the numerical constant includes $\kappa = 0.38$. (Compare with equation (2.10)). Biery and Delleur (1961) studied flow in channels having reinforcing bars close to the bed as roughness elements. The following equation was developed:

$$\frac{C}{\sqrt{g}} = 6.06 \log \left(\frac{y_n}{a}\right) + 4.6 \qquad (2.17)$$

where a is approximately equal to the diameter of the bars and equation (2.17) was compared to equation (2.16). A similar equation was used by Mirajgaoker and Charlu (1963) to express the effect of surface roughness in a channel. Stones 2.5 inches in diameter having densities of 15 to

114 stones per square yard were glued to the bed of a flow in patterns similar to those of Sayre and Albertson (1961), and the resistance to flow was measured.

O'Loughlin and Macdonald (1964) investigated flow in channels roughened with sand grains and small cubes in various concentrations. The surface roughness was expressed as a Nikuradse-type equivalent sand roughness. A semi-logarithmic expression for the friction factor gave reasonable agreement for small relative roughness values. Flow in a channel having various patterns and concentrations of 3.75 inch and 6.0 inch cubes was studied extensively by Herbich and Schulits (1964). The roughness coefficients were calculated differently for flows with submerged and protruding blocks and a flow resistance discontinuity was found at flow depths equal to the cube height. Ranga Raju and Garde (1970) developed a semi-logarithmic expression for the drag coefficient of two dimensional strip roughness in a flume for low Froude numbers on the assumption that total resistance was equal to the form roughness of the roughness elements. Roberson and Chen (1970) investigated flow in conduits with low roughness concentrations using shear stress distribution over the roughness elements. Shen and Li (1973b) used a multiple regression approach to analyze the resistance due to staggered roughness elements, and obtained

$$\frac{v}{v_f} = 2.92 \ln \left(\frac{y_n}{a\Omega}\right) \qquad (2.18)$$

where y_a = normal flow depth, a = roughness element height, and Ω is a dimensionless parameter to describe roughness geometry. Concepts used in the determination of resistance to flow by rigid roughness elements were extended to flow in channels lined with flexible plastic elements simulating vegetation by Kouwen and Unny (1973). The semi-logarithmic formula for velocity profile was found to be applicable, although the von Karman turbulence coefficient κ varied widely. Two values of the friction factor were found, one for erect elements and one for prone elements.

Sediment transport investigations have given impetus to the study of hydraulic roughness in alluvial channels, both in laboratory and natural channels. Simons and Richardson (1961) found that the friction factor f increased rapidly as ripples developed in a sand bed (F_r = 0.17 to 0.37) and then dropped markedly in the transition region (F_r = 0.55 to 0.67) before increasing slowly as the Froude number increased (F_r = 0.71 to 1.30). Similar results were found by Raudkivi (1967).

Taylor and Brooks (1961) proposed the division of the friction factor f into grain roughness effects f' and form roughness effects f'', and determined f' from a Moody pipe friction diagram. f/f' was found to be approximately unity for flat beds and f/f' was greater than

2 for bed forms such as ripples and dunes. Engelund (1966) used a similarity principle to compare studies of hydraulic resistance in natural and laboratory situations, while Raudkivi (1967) separated the total drag on the bed into surface drag and form drag in a similar way to that of Taylor and Brooks (1961). Raudkivi also considered resistance in terms of entrainment of particles into the flow.

Rouse (1965) suggested an equation of the form

$$\frac{1}{\sqrt{f}} = A \log \left(\frac{R}{DhE}\right) + B \qquad (2.19)$$

where f = friction factor, R = hydraulic radius, h = roughness height, E = exposure parameter and A, B, and D are parameters. For values of E greater than 0.15, E is replaced by (1-E). Equation (2.19) was used by Vanoni and Hwang (1967) for flow in alluvial channels, and E is the ratio of the area of the vertical projection of the bed forms to the total bed area. Experiments showed that hE adequately described the roughness length for beds having ripples of small steepness. Smith (1968) indicated the importance of bed formation in evaluating and comparing flow resistance. Annambhotla (1969) applied statistical analyses to bed heights taken from a stretch of the Missouri River to determine exposure parameters and roughness heights. Lovera and Kennedy (1969) presented a chart similar to the Moody pipe friction diagram for determining

friction factors in flows in the flat bed regime of sand bet channels. Alam and Kennedy (1969) developed a depth-discharge predictor for river channels based on a form drag friction factor as a function of grain size Froude number and hydraulic radius. Chang (1970) used equation (2.19) to determine the form-roughness friction factor in a study of ripple concentration effects on flow resistance. A modified Nikuradse-type equation was used to predict the grain roughness friction factor. Kundu (1971) developed expressions for the exposure parameter E in equation (2.19) for studies of overland flow over the grain-roughened surfaces of a laboratory catchment.

Burney (1973) described flow over stabilized eroded sand surfaces in terms of a nonlinear regression equation relating depth with discharge and slope. The equation used was of the form

$$DF = A\,QC^{B}SP^{C} \qquad (2.20)$$

where DF = mean detention depth (ft), QC = discharge in the center of the surface (in/hr) and SP = bed slope (percent). Coefficients A, B and C were obtained by regression analysis for each surface, and correlation coefficients of 0.98 were obtained. Results suggested that for the flow conditions investigated A = 0.004, B = 0.5 and C was a measure of surface roughness. Huggins, Burney, Kundu and Monke (1973) used equation (2.20) to

describe Kundu's results (1971), and obtained similar results, although values of coefficients A and B varied for individual surfaces, while there was less variation in coefficient C.

Random Surface Roughness Measurement and Analysis

Random surface roughness measurements vary widely with application, although similar analysis techniques are used. Spectral analysis techniques have been carefully documented for use in many different situations. Jenkins and Watts (1968) give a detailed treatment of the method. Surface roughness measurements of agricultural areas have been used for vehicle analysis, tillage assessment, evaluation of depression storage, and resistance to overland flow. Stream channel beds have been measured to determine characteristics for predicting flow resistance and for sediment transport analysis.

Surface roughness for tillage effectiveness was measured by Kuipers (1957) using a board holding 20 probe needles at 10 cm. spacing. A series of 20 profiles was collected manually at fixed intervals depending on the area to be covered. For most situations of measurements taken on cultivated surfaces before seed bed preparation, a normal distribution of heights was found. Surface roughness was expressed as

$$R' = 100 \log r \qquad (2.21)$$

where r = standard deviation of heights (in cm.) relative to a reference level.

Burwell, Allamaras and Amemiya (1963) used an apparatus similar to that of Kuipers (1957) for taking manual measurements over a 40 by 40 inch square area at a 2 inch grid spacing to obtain a three dimensional surface description. Surface roughness was estimated using the standard error among the natural logarithm of elevation heights. An automated method for obtaining height measurements at 1 inch intervals over a distance of 84 inches was developed by Schafer and Lovely (1967). A probe was mounted on a carriage moving laterally on a horizontal beam. Height readings were obtained by lowering the probe until it contacted the soil surface, the distance moved by the probe from a reference position being recorded on a chart. Currence and Lovely (1971) extended the concept by developing a fully automated profile meter consisting of a frame and cross carriage on which the probe was mounted. The probe took height readings to the nearest 0.01 inch on a 1 inch grid over an area of 60 by 80 inches, the readings being recorded on punched cards.

Curtis and Cole (1972) and Foster and Meyer (1972) used photographic methods to record profiles from the tops of pin-type profile meters similar to that of Kuipers (1957). The results were used in estimation of soil movement in erosion studies. Pin spacings of 1.2 inches

over a distance of 4 ft (Curtis and Cole (1972)), 0.25 inches over 7.5 inches and 1.0 inches over 12 ft (Foster and Meyer (1972)) were used.

Currence and Lovely (1970) compared indices of surface roughness using the standard deviation of height residuals after correcting for slope effects. Periodic components of the surfaces caused by tillage tool marks could be clearly distinguished from random roughness effects using a power spectral density analysis. Merva, Brazee, Schwab and Curry (1970) illustrated the difference between macro- and micro-surfaces, and directed attention to the micro-surface for overland flow analysis. Spectral density analysis was applied to micro-surface profiles measured at 0.79 inch spacings over a distance of 9.98 ft. Anisotropy of surfaces was estimated by comparing the spectra of cross and down slope profiles.

Mitchell (1970) developed an automatic profile meter similar to that of Currence and Lovely (1970) for determining heights on a 1.0 inch grid over a 3 ft square area to investigate depression storage as a function of depth in laboratory studies. Barron (1971) used Mitchell's profile meter to investigate the effect of tillage on the depression storage-depth relationship. Burney (1973) used an automatic micro-relief meter to obtain elevations on a 0.1 inch grid over a 24 inch square area of a stabilized sand surface used in a laboratory catchment investigation. The theory

of spectral analysis applied to random functions of two variables was presented by Longuet-Higgins (1957) and was used to analyze ground roughness for vehicle studies (Kozin, Cote and Bogdanoff (1963, 1968)). Burney (1973) used the technique to obtain area spectra of the eroded surfaces investigated.

Spectral analysis was applied to formations in sand-bed channels by Nordin and Algert (1966). Sonic sounder records were used to obtain profile data. For dune profiles investigated the spectra could be modelled by a second order Markov process. The standard deviation σ of the process was related to the average height of the highest one-third of the dunes in the form

$$H_{1/3} = 3\sigma \tag{2.22}$$

Ashida and Tanaka (1967) also found that a second order Markov process described the spectra of sand waves and substantiated equation (2.22) using their data. In addition relative roughness k_s, similar to a Nikuradse-type sand roughness, was related to the standard deviation of the profile in the form

$$k_s = a\sigma^b \tag{2.23}$$

where a and b are parameters. Wave lengths and amplitudes were characterized by a Rayleigh distribution. Profile measurements were taken using a sonic sounder, as did

Annambhotla (1969) and Squarer (1970), who both found bed heights from flumes and rivers to be normally distributed. Annambhotla (1969) found river profiles to differ significantly from flume profiles and showed zero-crossing distance and amplitude analysis to be more suitable for river profiles than spectral analysis. Squarer (1970) noted that the relationships between mean wave heights, highest one third wave heights and standard deviation corresponded to equation (2.22) using Rayleigh distribution and normal bed elevation distribution assumptions.

Kruse, Huntley and Robinson (1965) investigated equation (2.16) for flow in artificial rectangular and parabolic channels. The standard deviation was calculated from bed heights taken at 0.6 inch intervals. Regression analysis gave

$$\chi = 12.9\,\sigma^{1.66} \qquad (2.24)$$

which is similar to equation (2.23). For field conditions Kruse et al (1965) suggested that the standard deviation is calculated from 6 to 10 sections 12 inches long measured at 0.6 inch intervals with a precision of 0.01 inches. The calculation method acts as a band-pass filter to remove high and low frequency effects. Heerman, Wenstrom and Evans (1969) confirmed that equations (2.16) and (2.24) apply to flow in irrigation furrows. Bed elevation measurements were made at 0.125 in. spacing over a distance

of 9.5 ft using an automatic profile meter. Spectral analysis of the profiles did not determine significant periodic effects and spectra were considered not to be useful in describing roughness in irrigation furrows.

Brickman, Wambold and Zimmerman (1971) investigated highway roughness using spectral analysis techniques. It was noted that the frequency domain analysis did not indicate amplitude effects which were necessary to study vehicle response. Similarly amplitude distributions did not yield information on frequency of occurrence. A joint probability distribution giving amplitude and frequency components was developed, and analog/digital methods for profile analysis were indicated.

Conclusions

From the literature survey it was concluded that the kinematic wave approximation of the dynamic flow equations applies to overland flow conditions. Following Eagleson (1970) the general form of the kinematic equation is

$$q(x,t) = \alpha y^{m}(x,t) \qquad (2.25)$$

where $q(x,t)$ = discharge and $y(x,t)$ = flow depth at distance x and time t, and α and m are coefficients. Equation (2.25) is equivalent to Horton's equation (2.9), and equations (2.5), (2.6) and (2.7) can be expressed in a similar form, assuming equivalence between hydraulic

radius R and flow depth y(x,t). Coefficient α is then transformed into a function of roughness coefficient and slope for a given equation.

Investigation of the relationship of hydraulic radius and flow depth, and prediction of roughness parameters from surface properties (for example, equation (2.23)) appeared to be fruitful areas of study. Expression of surface roughness in terms of spectral analysis and the amplitude/frequency distribution indicated avenues of approach for quantification of roughness parameter estimation.

CHAPTER III

METHODS OF SURFACE ROUGHNESS ANALYSIS

In order to analyze natural surface roughness to determine hydraulically significant parameters, several approaches were used. As indicated in Chapter II, previous investigations have concentrated on either hydraulic testing or geometrical measurements of rough surfaces. The attempted unification of hydraulic and surface roughness aspects of overland flow has been limited to relatively few studies which include Kundu (1971) and Burney (1973).

The analytical techniques used in this study were as follows:

(i) Spectral analysis

(ii) Amplitude/frequency distribution

(iii) Area/wetted perimeter relationships

An outline of the theory of each method will be given where appropriate, together with the application of the techniques to the data obtained.

Spectral Analysis

Spectral analysis has been widely used to analyze frequency components of events separated in time. The method has been extensively documented, and many excellent

studies can be found (for example Jenkins and Watts (1968)). Spectral analysis has also been used to investigate occurrences separated in space, and the extension of spectral analysis methods to describe surface roughness has been a natural one.

The work of Kozin et al (1963, 1968) has applied spectral analysis to the problem of describing large scale rough surfaces for the determination of performance criteria for rough terrain vehicles. Merva et al (1970) investigated macro and micro surfaces using spectral analysis, and indicated the importance of the micro surface for overland flow conditions. Burney (1973) extended the concept of two-dimensional spectral analysis developed by Kozin et al (1963) to express surface roughness, but concluded that the spectra were more easily interpreted when collapsed into line spectra. From this conclusion it was decided to study line spectra in this investigation.

The calculation of spectral estimates from a finite segment of equally spaced data values $z(x)$ requires removal of trends and low frequency components which act as trends in the finite segment. To comply with this requirement the data may be detrended by fitting a linear regression line to the data. The data set for analysis $\hat{z}(x)$ then becomes:

$$\hat{z}(x) = z(x) - (a + bx) \qquad (3.1)$$

when a and b are linear regression coefficients.

The detrended data set $\hat{z}(x)$ may be written as a Fourier series of the form:

$$\hat{z}(x) = \sum_k (a_k \cos 2\pi f_k x + b_k \sin 2\pi f_k x) \qquad (3.2)$$

Arrangement of the squared amplitude values, $(a_k^2 + b_k^2)$, with frequency, f_k, forms the frequency spectrum in deterministic form. Considering the stochastic nature of the data from which the original data set, $z(x)$, was obtained, the autocovariance function must be used.

The autocovariance function, $\gamma(s)$, for the series $\hat{z}(x)$ is defined as

$$\gamma(s) = E(\hat{z}(x) \cdot \hat{z}(x+s)) \qquad (3.3)$$

where E represents the mathematical expectation. The autocovariance function is dependent on the separation or lag, s between the points. The variance spectrum $\Gamma(f)$ is the Fourier transform of the autocovariance

$$\Gamma(f) = \int_{-\infty}^{\infty} \gamma(s) e^{-i\,2\pi\,fs}\, ds \qquad (3.4)$$

where f is the frequency. The inverse transform is given by

$$\gamma(s) = \int_{-\infty}^{\infty} \Gamma(f) e^{-2\pi\,fs}\, df \qquad (3.5)$$

and hence equations (3.4) and (3.5) form a Fourier transform pair. Considering zero lag, then

$$\gamma(0) = \sigma^2 = \int_{-\infty}^{\infty} \Gamma(f)\, df \qquad (3.6)$$

which shows that the spectral function $\Gamma(f)$ describes the distribution of the variance of the $\hat{z}(x)$ process in the frequency domain.

To calculate the spectral estimates $S(f)$ the following procedure is used: after detrending the data the unbiased autocovariance estimates are calculated from

$$c(p) = \frac{1}{n-p} \sum_{q=1}^{n-p} \hat{z}(q) \cdot \hat{z}(q+p) \qquad (3.7)$$

$$c(-p) = c(p) \qquad p = 0, 1, 2, \ldots . m.$$

when n = number of points in the series, m = maximum number of lag intervals. The raw spectral estimate, $P(f)$, is obtained using

$$P(f) = 2 \sum_{p=n+1}^{n-1} c(p) e^{-i 2\pi fp} = 2 \left[c(0) + 2 \sum_{k=1}^{n-1} c(p) \cos 2\pi fp \right] \qquad (3.8)$$

The raw spectral estimates are smoothed by "hamming"

$$S(0) = 0.54\ P(0) + 0.46\ P(1)$$

$$S(h) = 0.23\ P(h-1) + 0.54\ P(h) + 0.23\ P(h+1) \qquad o < h < m$$

$$S(m) = 0.54\ P(m) + 0.46\ P(m-1) \qquad (3.9)$$

The smoothing process provides more stable spectral estimates for the $\hat{z}(x)$ process. The computer program, SPEC, used to compute spectral estimates is given in Appendix D.

Amplitude/Frequency Analysis

Brickman, Wambold and Zimmerman (1971) have developed the amplitude/frequency distribution to analyze road profile data to determine ride comfort in vehicles. It is pointed out that for vehicle response analysis, the spectral techniques consider amplitude only in that the spectrum indicates average roughness amplitude for a particular frequency. Amplitude domain descriptions, on the other hand, reduce observed roughness measurements to a table of values or a single number without reference to frequency components. Similar arguments apply for the analysis of surface roughness for overland flow description.

Combining the frequency and amplitude distributions into a joint probability distribution reduces a data series of roughness heights to a tabular array of numbers representing event counts in finite bands of amplitude and frequency. An event is defined as the determination of the separation of two points of equal elevation across a flow channel in the surface and is classified by amplitude from the mean elevation and by separation. Considering

N_{ij} to be the number of occurrences of events in the amplitude band, A_i, and the frequency band, f_j, the spectral estimate can be obtained by summing across the amplitude bands to yield the estimate of the spectral density

$$D(f_j) = \frac{1}{2\Delta f} \frac{\sum_{j=1}^{J} N_{ij} A_i^2}{\sum_{i=1}^{I} \sum_{j=1}^{J} N_{ij}} \tag{3.10}$$

and the spectral estimate, $S(f_j)$, is given as

$$S(f_j) = \sigma^2 D(f_j) \tag{3.11}$$

when σ^2 is the variance of the smoothed data. Similarly the amplitude distribution M(a) can be approximated from the amplitude/frequency distribution by summing across the frequency bands to obtain the estimated distribution $M(A_i)$

$$M(A_i) = \frac{\sum_{j=1}^{J} N_{ij}}{\sum_{i=1}^{I} \sum_{j=1}^{J} N_{ij}} \tag{3.12}$$

Wambold and Park (1974) gave analog/digital techniques for obtaining the amplitude/frequency distribution using the wavelength reciprocal to determine the roughness frequency. Since it was not possible to implement wavelength

analysis for the current data sets, a sorting technique was used to obtain a separation s of points of equal elevation using local gradient as an indicator to ensure than separation existed across a flow channel and not across a flow obstruction. Based on the assumption that separation indicated one-half of the wavelength, the frequency component could be estimated as

$$f = 1/2s \tag{3.13}$$

For the purpose of this analysis the frequency component was not included and the distribution was characterised by amplitude and separation. The computer program, AMSEP, is given in Appendix D.

Area/Wetted Perimeter Relationships

When considering flow equations for analysis and prediction purposes, the effects of surface form and roughness on the roughness coefficients in each equation must be considered. Of the flow equations considered in this study, the Chezy equation (2.5), and its alternate form the Darcy-Weisbach equation (2.6), are semi-empirical while the Manning equation (2.7) is empirical. The Burney equation (3.20) was developed from a nonlinear regression analysis relating average depth with independent variables of slope and discharge. The equation can be rewritten so that it predicts discharge in the form

$$QC = X\ DF^{Y} SP^{Z} \tag{3.14}$$

to predict discharge where X, Y and Z are regression coefficients. It should be noted that regression analysis, while evaluating correlation, does not imply functional dependence.

The Prandtl-von Karman equation was developed from the Prandtl mixing length theory. Following the development of Chow (1959), the shear stress at any point in the flow can be given by

$$\tau(y) = \rho l^2 \left(\frac{dv}{dy}\right)^2 \tag{3.15}$$

where ρ = mass density of the fluid, l = characteristic length, known as the mixing length, and dv/dy = velocity gradient at a distance y from the solid surface. Near the solid surface, Prandtl assumed (i) mixing length is proportional to y, which introduces the von Karman turbulence coefficient κ and (ii) the shear stress is constant, hence the shear stress is equal to the tractive force τ_o. Then

$$dv = \frac{1}{\kappa} \sqrt{\frac{\tau_o}{\rho}} \frac{dy}{y} \tag{3.16}$$

Integrating equation (3.16)

$$v = \frac{1}{\kappa} \sqrt{\frac{\tau_o}{\rho}} \ln\left(\frac{y}{y_o}\right) \tag{3.17}$$

where y_o is a constant of integration.

Since the tractive force τ_o can be expressed as

$$\tau_o = \rho g R S \tag{3.18}$$

where R = hydraulic radius and S = slope, then

$$\sqrt{\frac{\tau_o}{\rho}} = \sqrt{gRS} = V_f \tag{3.19}$$

by incorporating equation (2.11).

Velocity from equations (3.19) and (3.17) is

$$v = \frac{2.303}{\kappa} V_f \log_{10} \left(\frac{y}{y_o}\right) \tag{3.20}$$

which is known as the Prandtl-von Karman universal velocity distribution law.

From the work of Nikuradse (Schlichting (1951)), y_o can be considered a roughness coefficient. Keulegan (1938) substituted hydraulic radius R for y and hence from equation (3.20), discharge can be expressed as

$$Q = \frac{2.303}{\kappa} A\sqrt{gRS} \log_{10} \left(\frac{R}{\chi}\right) \tag{3.21}$$

where A = flow cross sectional area and χ = roughness coefficient.

From Burney's equation (2.20) a generalized flow equation can be developed.

$$Q = X R^Y S^Z \tag{3.22}$$

which is referred to below as the Burney discharge equation coefficient X incorporates the roughness

parameter, while coefficients Y and Z depend on the specific form of the flow equation used. Z has a value of 0.5 for the equations used. Alternately the coefficients can be optimized using non-linear regression.

For overland flow situations it is commonly assumed (for example Foster et al (1968)) that hydraulic radius R is approximated by flow depth $\bar{y}$. While the approximation is widely used (and probably valid) for wide shallow flows when the roughness elements are submerged, it was considered that for overland flow in which the roughness elements project through the flow, or when there is channelization of the flow, the hydraulic radius should be calculated. From a series of height values from a profile across the flow surface perpendicular to the flow direction the wetted perimeter P can be calculated for a particular flow cross-sectional area A. The hydraulic radius R is then calculated as

$$R = A/P \tag{3.23}$$

which can be applied in the flow equations (equations (2.5), (2.6), (2.7), (3.21), and (3.22)) to include the area/perimeter effect for varying flow situations. A computer program, ARPE, to compute the area/perimeter relationship is included in Appendix D.

CHAPTER IV

EQUIPMENT

In order to pursue the objectives given in Chapter I, a program of investigation was laid out which required the following three stages:

(i) construction of the bed surface for profile investigation and hydraulic response.

(ii) measurement of the surface geometry.

(iii) measurement of the hydraulic response of the surface.

The equipment required to satisfy the requirements of the study was derived from either existing equipment, modified existing equipment, or specially constructed apparatus. The existing equipment consisted of the micro-relief meter used by Burney (1973), and the rainfall simulator (Figure 1), the construction and operation of which is described by Das (1970), and was used by Das (1970), Kundu (1971), and Burney (1973). In addition, the TR-48 analog computer and the DES-30 logic unit used by the previous workers were available for experiment control and signal processing. The rainfall simulator was used without modification, while the micro-relief meter was substantially modified, and later replaced, by a specially designed profile meter (see Figure 2).

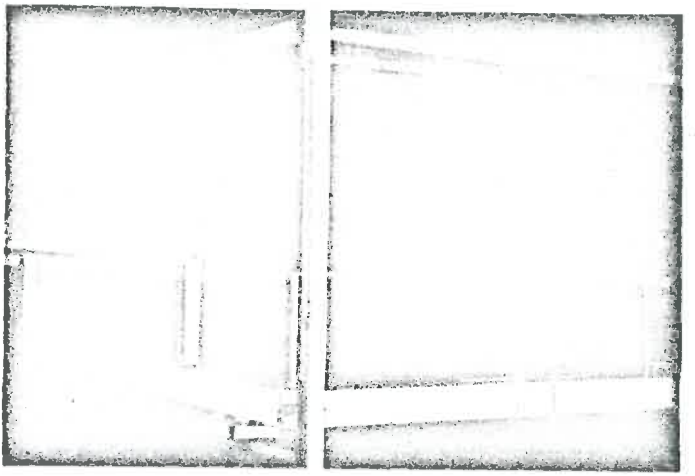

Figure 1. The rainfall simulator.

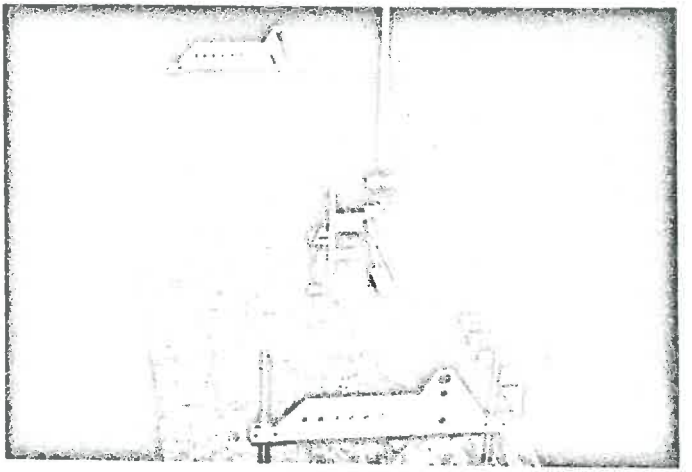

Figure 2. The profile meter shown mounted on Bed F1 (fiberglas rill replica).

Bed Surface Construction

The first surface to be investigated was the last surface used by Burney (1973), which was designated as Bed 4 in his study, and is denoted as Bed B4 in this study. Bed B4 was formed from a smooth sand surface subjected to an upstream flow of 6 in./hr. at a 5% slope. The rill pattern obtained consisted of converging and diverging flow channels forming a diamond pattern. Bed B4 is shown in Figure 3.

The second surface, designated Bed T1, was constructed using a similar technique to that described by Burney (1973) for Bed B4, but adapted to this application. The bed material selected was a #4 washed sand, passing a #4 sieve (0.156 in. aperture). To add large element roughness to the surface, a #9 gravel, passing a 0.75 in. sieve and retained on a #4 sieve, was used. Both the sand and the gravel were obtained from Western Materials Co. (formerly Western Indiana Aggregates), West Lafayette, Indiana. An initial bed thickness of 2 in. was proposed and, due to the load imposed on the flow table, was restricted in size to a width of 6.9 ft. and a flow length of 13.8 ft. as shown in Figure 1.

The bed was formed by laying a 2 in. layer of sand on top of a plastic sheet on the flow table, the plastic providing an impervious lower layer. Wooden guides 2 in. high were laid down either side of the flow table and the

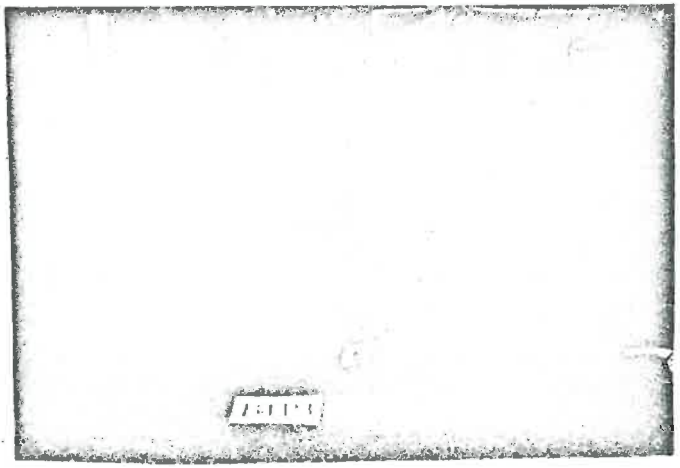

Figure 3. Bed B4 shown with areas sampled by the micro-relief meter (Burney (1973)).

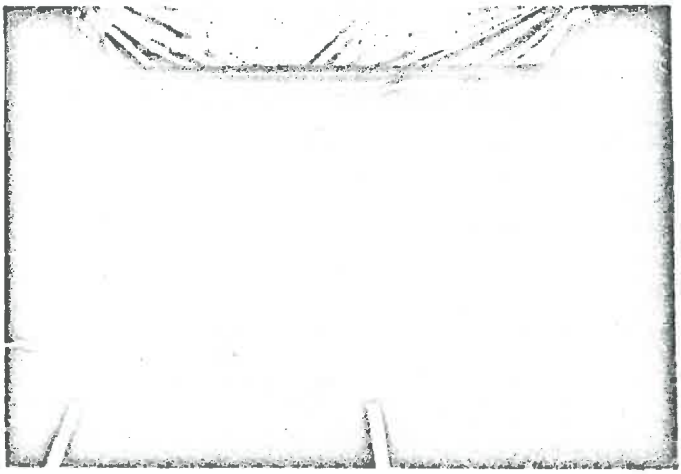

Figure 4. Bed T1 shown with locations of the measured cross and down-slope profiles.

sand was levelled using a 2 in. by 4 in. beam as a striker board. The guides were later removed and replaced with sand before flow was applied. At the downstream end of the bed a 1 in. high sheet metal barrier was placed to retain a minimum depth of sand on the bed. The downstream 6 in. of the bed was sloped from 2 in. depth to the top of the barrier. Gravel was scattered by hand on top of the sand at a density of approximately 60 stones per square foot.

The flow table was set at a 5 percent slope and water was applied from the upstream end at a rate of 12 in./hr. The dry sand slumped in places on wetting but the overall effect was not considered serious. The flow was applied for 45 minutes, during which it was noted that flow tended to concentrate along the sides, possibly due to different packing of the sand after removal of the guides. To reduce this effect the flow was partially diverted towards the center of the bed during the application. The bed was left to drain for 1 hour, and before restarting the flow, the sides of the bed were raised with sand to encourage the flow to remain in an area of the bed which could be measured using the profile meter. When the flow was restarted, it was observed that the modification of the sides had been successful. Water was applied for an additional 30 minutes and the surface left to dry at a 5 percent slope.

Bed T1 was distinctly different from Bed B4 in that well-defined flow channels were present, see Figure 4. At the upstream end of the bed erosion occurred forming four major flow channels, the material removed being deposited in the region 3 to 4 feet from the top of the bed. At a distance of 4 to 6 feet from the top many small flow channels formed which started to concentrate at around 7 feet. Below 7 feet the flow established three major flow channels, one in the center, approximately 12 in. wide and 1 in. deep, with the other channels on either side of the bed.

After the bed had drained for 4 hours the surface was treated to prevent slumping of the sand on drying. The surface was sprayed with 0.5 gallon of clear casting resin and styrene monomer mixed in a ratio of 2:1 with 1 ml. methyl-ethyl-ketone peroxide (MEK) as a catalyst. The styrene monomer provided sufficient dilution for spraying. The application left a thin crust on the surface which was sufficient to hold the material in place and yet was permeable enough to permit later application of clear casting resin to fix the bed surface relief. The surface was left to dry on a 5 percent slope.

After 2 days all gravitational water had drained from the bed. A fan was then directed onto the bed to accelerate evaporation. Three days after formation the upper end of the bed developed a lighter colour

and was dry to the touch, although the lower end was still wet. After five days the whole surface was light coloured and dry, and the fan was stopped. The bed was marked off into approximately 10 sq. ft. areas by dividing it down the center and into 3 ft. strips across the bed. Starting at the top a mixture of 1 gallon of clear casting resin, to which 10 percent by volume of styrene monomer and 3 percent by volume of MEK had been thoroughly blended, was applied to each 10 sq. ft. area using a sprinkling can. Initially the bed was at a 5 percent slope, but it was later raised to 1 percent, and then levelled prior to treating the bottom end. Some resin collected in the channels and depressions but it all moved into the surface within 5 minutes. At first 24 hours elapsed between applications to each 3 ft. strip, but since the surface rapidly hardened, it was not considered necessary to delay applications. In places, a second application covered areas where resin had concentrated and moved into the channels. In these areas the resin did not infiltrate completely into the surface, but instead formed a very smooth coating over the sand grains. However, these areas were a small percentage of the total and were not considered to be a serious defect. The remainder of the surface showed significant grain roughness effects.

Upon complete drying a few cracks occurred, especially along the sides of the bed, and these were filled with a

resin/sand mixture. The area underneath the upstream flow pipe was painted with resin and the bed was left to dry for two days, after which a final spray coat using the 2:1 mixture of clear casting resin/styrene monomer with 1 ml. MEK was added to seal the surface. Later drilling of the surface to mount the profile meter showed uneven penetration which was expected due to the elevation changes across the surface. However, a minimum thickness of approximately 0.25 in. was observed, and this was adequate to provide a stable, durable surface.

The Profile Meter

Following the conclusions drawn by Burney (1973), it was decided to concentrate on line profiles across and down the slope of the bed, and to utilize a smaller step size in an attempt to quantify the effect of the smaller grain sizes of which the surface was composed. According to Lambe and Whitman (1969), the M.I.T. particle size classification system gives 0.6 mm. (0.0236 in.) as the dividing line between medium and coarse sand. Accordingly, a step size of approximately 0.01 in. was chosen so that the effects of coarse sand and larger roughness elements could be measured.

Initially, Burney's (1973) micro-relief meter was modified to increase its lateral resolution to give a total of 2400 steps over a distance of 23.56 in. The

desired step size was achieved by using a 12-position bi-directional stepper motor driving an 80 tooth 1.667 in. pitch diameter anti-backlash worm wheel using a double thread worm gear. The drive was transmitted to a 0.0982 in. linear pitch precision rack through a 48 tooth 1.50 in. pitch diameter anti-backlash spur gear. The resulting drive system gave an incremental step of 0.00982 in. (.249 mm) for each increment of the stepper motor. The drive system was mounted on a cross-carriage and is shown in Figure 5. The cross-carriage was mounted on a rail consisting of a 0.75 in. diameter hardened ground steel shaft supported underneath by an aluminum backbone. The cross-carriage was supported on the rail with open linear bearings which were adjustable to reduce play. The provision for two-dimensional traversing at .1 in. intervals was retained but not used due to the time involved for each 2400 point profile (approximately 40 min.). The cross-carriage was later transferred to a 78 in. rail using the same drive system and providing a 72.65 in. (7400 steps) traverse. The rail length was limited by the width of the bed (83 in.). Approximately 2 hours was required to collect 7400 data points.

The profile height measurements were obtained using a ± 0.5 in. linear variable differential transformer (LVDT). The LVDT consisted of a central iron core which causes inductive coupling between a primary coil, excited by a 1.6 kHz ac voltage, and two secondary sensing coils. The

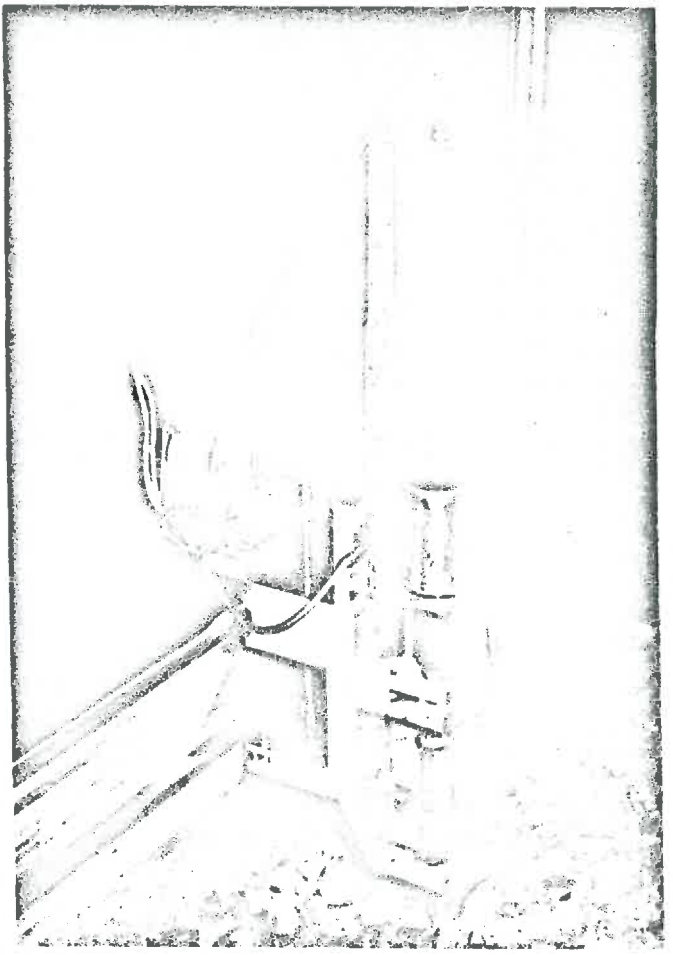

Figure 5. Profile meter cross-carriage showing the drive and probe lift systems.

position of the core is indicated by the amplitude and phase of the two secondary coil outputs. The secondary coil outputs were transformed into a proportional current by a demodulator unit. An ancillary circuit (Figure A3) incorporating a resistance and low pass filter, converts the signal to a voltage output, resulting in a linear relationship between core position and output voltage. The response of the LVDT is very rapid and provides continuous resolution of ± 0.0002 in. over a range of 1.3 in.

The LVDT core was bonded to a surface elevation sensing probe using epoxy glue, the probe consisting of a nominal 0.125 in. diameter stainless steel tube which was precision ground for straightness and circularity. The tube had a phonograph needle swaged into the lower end and the 8 in. long probe was laterally supported by circular low tolerance Teflon bearings mounted 4 in. apart. The probe lift mechanism was provided by a tubular pull-type 24 volt dc solenoid having an intermediate duty rating and a 6.0 oz. pull at 1.5 in. stroke. Since the probe weighed 6.2 oz., the solenoid core was lightened by drilling out the center, and a sliding connection was provided between the solenoid core and the probe. A diagram of the connection is shown in Figure 6. The connection allowed the solenoid core to continue its descent after the probe tip had contacted the surface, thus reducing the impact force on the surface being measured.

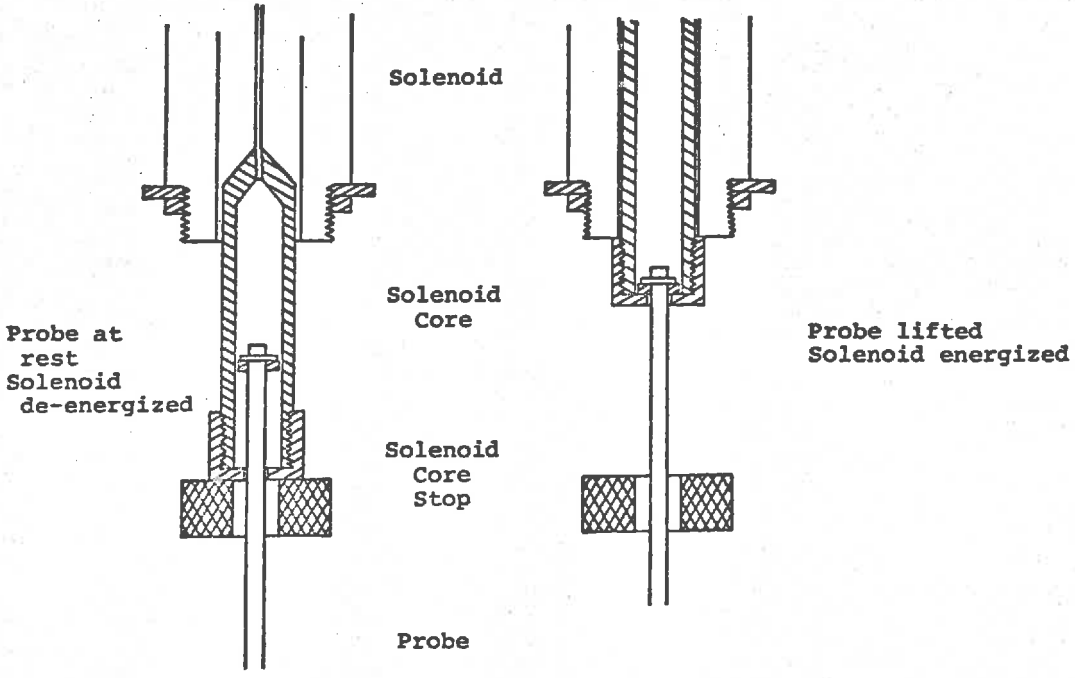

Figure 6. Diagram of sliding connection between the solenoid core and the elevation sensing probe.

Lateral deflection of the probe due to bending was affected by probe descent velocity and surface angle of incidence, and caused errors in the height readings. In order to reduce the magnitude of such errors and the probability of probe penetration into the surface, the probe fall velocity was reduced to approximately 0.5 in./sec. using an adjustable pull-type dashpot attached to the solenoid core. The complete probe lift mechanism is shown in Figure 5.

To mount the profile meter in the desired locations on the flow surface, the bed was drilled to receive 0.125 in. diameter brass pins, which fitted into locating holes in the legs at either end of the profile meter. The pins were glued in place. Before collecting data the meter was positioned on the bed and the height adjusted so that the probe tip cleared the high points of the profile. The meter was then levelled by adjustment of its threaded support legs. The cross-carriage was positioned at one end of the rail, and the probe lowered to the surface.

Data were recorded from the LVDT by transmitting the voltage output, with a full-scale range of 0-3.8 volts, over high grade shielded instrumentation lines to the analog/digital hybrid computer, which controlled the operation of the profile meter and recorded the data on magnetic tape. Data acquisition was achieved using the DES-30 digital logic computer to control the profile

meter and to issue analog-to-digital conversion (ADC) requests to a PDP-11/20 digital computer. Signal processing necessary to control the operation of the data acquisition was achieved using the TR-48 computer.

The operation cycle of the profile meter commences with the probe in the lowered position with the tip resting on the bed surface. An ADC is requested and after a delay of 10 ms. the lift solenoid is energized until the probe rises above a preset level, sensed by a comparator in the TR-48 monitoring LVDT output. After the probe is raised, a 60 ms. pulse is sent to the stepper motor to move the cross-carriage one step. The probe falls at approximately 0.5 in./sec. and when it descends below the preset level detected by the comparator, the ADC request is enabled. As the probe is lowered the derivative of the LVDT signal is generated and monitored by the analog computer. When the derivative falls below a preset threshold level the signal proportional to the surface elevation (the LVDT output) is considered to be stable. The ADC is then requested, which initiates the next cycle. The ADC's are counted and after completion of a preset number (e.g. 7400) the test is terminated. Details of the operation, control and calibration of the profile meter are given in Appendix A.

The Rainfall Simulator

Chow and Harbaugh (1965) reviewed many techniques for

producing simulated rainfall in a laboratory situation, with particular reference to producing rainfall variations with space and time. A basic design for a rainfall producing module was developed, consisting of a 24 in. square Plexiglas box having drop formers at 1 in. centers on the underside and four calibrated supply lines and an air release valve on the upper side.

The basic design has been used by several workers, including Das (1970) who described the rainfall simulator built by him and also used by Kundu (1971) and Burney (1973). The rainfall simulator consists of a 14 ft. square flow table which is supported on four strain-gauged aluminium rods to provide continuous monitoring of the bed weight. Each rod is equipped with two strain-guage pairs to form a temperature compensated bridge and to eliminate bending effects. The flow table can be inclined at slopes from 0.00 to 0.05 ft./ft. using two motor-driven screw jacks. A runoff collection tank is situated at the downstream end of the flow table, and is supported on two strain-guaged cantilever beams. A constant current power supply is connected to the two strain-guage circuits which are connected in series. Low-level voltage signals from the two strain-guage circuits provide continuous outputs proportional to the bed weight and the collecting tank weight.

Rainfall is provided using 49 modules mounted on a frame suspended over the flow table. The height of the

frame above the bed can be adjusted using four electric winches which can be controlled simultaneously or separately. Each module is 2 ft. square and has 0.023 in. I.D. drop tubes at 1.25 in. spacing. Since only half the flow table was utilized in this study, 28 modules were used. The modules are connected to each of four water supply lines, which enter each box through calibrated nozzles. The nozzles provide intensities of 0.5, 1, 2, and 4 in./hr. from each module under a 25 psi. supply pressure. Each supply line is controlled by a solenoid valve so that a particular rainfall rate could be obtained by a combination of open valves. Water is supplied to the rainfall modules by means of a pump and filter unit from a sump underneath the flow table.

Across the upstream end of the flow table a P.V.C. pipe having 0.125 in. I.D. tubes at 1 in. spacing supplies water to the bed simulating an upstream extension of the surface. Water is pumped from the sump through a flow regulating manifold consisting of two branches controlled by solenoid valves. One branch contained a calibration valve, while the other divided into two, one branch having a calibration valve while the other contained a calibration valve and a gate valve. At 20 psi. supply pressure the solenoid and gate valves were manipulated to produce 6, 12 and 18 in./hr. flow rates. Supply pressures from each of the two pumps were controlled using bypass gate valves.

The rainfall simulator was set up for semi-automatic operation. Local controls were used to set rainfall module height, bed slope and to select application rates for rainfall and/or upstream flow. Local override during automatic control of hydraulic tests was also available. The bed weight and collecting tank weight signals were transmitted to the analog/digital hybrid computer system using high grade shielded instrumentation lines. The TR-48 analog computer processed the signals to obtain values of bed weight, collecting tank weight, and the derivative of the collecting tank weight. By calibration prior to testing these signals gave instantaneous values of detention, accumulated mass flow, and flow rate respectively. Detention and flow rate signals were fed back to the laboratory for recording on a chart recorder to monitor test progress and provide a permanent test record. The control of the solenoid valves and the ADC requests were handled by the DES-30 digital logic computer, while the PDP-11/20 controlled the analog-to-digital conversions and data recording on magnetic tape.

Prior to each series of tests the rainfall module frame was tilted and air was evacuated from the modules using a vacuum pump connected to each module via an air release valve. After evacuation the module frame was levelled at the required height above the bed (4.5 ft.). Rainfall and upstream flow application and cut-off,

activated by computer control, were almost instantaneous and provided close control. For tests in which both rainfall and upstream flow were applied, the local override was used to produce a second rainfall application so that the rainfall and upstream flow application rates could be separated. The operation, control and calibration of the rainfall simulator are discussed in Appendix B.

CHAPTER V

DATA ACQUISITION

It is the purpose of this chapter to describe the measurements taken in order to establish a data base on which analyses were performed. The analytical methods and results obtained will be discussed in the next chapter. However, it should be noted that some data were partially analyzed soon after being taken, and decisions on the necessity or desirability of collecting more data were made. Since data acquisition and preliminary analyses formed a continuing process during the data collection phase of the investigation, the decisions and the reasoning behind them will be noted here.

Profile Measurements

The last surface used by Burney (1973) remained following his investigation as a "benchmark" surface to link the studies and is denoted as Bed B4. The recommendations following Burney's study indicated the spectral analysis technique used was restricted in its usefulness by the range of frequencies covered. Considering that height measurements were taken at approximately 0.1 in. spacing, the Nyquist frequency is 5 cycles per inch (cpi).

Following a stability analysis, Burney used a maximum lag of 20, corresponding to a lower frequency bound of 0.5 cpi. In addition, a moving average filter was used to remove trends and limit low frequency, high power components, while at higher frequencies errors due to "aliasing", or folding of frequencies higher than the Nyquist frequency back into the spectrum occurred.

Initially it was decided to modify the profile meter to obtain height measurements at a spacing of approximately 0.01 in., corresponding to a Nyquist frequency of 50 cpi. In addition, the probe fall velocity was reduced to limit lateral deflection of the probe due to wedge effects, i.e. probe lateral deflection errors, due to particles on the bed surface. The mechanism to achieve these modifications have been described in Chapter IV. The profile length of the meter was kept at 24 in.

Positions 1, 2, and 3 on Bed B4 used by Burney were marked by the brass pins used to locate the profile meter. Profiles were taken across and down the slope in the center of each position. Analysis of the profiles yielded spectra that did not indicate significant detail for the higher frequencies, and showed little effect of the grain roughness present in the surface. On the basis of these spectra, it was decided that an investigation of the low frequencies might be more profitable. Visual inspection of the surface indicated the presence of low frequency components due to the rill pattern created by the flow.

To achieve low frequency measurements within the limitations of the bed surface, which had a width of 82.5 in., a profile meter allowing for the measurement of a 72 in. profile was constructed. The carriage conveying the drive mechanism and probe assembly from the previous meter was used without modification. This meter is described in detail in Chapter IV.

Since the flow surface was formed using only overland flow introduced at the upstream end of the bed, it was considered that the area close to the region of introduction of the flow would not be representative of the overall flow situation. Similarly the lower end of the bed was influenced by the free overfall when the flow left the surface, which was indicated by a general lessening of surface undulation as the flow pattern became less distinct. Accordingly the lower end of the bed was considered unrepresentative and not measured. The effect of the sides parallel to the flow direction on the flow properties forming the surface was uncertain, and consequently the "edge effects" were avoided by taking measurements no closer than within 5 in. of the sides of the bed. Surface profile information for 2 ft. by 2 ft. square areas was already available (Burney (1973)) and so it was decided to take profile measurements on a 2 ft. grid over the surface. Profiles taken perpendicular to the flow direction, i.e. across the slope, were referenced

to the top of the slope, and were taken at 3, 5, 7, 9, and 11 ft. Profiles taken parallel to the flow direction, i.e. down the slope, were referenced to the left side of the surface viewed in the up-slope direction, and were taken at 1.5, 3.5, and 5.5 ft., the profiles being centered on the 7 ft. cross-slope profile. Example profiles for Bed B4 are shown in Figure 7. A similar set of cross-slope and down-slope profile measurements were taken for Bed T1, examples of which are shown in Figure 8.

The conversion of the height reading to a voltage signal for transmission to the central computer system for processing and storage on magnetic tape has been discussed in Chapter IV and Appendix A.

Hydraulic Tests

Following construction of Bed T1, as described in Chapter IV, a comprehensive series of hydraulic tests was performed. The series consisted of two replications of a complete factorial design, the order of testing being separately randomized within each replication. The variable levels used in the tests were as follows: five levels of bed slope (1, 2, 3, 4 and 5 percent), four levels of rainfall (0, 2, 4 and 6 in./hr.) and four levels of upstream inflow (0, 6, 12 and 18 in./hr.). The first replication was completed and checked before the second replication was commenced. The complete series comprised 160 tests, of which 10 were null tests having zero rainfall

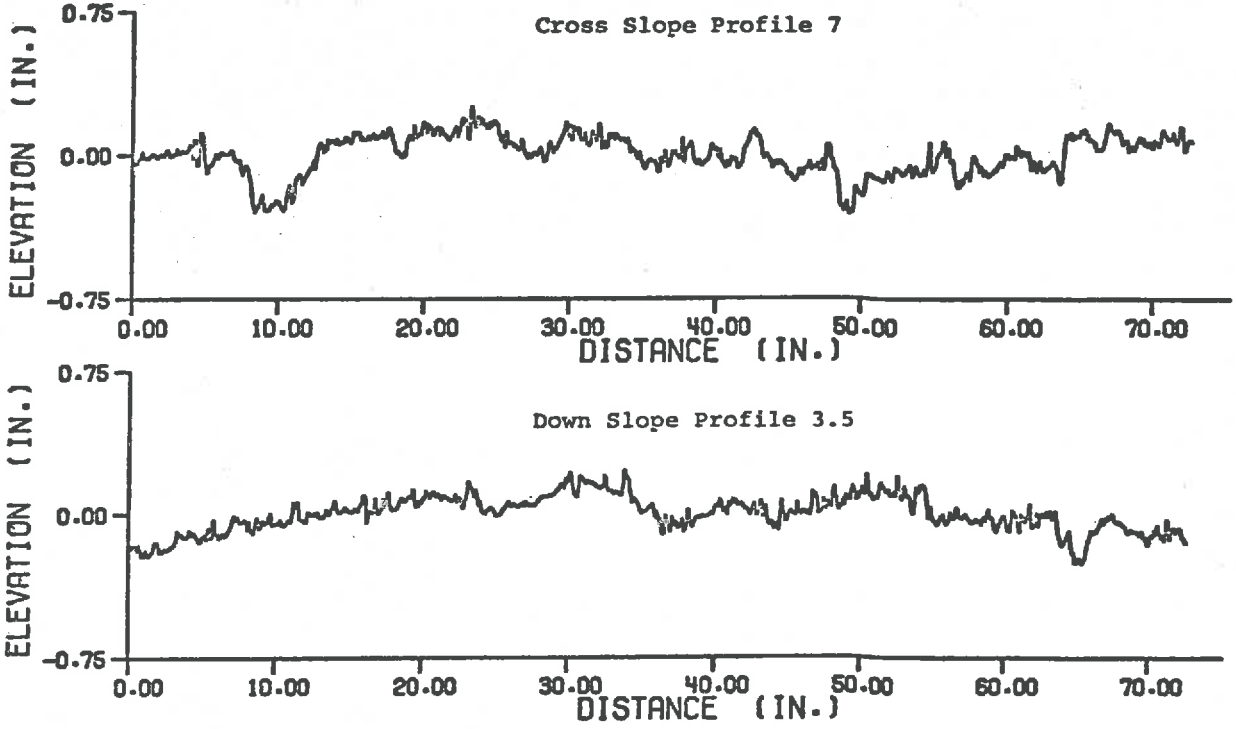

Figure 7. Profiles obtained from Bed B4.

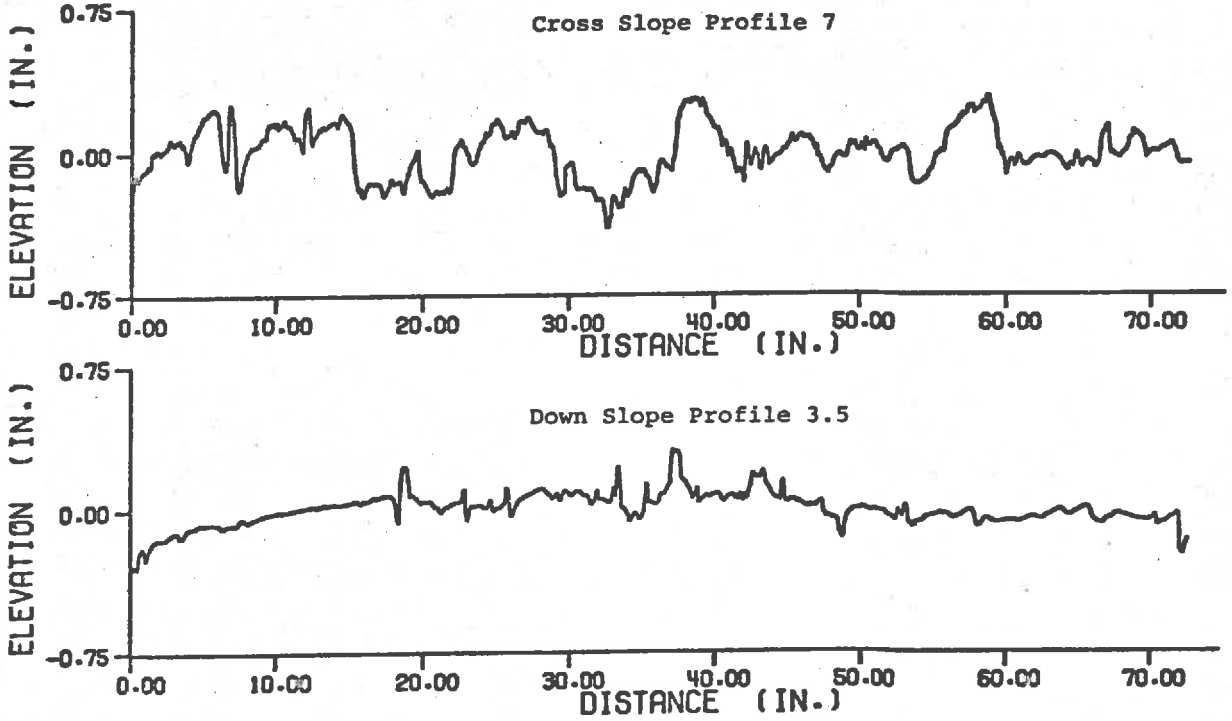

Figure 8. Profiles obtained from Bed T1.

and upstream inflow (two replications for each level of slope), resulting in 150 data sets. Each set consisted of steady-state values of total discharge rate, rainfall rate, and mean detention together with the bed slope value.

Before testing, the three signals indicating detention (from bed weight), mass runoff (from weighing tank weight) and runoff rate (from weighing tank derivative) were calibrated as described in Appendix B. Prior to each test sequence the rainfall modules were placed under reduced pressure to remove air as described in Chapter IV. Rainfall was applied to the surface between tests to ensure that the surface retention component for the bed was satisfied prior to the start of a test. The initial bed weight was used to calculate detention throughout a test. Values of runoff rate, detention and mass runoff were calculated from averaged values of the voltage signals from the weighing tank derivative, bed weight and weighing tank weight respectively. Procedures for collection and recording of the data on magnetic tape are described in Appendix B. The digital computer program, HYDAN, used to analyze the steady-state conditions for each test is given in Appendix D.

Expansion of the Data Base

Foster's Surface

The surface used by Foster (1975) to study rill flow

was made available to this investigation together with the hydraulic test data, which consisted of bed slope, rainfall rate and upstream inflow information, together with flow area values for 15 cross-sections of the rill. An average value of flow cross-sectional area was calculated for each test.

The surface consisted of a fiberglas replica of a rill which was developed in field tests under conditions of simulated rainfall. A plaster cast of the field surface at the end of a simulated runoff event was made from which the fiberglas replica was constructed. Details of the surface formation and testing are given by Foster (1975).

The rill surface, which is denoted as Bed F1, consisted of an area 14 ft. long and 3 ft. wide having the rill running lengthwise down the bed. The rill, which is approximately parabolic in cross-section, is situated to the right of center when viewed in the up-slope direction. Cross-sectional profiles of the rill were taken at 3, 5, 7, 9 and 11 ft. from the top of the surface, and a down-slope profile centered about the 7 ft. cross-section was taken approximately along the centerline of the rill. Example profiles for Bed F1 are shown in Figure 9.

Since the depth of the rill (approximately 2 in.) was greater than the stroke of the probe (1.3 in.), each cross-section was acquired in two parts, and matched to give a

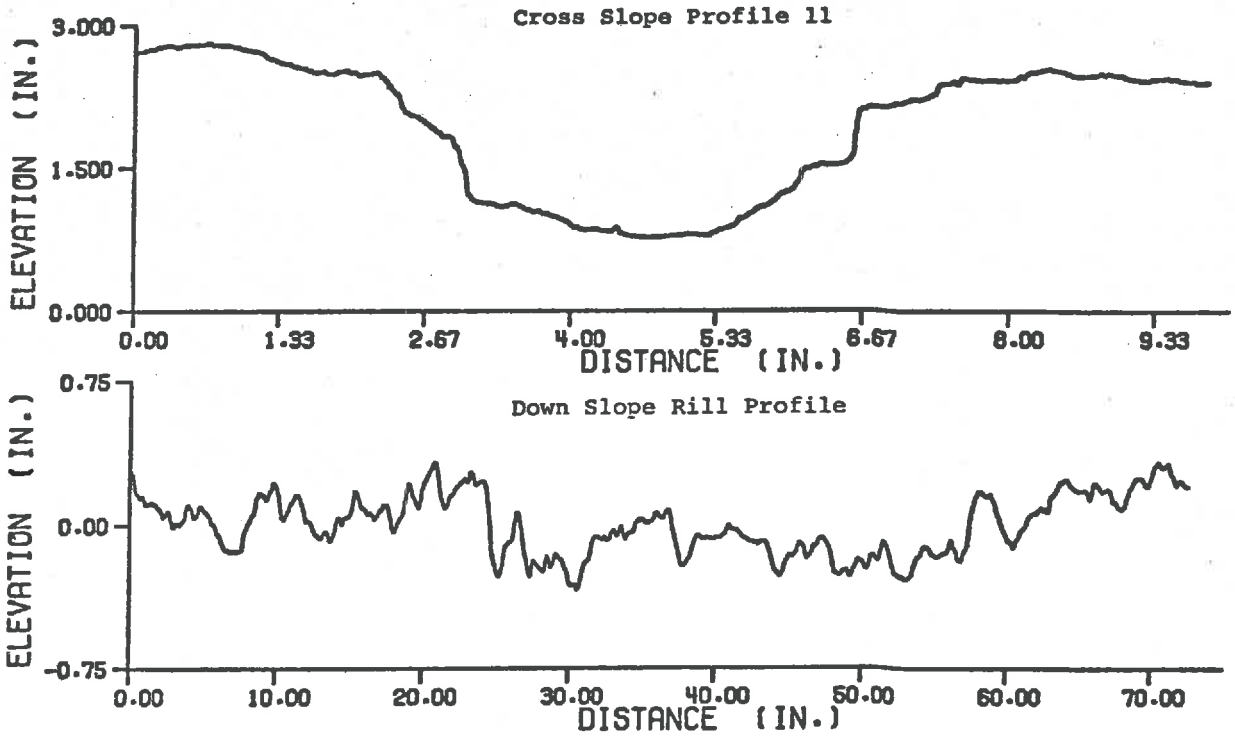

Figure 9. Profiles obtained from Bed F1.

complete profile. First the profile meter was set up to measure the center section of the rill which included the lowest elevations of the section. The location of the cross-section was fixed by clamping a board across the surface on which the profile meter was located. Following the collection of the data, a calibration block was placed in the rill and a series of measurements taken across the block. The elevation of the profile meter was increased to enable the remainder of the cross-section to be measured, and a second series of measurements on the calibration block was taken. The calibration block was removed, and the upper section of the profile was measured. To obtain the complete cross-section for each station, the two parts of the profile were matched using the known difference in elevation of the two data sets.

Kundu's Surfaces

Hydraulic test data similar to that described above for Bed T1 were available for the plane grain-roughened surfaces used by Kundu (1971). In addition, information concerning particle size and distribution for each surface was used. The surfaces tested by Kundu were denoted as Beds K1, K2, and K3 respectively. Bed K1 approximated a Poisson distribution. For surfaces K2 and K3 the particle distributions were controlled to closely conform to a Poisson distribution. Surfaces K2 and K3 were formed by adding particles to the previous surface. The

particle sizes and distribution densities are given in Table 1.

The distance between occurrences for a Poisson process is given as an exponential distribution (Griffin (1971)) having a mean of $1/\lambda$, where λ is the particle density. The probability of distance between occurrences is then

$$F(x) = 1 - e^{-\lambda x} \tag{5.1}$$

The profile for a single particle distribution was determined using a computer program which assigned the distance between particle occurrences using equation (5.1), and also the effect from the profile centerline to a maximum of $\pm$ 0.5 $\bar{d}$, when $\bar{d}$ is the mean particle diameter. The actual particle diameter is also assigned within the particle size range specified, assuming that the particles are approximately spherical. The computer program assigned values using a uniformly distributed random number generator with a random starting point. Subsequent profiles were developed by overlaying the generated profiles for single particle distributions. The computer program, POIS, given in Appendix D, was used to generate the profile for Bed K3, using the generated profile for Bed K2 as input. The generated profiles for surfaces K1, K2 and K3 were used in conjunction with the hydraulic test data to characterize the response of plane grain-roughened surfaces.

Table 1: Particle distributions for Kundu's surfaces.

Surface	Equivalent Particle Diameter (in.)			Particle Density (No./in.^{2})
	Minimum	Mean	Maximum	
K1	0.0327	0.0433	0.0552	84.40
	0.1311	0.1575	0.1874	6.67
K2	0.3750	0.4374	0.500	1.46
K3	0.2500	0.3126	0.3750	2.42

CHAPTER VI

ANALYSIS AND DISCUSSION OF RESULTS

In Chapter V, the data collection procedure was discussed, together with the decisions incorporated in each step. The analysis of the data, and discussion of the results obtained is the substance of the present chapter. As explained in the introduction to Chapter V, data collection and preliminary analysis were often concurrent operations in the investigation, and hence the directions taken in later work were indicated from the conclusions drawn from the initial analysis.

Since the first overall objective of the study concerned the development of expressions to characterize surface roughness, it is convenient to discuss the techniques used and their results first. The analysis of the hydraulic test results, and the inclusion of estimated parameters in prediction equations, follow logically. Comparisons between laboratory and field data form the final section of this chapter.

Spectral Analysis

Height profiles were taken across and down the centerlines of the three positions used by Burney (1973) on Bed

B4. The positions were denoted as Positions 1, 2 and 3 and are shown in Figure 3. Profiles consisted of n = 2400 readings at 0.00982 in. spacing, corresponding to a profile length of 23.56 in., while Burney's data consisted of 240 profiles of 240 readings each at ten times the spacing interval. Burney (1973) gave the collapsed line spectra up to a Nyquist frequency of 5 cpi. as a semilogarithmic plot of spectral estimate against frequency. For the purposes of this study the spectra obtained will be expressed graphically in a log-log form, an example of which (Bed B4 profile 7) is given in Figure 10. The spectra in log-log form are remarkably linear, showing some variation in the lower frequencies due to a reduced number of estimates, which is a characteristic of the method of spectral analysis. A discussion of the uncertainty associated with spectral analysis is given in Appendix C. Regression equations were fitted to the spectra, which plot linearly in log-log form. The model used for the spectra, obtained from log transformations of the data, is as follows:

$$S(f) = A f^{B} \tag{6.1}$$

when A and B are regression coefficients. For Bed B4, positions 1, 2 and 3, the regression coefficients are given in Table 2. The spectra were obtained using the spectral analysis program, SPEC, given in Appendix D.

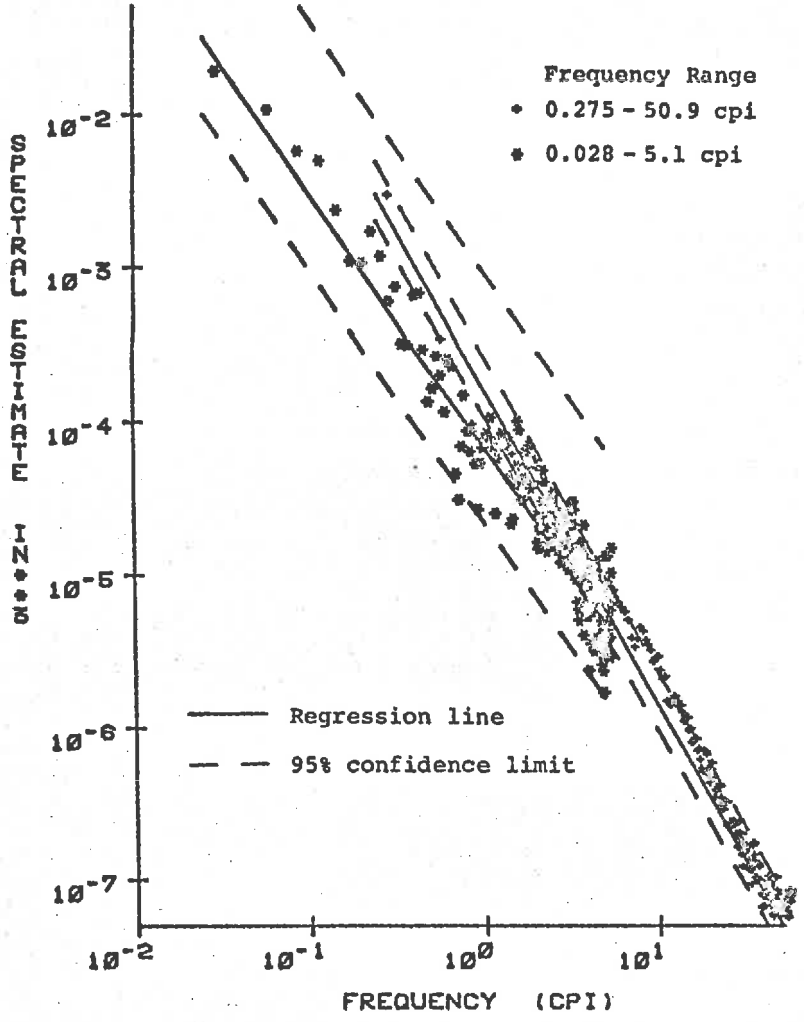

Figure 10. Spectra for Bed B4 profile 7. Regression equations and 95% confidence limits are given for the spectra.

Table 2: Regression coefficients for spectra from Bed B4 (23.56 in. profiles).

Equation: $S(f) = Af^B$

Frequency range: 0.255 - 50.9 cpi

Position	Direction	Coefficients A($\times 10^{-5}$)	Coefficients B	Correlation Coefficient r^2
1	Cross	1.850	-1.465	0.953
1	Down	9.040	-1.722	0.956
2	Cross	20.950	-1.378	0.979
2	Down	5.634	-1.475	0.977
3	Cross	0.565	-1.396	0.959
3	Down	5.786	-1.535	0.966

Generally, the maximum lag used varies between 10 and 25 percent of the total number of points in the data set. Since stable estimates of the spectra were required, a maximum lag m = 200 (8.3 percent) was used. Using the approximate degrees of freedom formula developed by Kozin et al (1963)

$$\nu = \frac{n - m}{m} \tag{6.2}$$

when ν is the number of degrees of freedom, 11 in this case. Confidence limits on the spectral estimates were derived using the χ^2 distribution as given by Jenkins and Watts (1968):

$$P\left[\frac{\nu}{\chi_\nu(1-\alpha/2)} < \frac{\sigma^2}{S^2(f)} \leq \frac{\nu}{\chi_\nu(\alpha/2)}\right] = 1 - \alpha \tag{6.3}$$

For a 95% confidence interval with 11 degrees of freedom the spectral estimate confidence limits are 0.502 and 2.880 times their values. Reducing the maximum lag m has the effect of increasing the number of degrees of freedom according to equation (6.2) which would reduce the confidence limits at a given confidence level. However, reducing m leads directly to a reduction in the frequency band investigated, and a larger frequency interval between estimates. The frequency range for the spectra given in Table 2 is 0.255 to 50.9 cpi. Despite the range of the 95% confidence interval, the spectra

closely conform to their respective regression equations, with correlation coefficients between 0.95 and 0.98.

In order to compare the results obtained from Bed 4 positions 1, 2 and 3 with those obtained by Burney, the variances of the profiles are given in Table 3. Single profile detrended and non-detrended variances from 2400 point profiles are compared with the mean non-detrended 2400 point profile variances since the gradient of the linear regression equations was always less than 0.01.

Interpretation of the results in Table 3 is aided by knowledge of the bed forms in the positions measured. Position 1, located near the upper end of the bed, contained relatively large elevation changes due to flow channels formed by concentration of the upstream inflow. Burney's data gives a larger mean variance in the cross-slope direction which indicates the presence of the flow channels. However, for the particular profiles measured in this study, the opposite case was true. A similar situation occurred in Position 3, located near the lower end of the bed. The overall uniform lower variance condition having a general lack of well defined flow channels is shown by Burney's data, while the present study shows a considerably greater variance in the down-slope direction when compared to the cross-slope direction. Position 2, near the center of the bed showed uniformly distributed flow channels from Burney's data, while the present study

Table 3: Comparison of variances from Bed B4.

Position	Direction	Single 23.56 in. Profile		Mean of 240 Profiles (Burney's data)
		Detrended ($\times 10^{-4}$ in.^{2})	Not Detrended ($\times 10^{-4}$ in.^{2})	Not Detrended ($\times 10^{-4}$ in.^{2})
1	Cross	4.780	4.789	77.782
1	Down	47.350	52.450	42.106
2	Cross	48.280	49.211	53.258
2	Down	12.505	15.600	56.727
3	Cross	1.936	2.069	33.015
3	Down	12.793	12.799	28.470

showed a higher variance in the cross-slope direction. The mean variance data from the area measurements in Burney's study proved superior in description of general trends when compared to single profiles in arbitrary locations. However, a knowledge of the surface form was necessary to assist interpretation of the results.

The regression coefficient A of the spectra in Table 2 is interpreted in a similar way to the variance in Table 3, since the B coefficients for the spectra are approximately equal. Increasing the A coefficient, which is the intercept at unit frequency, increases the area under the curve, which is equivalent to increasing the variance. Since the spectra obtained from the 23.56 in. profiles showed no significant characteristics in the frequency domain, it was concluded that the frequencies due to the grain roughness of the surface could not be identified. In addition, the uncertainty analysis given in Appendix C shows the high frequency components are masked by the white noise added to the spectra by uncertainty of the probe position. Accordingly, it was decided to direct attention to the low frequency components caused by the flow channels present in the surface.

The profile meter was rebuilt to enable a 72 in. profile to be measured, the length of the profile being limited by the width of the bed (82.5 in.). The new profile meter is shown in Figure 2. Since detailed

information was already available for 2 ft. by 2 ft. areas of the surface, it was decided to take profiles on a 2 ft. grid, avoiding the side and end affects. Profiles were taken at 3, 5, 7, 9 and 11 ft. from the upper end of the bed, and at 1.5, 3.5, and 5.5 ft. from the left-hand side looking up-slope. The profiles are denoted by their direction and their position (in feet) on the bed. The profiles consisted of 7400 data points at 0.00982 in. spacing, corresponding to a profile length of 72.65 in.

For the low frequency analysis, a "window closing" test was performed as described by Jenkins and Watts (1968). Since spectrum resolution and stability are incompatible, a series of tests with varying maximum lag was run on a typical profile (Bed B4 position 7 shown in Figure 10). The results indicated that a maximum lag of 25 percent was possible without excessive noise in the spectrum. By equation (6.2), the spectrum has 3 degrees of freedom for m = 1850. In order to reduce computation time without changing the degrees of freedom, a filtering procedure was used. The data was reduced by a factor of 10 by "clustering" the points, which consisted of taking each group of ten points in the series, calculating the mean, and creating a new series consisting of the means at ten times the original data spacing. Since each point in the clustered series is derived from ten original values, increased confidence is associated with each point.

The effect of clustering is to subject the data to a low pass filter, the Nyquist frequency being reduced to 5.1 cpi.

Each profile was analyzed for high and low frequency components. The high frequency analysis used the original data series of 7400 points and a maximum lag of 185, giving a spectrum having 39 degrees of freedom and, from equation (6.3), 95% confidence limits of 0.671 and 1.646 times the estimate value. The frequency band for the high frequency analysis is 0.275 to 50.9 cpi. The low frequency analysis used the clustered series of 740 data points, and a maximum lag of 185, which gave 3 degrees of freedom for the spectral estimates, corresponding to 95% confidence limits of 0.32 and 13.89 times their values. However, the effect of clustering on each derived data point is considered to moderately increase the effective degrees of freedom. A frequency band of 0.0275 to 5.1 cpi. was obtained for the analysis.

Profiles obtained from Bed B4 were analyzed for high and low frequency components. An example is shown in Figure 10. The high frequency spectrum conforms closely to the respective regression equation due to the increased degrees of freedom. The low frequency analysis shows a greater degree of variability due to the few degrees of freedom involved. However, the linear trend is marked for both data sets.

Regression equations were fitted to each of the spectra obtained from Bed B4, and the coefficients are given in Table 4. For the high frequency analysis the coefficients have similar values for the cross and down-slope profiles, the down-slope values being slightly lower. The coefficient B is approximately -2, which corresponds to the model suggested by Akaike (Kozin et al (1968)). The model indicates a randomly rough surface whose profile components are similar in geometry over the frequency range. Considering that the largest single particles contributing to grain roughness were of the order of 0.25 in. diameter, and assuming approximate geometrical similarity of the particles over the range, then the assumption applies from 2 to 50 cpi.

For the low frequency analysis, the spectra depart from the B = -2 condition as indicated by Kozin et al (1968). The B coefficients are generally -1.7 for the cross-slope profiles, except for profile 11 which had little distinguishable surface geometry. The A coefficients for the down-slope profiles are slightly lower than those for the cross-slope profiles, indicating a greater variance in the cross-slope direction. The cross-slope profiles have lower B coefficients than the down-slope profiles, which indicates that the cross-slope profiles have larger variance contributions in the low frequency range.

Table 4: Regression coefficients for spectra from Bed B4 (72.65 in. profiles).

Equation: $S(f) = Af^B$

Profile	Frequency Range					
	0.275 - 50.9 cpi			0.028 - 5.09 cpi		
	$A(\times 10^{-5})$	B	Correlation Coeff. (r^2)	$A(\times 10^{-5})$	B	Correlation Coeff. (r^2)
Cross-slope						
3	15.273	-2.113	0.956	7.314	-1.792	0.926
5	11.852	-2.019	0.961	6.421	-1.749	0.917
7	16.681	-2.079	0.948	6.854	-1.661	0.915
9	11.265	-2.028	0.965	4.705	-1.753	0.904
11	15.620	-2.021	0.950	5.138	-1.344	0.921
Down-slope						
1.5	8.813	-1.937	0.949	3.202	-1.515	0.913
3.5	14.977	-2.029	0.952	5.696	-1.448	0.923
5.5	9.714	-1.966	0.961	4.753	-1.659	0.917

A similar series of analyses was performed on the profiles from Bed T1, which had a considerable degree of rilling of the surface. The rilling became more pronounced with distance down the slope. The regression coefficients for the spectra of Bed T1 are given in Table 5. The A coefficients for the T1 spectra are higher, and the B coefficients are lower, than those for the B4 spectra, indicating increased variance in the low frequency range. The B coefficients for the high frequency analysis are greater than -2 except for profile 5.5 in the down-slope direction. Profile 5.5 crossed over the flow channel near the edge of the bed, and consequently shows different properties from the other down-slope profiles. For the low frequency analysis the B coefficients became closer to -2, although the cross-slope values were greater than the down-slope values.

The spectral analyses of Beds B4 and T1 did not show characteristic frequency components for the frequency range tested (0.0275 to 50.9 cpi.); however, the effective frequency range was reduced to an upper limit of approximately 10 cpi. due to white noise effects resulting from probe placement errors. The spectra were notable for their linearity in a log-log form, and could be adequately described by equation (6.1), the coefficients being determined by regression. The random roughness characteristics indicated by the spectra suggest the possibility

Table 5: Regression coefficients for spectra from Bed T1 (72.65 in. profiles).

Profile	Frequency Range					
	0.275 - 50.9 cpi			0.028 - 5.09 cpi		
	A($\times 10^{-5}$)	B	Correlation Coeff. (r^2)	A($\times 10^{-5}$)	B	Correlation Coeff. (r^2)
Cross-slope						
3	14.794	-2.439	0.949	10.174	-2.181	0.891
5	19.286	-2.407	0.948	11.246	-2.142	0.901
7	12.567	-2.252	0.957	8.774	-2.198	0.936
9	17.015	-2.619	0.960	8.515	-2.478	0.921
11	21.002	-2.227	0.954	19.754	-2.296	0.947
Down-slope						
1.5	7.944	-2.132	0.954	5.702	-2.076	0.901
3.5	5.838	-2.109	0.938	4.922	-1.905	0.927
5.5	2.962	-1.357	0.947	5.295	-2.149	0.917

of more easily characterizing the spectra by computing only the variance. From equation (6.1), using B = -2

$$\sigma^2 = \int S(f)df = \int \frac{A}{f^2}\, df \qquad (6.4)$$

which relates the variance σ^2 to A, the intercept at unit frequency.

Amplitude/Frequency Distribution

The amplitude/frequency distribution described by Brickman, Wambold and Zimmerman (1971) has been approximated by the amplitude/separation method given in Chapter III. Separation has been related to frequency by equation (3.13). An event in the distribution is defined as the determination of the separation of two points of equal elevation across a flow channel in the surface and is classified by amplitude from the mean elevation and by separation. The amplitude/separation gives the number of events N_{ij} occurring in a profile for amplitude band a_i and separation band s_j. The program, AMSEP, used to compute the amplitude/separation distribution from the profile data is given in Appendix D. The amplitude/separation distribution for Bed T1 profile 7, taken across the center of Bed T1, is given in Figure 11.

The pattern of event distributions shown in Figure 11 is similar for all the profiles of Beds B4 and T1. The occurrence of large separations in amplitude ranges

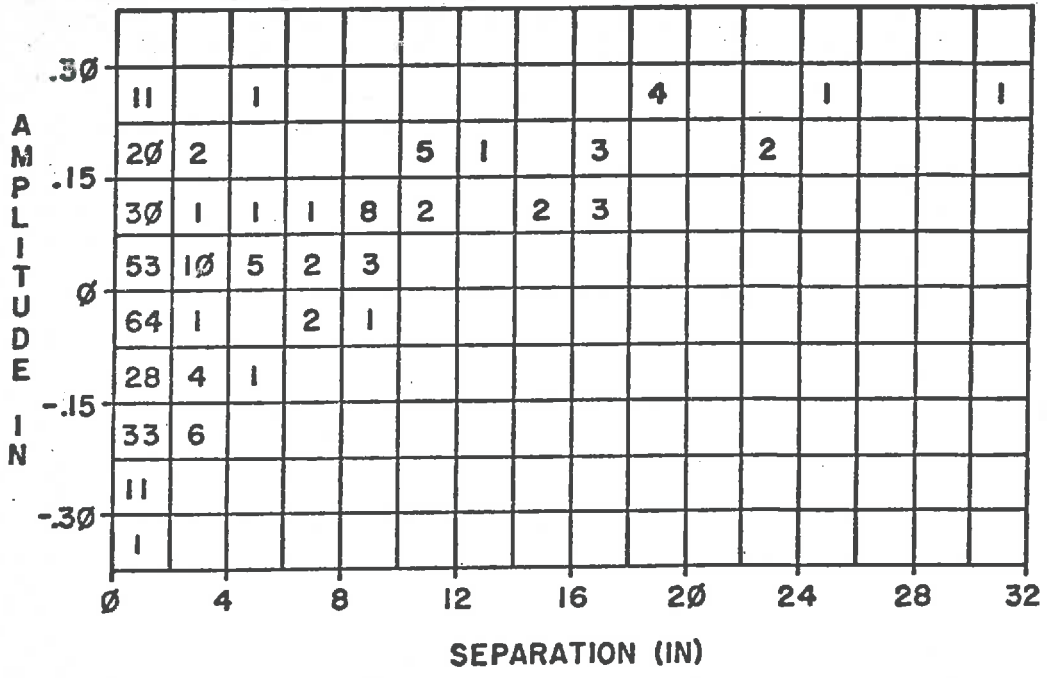

Figure 11. Amplitude/separation distribution for Bed T1 profile 7.

above the mean elevation is characteristic of the method of analysis, and indicates the separation of flow boundaries at a given amplitude or elevation. In order to compare the results from each profile, the amplitude and separation distributions were obtained by summing across the separation and amplitude bands respectively.

The amplitude distributions for Beds B4 and T1 are given in Tables 6 and 7 respectively. Example amplitude distributions for Beds B4 and T1 are given in Figures 12 and 13 respectively. Since Bed B4 contained a limited range of profile elevations, increased resolution was necessary. An amplitude band width of 0.025 in. was used for Bed B4, while a 0.075 in. band width was used for Bed T1. The amplitude distributions of Bed B4 show generally similar characteristics for both the cross slope and down-slope profiles, the majority of points (69.4%) being grouped within ± 0.1 in. of the mean elevation. Outside the ± 0.1 in. range the cross and down-slope profiles remain similar over the ± 0.25 in. range. Exceptions are the 9 and 11 profiles, profile 9 showing a wide range of amplitudes indicating considerable effects of flow channels which are not present in the other profiles. By contrast, profile 11 shows a reduced amplitude range which indicates the smoothing of the surface near the downstream end of the bed. The extreme amplitude range greater than 0.25 in. is confined to profile 9 (2

Table 6: Amplitude distributions for Bed B4.

Amplitude (in.)	Number of Events in each Profile							
	3	5	7	9	11	1.5	3.5	5.5
>0.250	-	-	-	2	-	-	-	-
>0.225	1	1	-	13	-	-	-	-
>0.200	4	3	-	18	-	-	1	2
>0.175	15	6	4	11	-	-	8	7
>0.150	22	4	11	18	2	4	10	8
>0.125	17	16	24	33	5	12	18	8
>0.100	20	22	29	30	13	19	24	27
>0.075	20	27	43	15	26	55	32	26
>0.050	26	50	29	12	39	60	29	35
>0.025	30	42	20	4	46	44	28	43
>0.000	29	35	40	3	78	29	48	60
>-0.025	27	26	29	3	65	19	35	24
>-0.050	22	18	36	21	36	20	32	15
>-0.075	29	31	26	28	15	23	20	23
>-0.100	16	20	20	45	15	16	21	18
>-0.125	19	16	16	25	11	13	20	15
>-0.150	15	3	3	24	3	6	5	13
>-0.175	17	3	5	21	3	12	7	7
>-0.200	14	10	2	9	1	10	5	3
>-0.225	4	3	4	7	1	10	4	2
>-0.250	2	2	5	6	-	2	1	1
>-0.400	5	8	10	8	-	3	1	6
Number of Events	354	346	356	356	359	357	349	353
No. of High Points	16	28	9	21	11	13	15	4
Total Points	724	720	721	733	729	727	713	710

Table 7: Amplitude distributions for Bed T1.

Amplitude (in.)	Number of Events in each Profile							
	3	5	7	9	11	1.5	3.5	5.5
>0.450	-	-	-	13	26	-	-	-
>0.375	-	-	-	15	29	-	-	-
>0.300	5	3	-	20	23	-	1	-
>0.225	16	8	18	2	32	5	1	24
>0.150	24	25	33	28	27	4	8	64
>0.075	57	64	48	45	41	58	43	33
>0.000	84	84	73	58	31	146	101	17
>-0.075	74	59	68	23	5	102	109	57
>-0.150	60	61	33	51	10	21	13	81
>-0.225	19	37	39	42	24	20	6	19
>-0.300	13	11	11	13	14	4	5	5
>-0.375	6	-	1	14	14	1	-	2
>-0.450	-	-	-	21	5	-	-	-
>-0.525	-	-	-	-	6	-	-	-
>-0.600	-	-	-	-	26	-	-	-
>-0.675	-	-	-	-	12	-	-	-
>-0.750	-	-	-	-	9	-	-	-
Number of Events	358	352	324	345	334	361	287	307
No. of High Points	29	26	21	35	24	10	20	48
Total Points	745	730	669	725	692	732	594	652

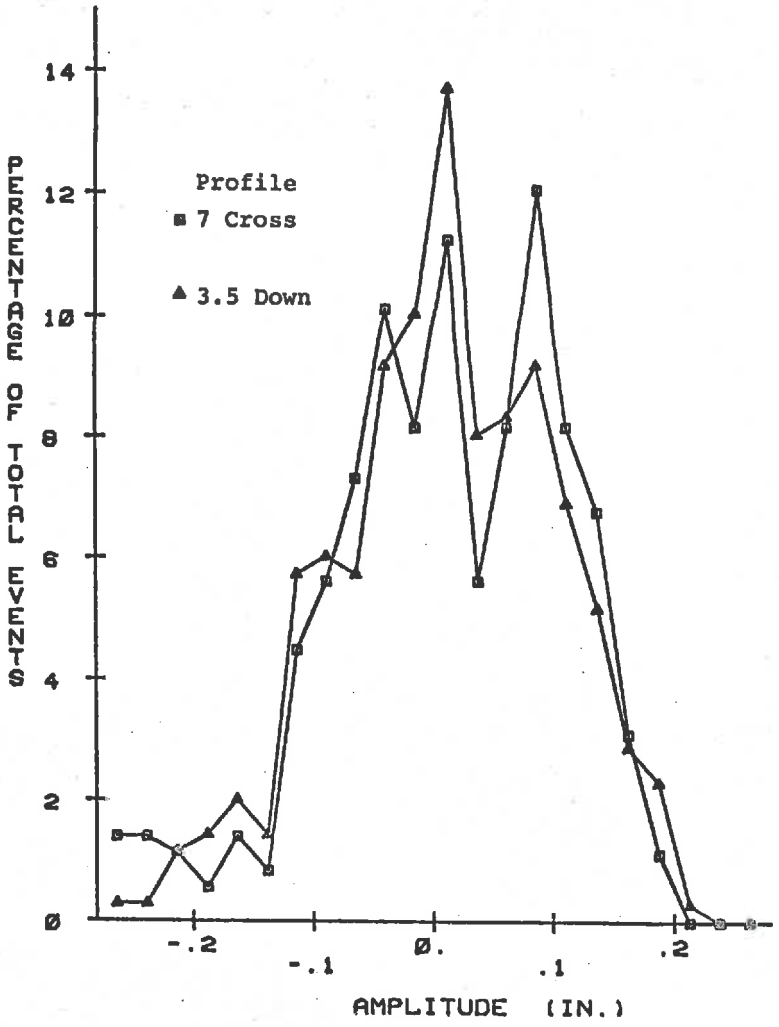

Figure 12. Amplitude distributions for Bed B4.

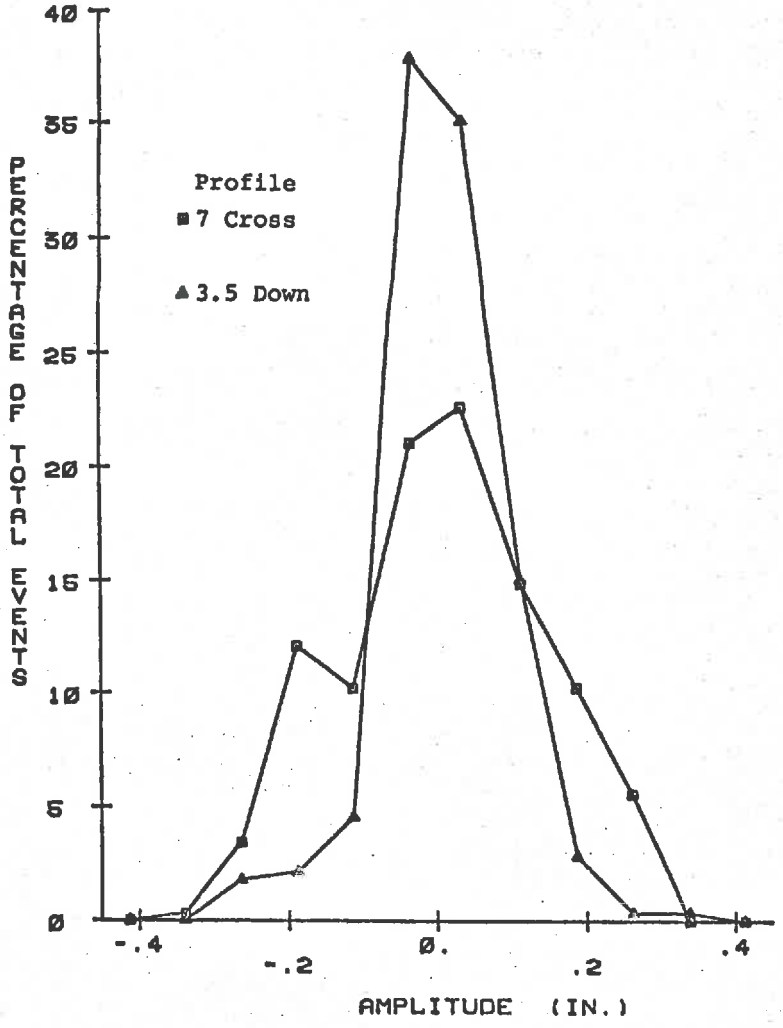

Figure 13. Amplitude distributions for Bed T1.

events), while at the other end of the scale the amplitudes less than -0.25 in. are present in relatively larger numbers for the cross-slope profiles (31 events against 10 for the downslope profiles). Apart from the local variations of profiles 9 and 11, the amplitude distributions for Bed B4 show a uniformly distributed surface in the range ± 0.25 in., which accounted for 98.5% of the total events. The number of events in each distribution correspond to approximately half of the 740 points used in the profile analysis. (A mean of 47% for Bed B4 and 45% for Bed T1.) From the analysis this conclusion is logical since each event matches two points of equal elevation. The high points determined for the profile are points for which no corresponding point exists in the profile. The majority of the high points occur in profiles having negative gradients at their extremes accounting for the variation in numbers of high points for each profile.

The amplitude distributions for the profiles of Bed T1 are given in Table 7. The distributions are generally similar except for profiles 9 and 11 which showed marked effects of the developing rill pattern. From observation of Bed T1 (Figure 4) the rill pattern develops on the lower half of the bed, which can be seen from profiles 7, 9 and 11. Apart from profiles 9 and 11, the majority of events (83.7%) lie in the range ± 0.225 in. which is

similar to that for Bed B4. In addition, the events are grouped around the zero amplitude in the range ± 0.075 in. (41%), the down-slope profile values (56%) being grouped more closely than the cross-slope profile values (32.6%). The difference in grouping indicated the dominance of the flow channels perpendicular to the cross-slope profiles. The amplitude distributions of Bed T1 account for 90% of the profile points. There are slightly more high points in the cross-slope profiles compared to the down-slope profiles due to the more uneven nature of the cross-slope profiles.

The separation distributions for Beds B4 and T1 are given in Tables 8 and 9 respectively. Overall the separation distributions for each bed are remarkably similar. For Bed B4 82.5% of the events have separations less than 2 in. (77.9% for Bed T1) while for events with separations less than 10 in. Bed B4 has 95.8% (96.7% for Bed T1). For separations between 10 and 20 in. Bed B4 has 3.4% (2.4% for Bed T1) and for separations greater than 20 in. Bed B4 has 0.8% (0.9% for Bed T1). For the profiles of each surface it is difficult to discern trends in the separation distributions. The cross-slope and down-slope profiles have similar distributions and there is no noticeable effect caused by the flow patterns.

The amplitude/separation joint distribuiton, an example of which was shown in Figure 11, gave the distribution of equal elevation events for a profile classified by

Table 8: Separation distributions for Bed B4.

Separation (in.)	Number of Events in each Profile							
	3	5	7	9	11	1.5	3.5	5.5
>0.	287	280	292	289	304	300	312	277
>2.	34	27	28	34	29	27	22	35
>4.	9	11	19	18	16	6	7	9
>6.	2	11	4	8	6	6	4	4
>8.	4	4	4	4	-	3	-	11
>10.	2	5	3	-	1	1	-	3
>12.	4	2	-	1	1	10	2	1
>14.	2	3	-	1	2	1	-	4
>16.	5	-	-	-	-	5	2	3
>18.	-	-	-	-	-	-	-	-
>20.	-	1	2	-	-	-	-	2
>22.	-	-	2	-	-	2	-	-
>24.	-	1	-	-	-	1	-	1
>26.	-	-	-	-	-	-	-	-
>28.	-	-	-	-	-	-	-	-
>30.	5	1	2	-	-	-	-	3
Number of Events	354	346	356	356	359	357	349	353

Table 9: Separation distributions for Bed T1.

Separation (in.)	Number of Events in each Profile							
	3	5	7	9	11	1.5	3.5	5.5
>0.	292	262	251	268	251	270	241	240
>2.	28	23	24	25	45	36	27	40
>4.	8	25	8	13	16	22	12	11
>6.	12	30	5	10	7	12	3	1
>8.	-	8	12	18	5	7	-	2
>10.	2	2	7	2	4	-	1	-
>12.	2	-	1	6	6	-	-	-
>14.	5	1	2	-	-	1	2	1
>16.	-	-	6	-	-	1	-	-
>18.	7	-	4	-	-	-	1	1
>20.	-	-	-	-	-	-	-	-
>22.	-	-	2	-	-	-	-	3
>24.	-	1	1	3	-	4	-	3
>26.	1	-	-	-	-	-	-	-
>28.	-	-	-	-	-	-	-	-
>30.	1	-	1	-	-	7	-	-
Number of Events	358	352	324	345	334	361	287	302

amplitude and separation. The two dimensional distribution contains considerable information in a similar manner to the area spectra developed by Burney (1973). It was necessary to collapse the joint distribution into separate amplitude and separation distributions by summing across separation and amplitude bands respectively. The amplitude distributions could be related to the descriptive characteristics of the flow surfaces, while the separation distributions were not distinguishable between and within surfaces.

Area/Wetted Perimeter Analysis

For each cross-slope profile of the two surfaces investigated initially an area/wetted perimeter relationship was derived. From the original data, a clustered detrended profile was obtained, a cluster size of 10 points being used as for the low frequency spectral analysis and the amplitude/separation analysis. For equal increments of flow cross-sectional area, the wetted perimeter was determined using the computer program, ARPE, given in Appendix D.

The area/perimeter curves for Bed B4 are given in Figure 14. The curves show the increase of perimeter with flow cross-sectional area, the maximum perimeter being slightly greater than the profile length (72.65 in.). Profile 7, taken across the center of the bed, gives a smooth profile indicating a departure from the assumption

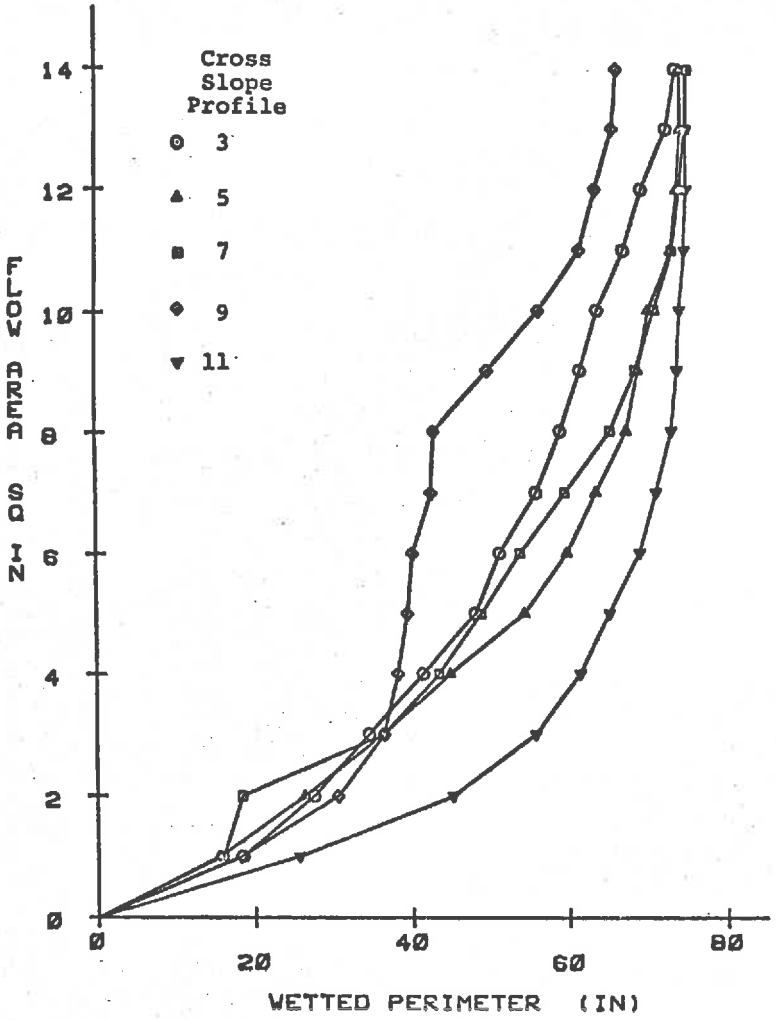

Figure 14. Area/wetted perimeter curves for Bed B4.

that wetted perimeter equals the bed width, which is inherent in the approximation of hydraulic radius to mean flow depth for wide shallow flows. Below a flow cross-sectional area of 12 sq. in. (corresponding to a mean flow depth of 0.165 in.) the deviation of calculated perimeter from profile length becomes pronounced for decreasing flow area. Flow depths of less than 0.165 in. were frequently measured in the hydraulic tests.

Comparing the other profiles to profile 7, it can be seen that profile 5 is very similar to profile 7. Profile 3 differs from profile 7 in the 6 to 14 sq. in. range, the gradient of this section showing that perimeter is increasing less rapidly with area than for profiles 5 and 7. The deviation of profile 3 is due to flow channels caused by the upstream inflow used to form the surface. Profile 9 shows a greater effect of flow channels indicated by the departure from profile 7 above a flow area of 3 sq. in. The effect of the flow channels is noticeable over the remainder of the area range. Profile 11 corresponds to a profile having ill-defined flow channels, since the perimeter increases rapidly below a 3 sq. in. flow area, and increasing more gradually above 3 sq. in. A flow of 3 sq. in. corresponds to a mean flow depth of 0.04 in.

The area/wetted perimeter curves for Bed T1 are given in Figure 15. The 3, 5, and 7 profiles give almost

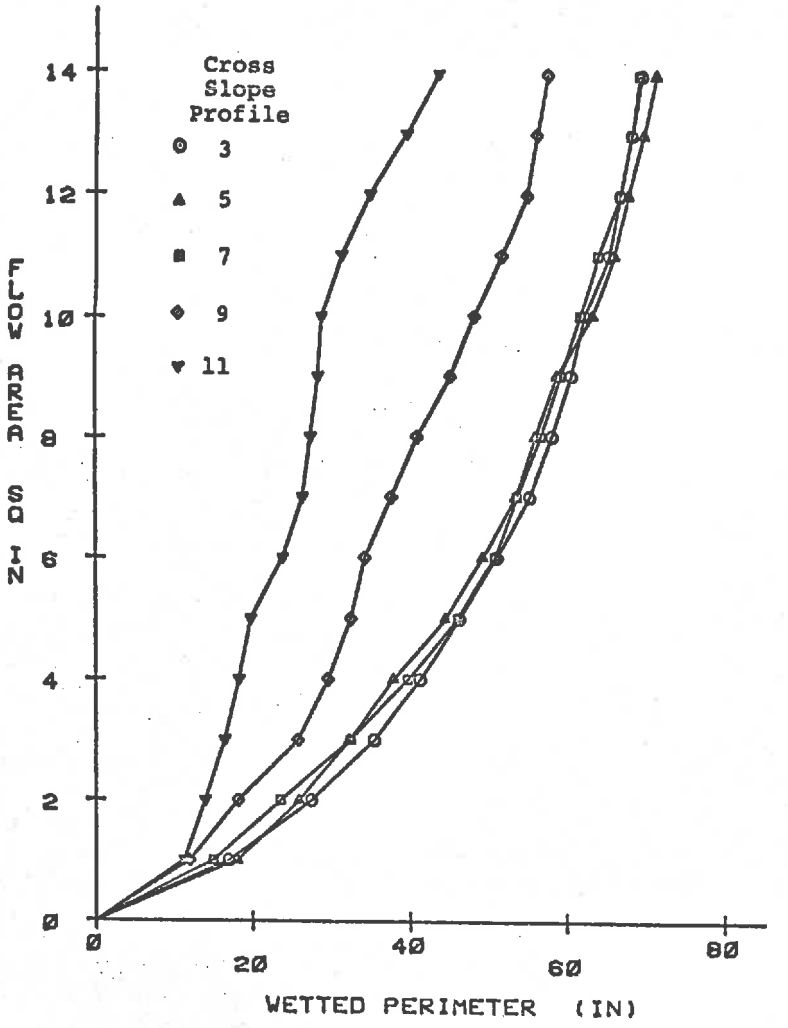

Figure 15. Area/wetted perimeter curves for Bed T1.

identical curves for Bed T1, while profiles 9 and 11 showed significant deviations. The shift of curves 9 and 11 towards the area axis shows the effect of the establishment of the flow pattern with increasing distance below the center of the bed. The formation of well defined channels has the effect of increasing the gradient of the curve for profile 11 in the 7 to 11 sq. in. area range.

Mean area/wetted perimeter curves for Beds B4 and T1 were calculated from the five curves obtained for each bed. These mean curves, together with analogous curves for the other surfaces evaluated, are given in Figure 16. It can be seen that Bed T1 has a more fully developed flow pattern than Bed B4 since the T1 area/perimeter curve has a higher gradient over the range than that for B4. Average area/perimeter curves are also shown for Bed B3 (Burney (1973)), Kundu's (1971) surfaces K1, K2 and K3, and for Foster's (1975) rill surface F1, since hydraulic data already existed for these surfaces.

Since profile data for Burney's Bed B3 was available as 24 in. profiles having 0.0982 in. spacing, an area/perimeter curve based on a 24 in. profile was developed from data taken from the five positions used by Burney to take height readings across the slope. The mean area/perimeter curve for a 72 in. profile was then approximated by multiplication of the 24 in. profile values by 72.65/24. The resulting mean curve is shown in Figure 16.

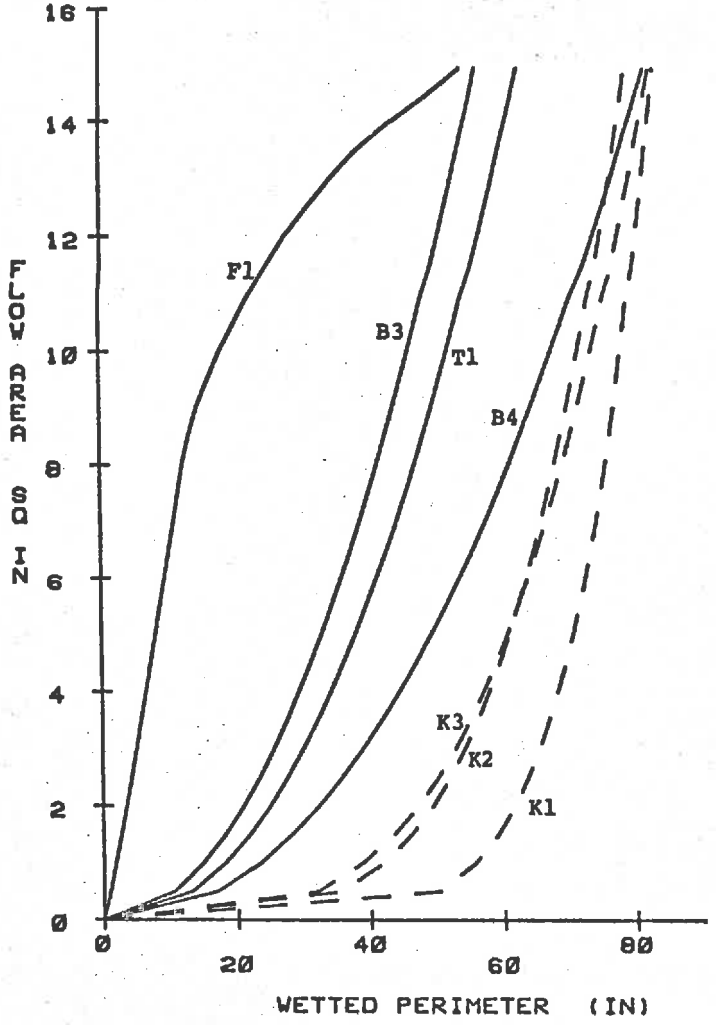

Figure 16. Mean area/wetted perimeter curves for the surfaces evaluated.

Rill cross-section measurements were taken at 2 ft. intervals for Foster's (1975) surface as described in Chapter V. Since the hydraulic tests on Bed F1 gave results for a 3 ft. wide surface, a similar scaling was applied to the mean curve obtained from the 3 ft. long area/wetted perimeter analysis for the F1 surface so that a comparable curve could be shown in Figure 16.

The profiles for Kundu's surfaces were simulated using the assumption of a Poisson distribution of particles of known densities and size ranges (Kundu (1971)). Profiles were first generated to correspond with those derived from Beds B4 and T1, having 7400 points at a 0.00982 in. spacing. Clustering of the points by groups of 10 was then used in the computer program to develop area/perimeter curves. Since the surfaces were assumed to be homogeneous, one profile was generated for each surface. These area/perimeter curves are also plotted in Figure 16.

Bed F1 gives a very steep curve, with little increase in wetted perimeter for a large change in flow area, which is characteristic of a well defined flow channel. The effect of such channels was noted on individual profiles for Beds B4 and T1. Above an area of 8 sq. in. the perimeter increases rapidly as the rill is overtopped and the top width of the flow cross-section increases.

The plane grain roughened surfaces of Kundu give curves similar in form to that of Bed B4 profile 11. The

wetted perimeter increases rapidly for a small change in area, but reaches a maximum as the flow area increases to cover all of the flow obstructions. Since K3 was formed by adding more particles to K2, which was similarly formed from K1, it could be expected that, in order of gradient for low flow area, K3 would be steeper than K2 which in turn would be steeper than K1. From Figure 16 these expectations are confirmed, but while the K1 curve remains below the other curves, the K2 and K3 curves cross at a flow area of 6 sq. in. Perimeter then increases less rapidly with flow area for K2 than for K3.

The area/wetted perimeter curves in Figure 16 can be used to describe the flow situation in general terms, as well as to calculate the hydraulic radius for a given flow cross-sectional area. Bed K1 approximates closely a wide rectangular channel for low flow areas, but the effect of the grain roughness causes the wetted perimeter to exceed the length of the profile (or assumed width of the channel) as the flow area increases. The K2 and K3 curves show similar effects to those of K1 but have more grain roughness on the surfaces. Curves B4, T1, B3 and F1 show increasing channelization of the flow pattern, with F1 representing an extreme case.

The area/wetted perimeter curves show the area and wetted perimeters are not related by a fixed proportionality for a wide range of flow areas, while assumptions of a

wide rectangular channel for overland flow do not have the ability to accurately estimate the hydraulic radius for a flow situation with a significant amount of rilling. The area/wetted perimeter curves were considered to give the form of the surface roughness in the cross-slope direction as it affected the flow.

Hydraulic Analysis

The hydraulic analysis used the hydraulic data derived from the tests run on Bed T1. The data consisted of two replications of tests having 5 levels of slope, 4 levels of rainfall and 4 levels of upstream inflow giving 150 data points. Two estimates for rainfall intensity and upstream inflow rate were available from each test analysis, namely the averaged runoff rate due to the differentiation of the weighting tank signal, and the slope of the weighing tank signal as determined by linear regression. The computer program, HYDAN, (Appendix D) calculated each estimate from 20 steady-state readings. The runoff rates and detention values were subjected to Chauvenet's criterion (Holman (1966)) which rejected spurious values. For the hydraulic analysis a mean steady-state runoff rate was determined from the average of the two estimates.

In order to broaden the range of hydraulic conditions available for correlating with roughness parameters, data from previous studies were also re-evaluated.

Kundu (1971) obtained two replications for an incomplete factorial sequence for 5 levels of slope, 6 levels of rainfall, and 6 levels of upstream inflow. The results available for analysis consisted of 70 data points for Bed K1 and 122 data points for each of Beds K2 and K3. For Burney's (1973) B3 and B4 surfaces, hydraulic test data similar to that for Bed T1 were available. Foster (1975) used 3 levels of slope, 3 levels of rainfall and 5 levels of upstream inflow, which for two replications gave a total of 90 data points.

The hydraulic analysis commenced with the investigation of the data from Bed T1. Bed T1 was formed on a 5 percent slope as described in Chapter IV. From observation of the flow it appeared that deposition of eroded material from the upper portion of the bed occurred on the region 4 to 6 feet from the top of the bed. While flow appeared normal for 4 and 5 percent slopes, retention occurred above the deposition area for tests with lower slopes. Since retention storage was satisfied between tests by rainfall application, the effect was removed from the data by referencing bed weight values to the readings taken in the first 10 seconds of the test. Detention values were obtained from the calibration equation; however, it was not possible to delay starting a test until the drip rate from the surface was reduced to zero since complete drawdown took approximately 20 minutes.

The Bed T1 hydraulic data was tested using Burney's non-linear depth prediction equation (2.20) which yielded

$$\hat{DF} = 0.00242\ QC^{0.611}\ SP^{-0.327} \qquad (6.5)$$

where ^ indicates predicted values. The equation gave a correlation coefficient of 0.997 which was similar to those obtained by Burney for Beds B3 and B4. However, the coefficients A and B are significantly different from the values of 0.004 and 0.5 suggested by Burney. The "goodness of fit" of the regression equation was tested using the coefficient of variation, CV (Ostle (1963)), where

$$CV = \frac{\sigma_d}{\bar{x}} = \frac{1}{\bar{x}} \left[\frac{\Sigma(\hat{x}-x)^2}{N-1} \right]^{1/2} \qquad (6.6)$$

where σ_d is the standard deviation about regression, which is related to the mean of the actual values $\bar{x}$. A coefficient of variation of 6.5% was obtained for the Bed T1 data while Beds B3 and B4 had CVs of 4.4% and 6.0% respectively. Since Burney's equation allows variation of coefficients A, B and C, high correlation coefficient values are obtained.

The coefficients A and B for Bed T1 are appreciably different from the values of 0.004 and 0.5 suggested by Burney. A non-linear regression was made holding A and B

at the above values. The optimized slope exponent C was -0.502 with a correlation coefficient of 0.972 and a CV of 16.1%, which suggested a considerable change in the ability of the equation to fit the data with A and B fixed. A scattergram showing the comparison of equation (6.5) with the suggested A = 0.004, B = 0.5 equation is given in Figure 17 to indicate the predictive capabilities of each equation.

Testing of Prediction Equations

The present investigation was directed to determining flow equations which incorporate physically measureable surface roughness parameters to predict discharge from flow depth. It is anticipated that such equations will have application in the area of hydrologic simulation, e.g. the distributed parameter watershed model discussed earlier. The separation of a watershed into elements within which conditions are assumed constant allows the flow equation to contain constant parameters. The laboratory flow surface used in this study represents a full scale model of such a watershed element; hence, the desire to describe it with average roughness parameters even though the surface profiles or roughness measures change with location within the element.

To test various possible prediction equations data files were set up containing hydraulic data including slope, discharge, detention, rainfall intensity and

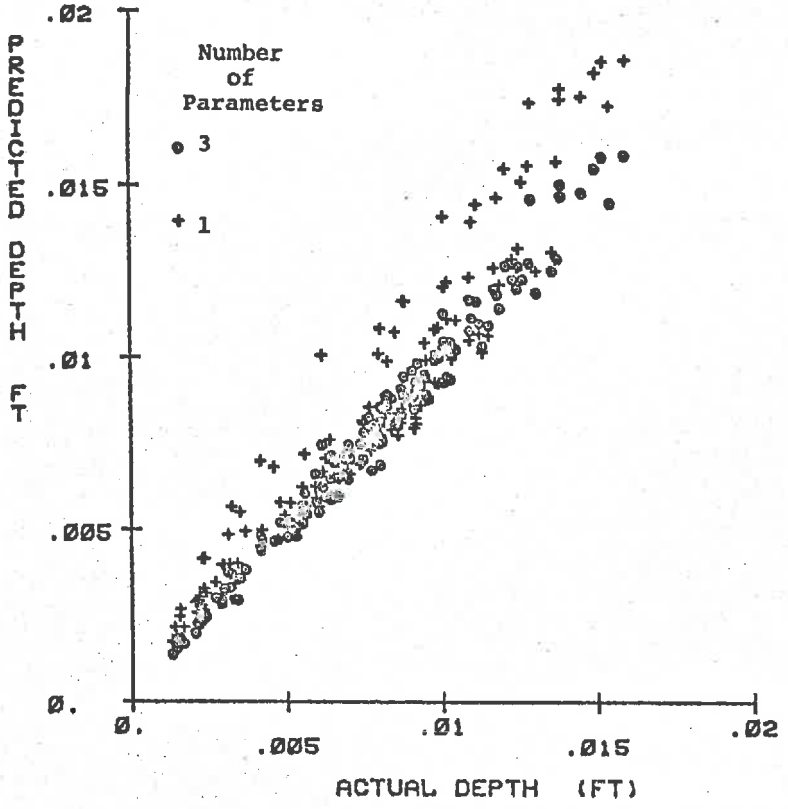

Figure 17. Comparative scattergram for Bed T1 depth prediction equations.

hydraulic radius (determined from the area/wetted perimeter curves). These data from Beds K1, K2, K3, B3, B4, T1 and F1 were evaluated to determine how well they could be characterized by the following equations:

(i) Manning's equation (2.7)

(ii) Chezy equation (2.5)

(iii) Burney discharge equation (3.22)

(iv) Prandtl-von Karman equation (3.19)

Several variations of each equation were tested with each of the seven data sets. Regression analysis was used to optimize the coefficients for each equation in order to compare flow prediction equations for each surface. Since the Prandtl-von Karman equation was developed for turbulent conditions some data was eliminated for that analysis. The transition Reynolds number range for laminar/turbulent overland flow conditions is usually 500 to 2000 (Chow (1959)) using mean depth as the length parameter. Preliminary analysis using the Prandtl-von Karman equation indicated the equation gave acceptable results for Reynolds numbers as low as 200, probably due to induced turbulence caused by rainfall. The data values provided a convenient break-point at a Reynolds number of 180, which was used as the lower limit for application of the Prandtl-von Karman equation.

The results of the regression analyses for the various equations with their options are given in Table 10,

Table 10: Review of prediction equations.

Equation	Optimized Parameter	Correlation Coefficient (r^2)	Coefficient of Variation (%)
Manning (R)	n	0.983	14.0
Manning ($\bar{y}$)	n	0.981	14.8
Chezy (R)	C	0.981	15.5
Burney (discharge)*	X,Y,Z	0.996	7.4
Burney (discharge)*	X,Z	0.994	8.8
Burney (discharge)*	Z	0.873	29.4
Prandtl-von Karman			
$\kappa = 0.38$	χ	0.981	12.6
$\chi = \sigma$	κ	0.921	21.3
$\kappa = 0.38$, $\chi = \sigma$	-	0.683	20.9

R signifies hydraulic radius used in equation

$\bar{y}$ signifies mean depth used in equation

*$\bar{y}$ used in Burney (discharge) equation.

the mean r^2 and mean CV values for the 7 surfaces being also included. In order to more clearly assess the applicability of some of the equations tested which gave r^2 values greater than 0.98 the individual regression results are given in Tables 11 to 14. Equations having more than one optimized parameter (Burney's equations and the Prandtl-von Karman equation) have higher probabilities for attaining high r^2 and low CV values than single parameter equations. However, multiple parameters increase the complexity of transforming optimized equations into prediction equations applicable to field situations for which hydraulic test data is unavailable. The equations for which hydraulic radii were used included the surface geometry effects as represented by the area/wetted perimeter curves. The most marked effect of hydraulic radius compared to mean depth occurred with Bed F1: mean depth Manning's n = 0.0072 compared to hydraulic radius Manning's n = 0.023. Bed F1 consisted of a well defined rill for which the area/perimeter curve (Figure 16) has a pronounced effect. Thus, for this surface especially, the use of hydraulic radius was much superior to mean depth for characterizing the flow.

In order to relate the optimized roughness coefficients to a measure of surface roughness parallel to the flow, i.e. in the down-slope direction, an expression of the standard deviation of height readings about a mean regression

Table 11: Optimized coefficients for Manning (R) equation.

Surface	Optimized n	Correlation Coefficient (r^2)	Coefficient of Variation (%)
K1	0.0361	0.990	11.3
K2	0.0542	0.994	8.4
K3	0.0644	0.979	16.5
B3	0.0243	0.956	24.2
B4	0.0302	0.986	13.3
T1	0.0269	0.989	11.8
F1	0.0235	0.989	12.7
	Mean	0.983	14.0

Table 12: Optimized coefficients for Chezy equation.

Surface	Optimized C	Correlation Coefficient (r^2)	Coefficient of Variation (%)
K1	20.04	0.982	15.4
K2	13.85	0.990	11.3
K3	11.62	0.972	19.0
B3	29.22	0.967	20.9
B4	23.63	0.980	15.8
T1	27.12	0.986	13.4
F1	38.77	0.989	12.5
	Mean	0.981	15.5

Table 13: Regression coefficients for Burney discharge equation.

Surface	Optimized Coefficients X	Y	Z	Correlation Coefficient (r^2)	Coefficient of Variation (%)
K1	92.955	1.953	0.465	0.998	4.5
K2	19.569	1.684	0.465	0.998	4.9
K3	71.968	2.094	0.478	0.996	7.2
B3	60.054	1.812	0.939	0.996	7.4
B4	57.323	1.774	0.520	0.993	10.0
T1	30.765	1.569	0.532	0.992	10.0
F1	11.064	1.380	0.716	0.996	7.7
			Mean	0.996	7.4

Table 14: Regression coefficients for Prandtl-von Karman equation.

Surface	Optimized $\chi(\times 10^{-3})$	Correlation Coefficient (r^2)	Coefficient of Variation (%)
K1	3.549	0.997	5.6
K2	6.650	0.985	12.7
K3	7.646	0.996	6.7
B3	1.570	0.916	30.6
B4	2.530	0.993	9.2
T1	2.277	0.992	9.4
F1	3.916	0.987	14.0
	Mean	0.981	12.6

line was selected. The use of standard deviation as the roughness measure was prompted by the works of Nordin and Algert (1966), Ashida and Tanaka (1967) and Squarer (1970) and the results of this study as discussed earlier in this chapter. Kruse et al (1965) suggested determining standard deviation from 6 to 10, 12 in. sections measured at 0.6 in. intervals. Data was available for profiles 24 in. long in the down-slope direction for all the surfaces considered and hence the standard deviations of 240 points at 0.0982 in. spacing about a mean regression line were calculated for each surface. The values obtained are given in Table 15.

The relationships between single optimized parameter values and standard deviation for the Manning, Chezy and Prandtl-von Karman equations are shown in Figures 18 to 20 respectively. In all these cases linear trends between roughness coefficients and standard deviation are noticeable for the plane grain-roughened surfaces. The prediction equations indicated by linear regression are:

Manning's equation

$$n = 0.0282 + 3.191\,\sigma \qquad (6.7)$$

Chezy equation

$$C = 22.34 - 977.2\,\sigma \qquad (6.8)$$

Prandtl-von Karman equation

$$X = 0.0024 + 0.479\,\sigma \qquad (6.9)$$

For the remaining "natural" surfaces no discernable trend could be detected for the Prandtl-von Karman equation,

Table 15: Summary of standard deviations.

Surface	Standard deviation of 23.56 in. profile at 0.098 in. spacing ($\times 10^{-3}$ ft.)
K1	2.342
K2	8.713
K3	10.944
B3	8.175
B4	6.973
T1	8.487
F1	10.885

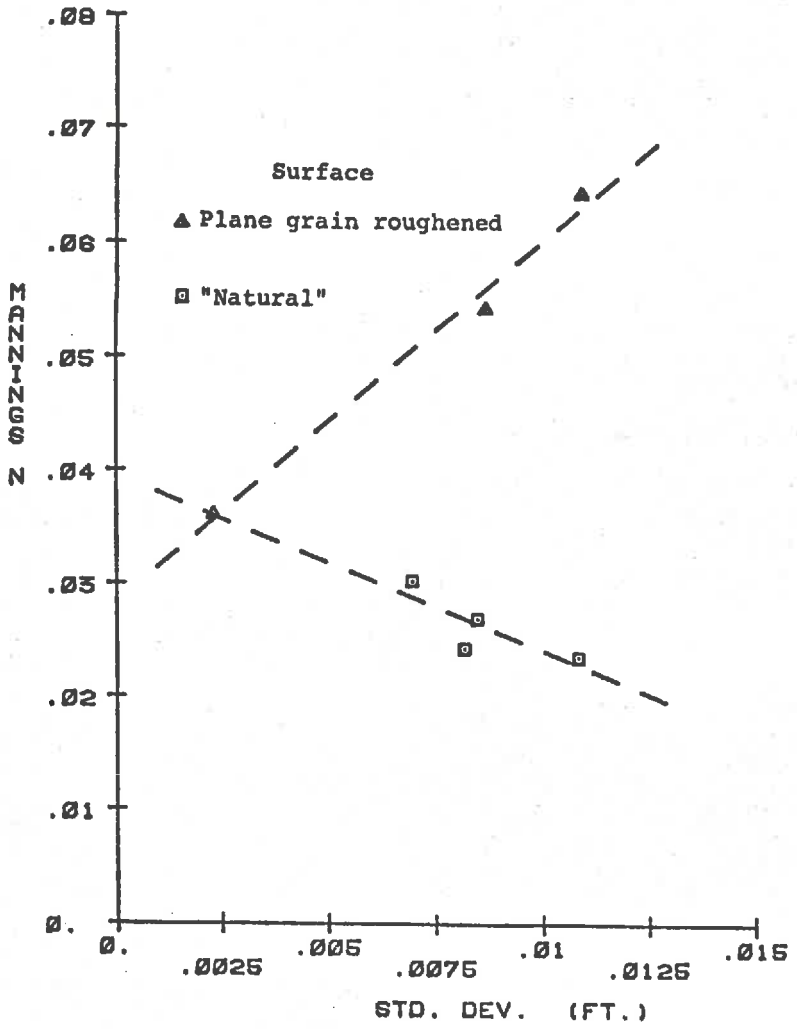

Figure 18. Plot of Manning's n against standard deviation.

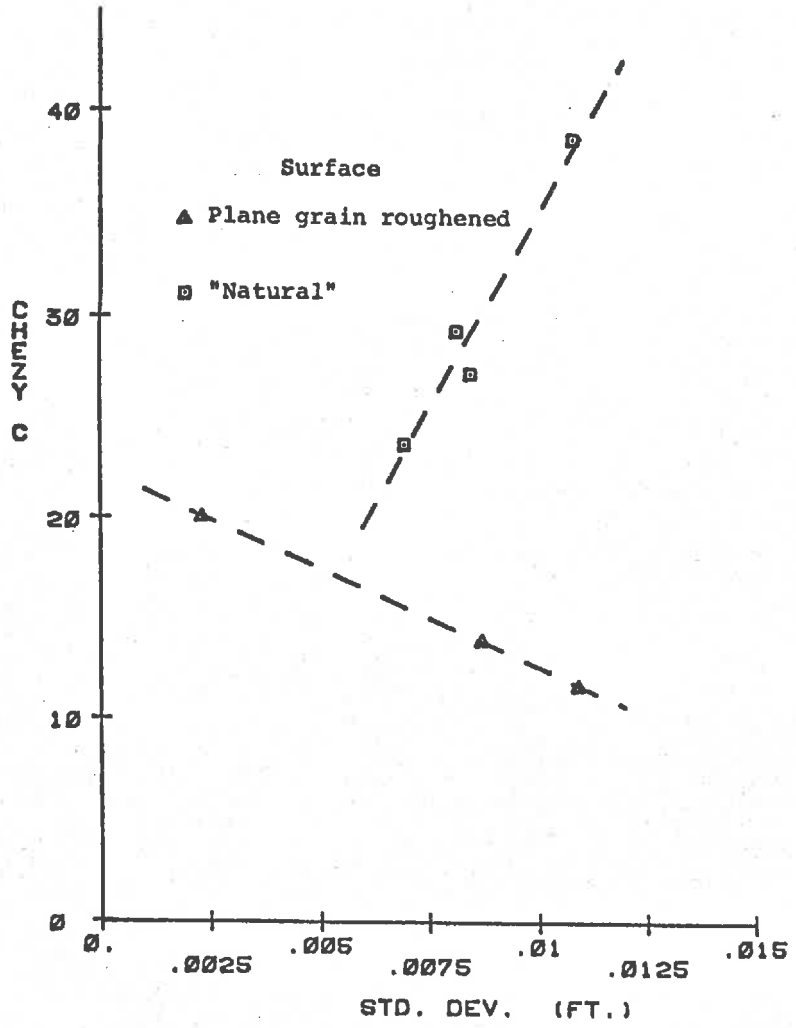

Figure 19. Plot of Chezy C against standard deviation.

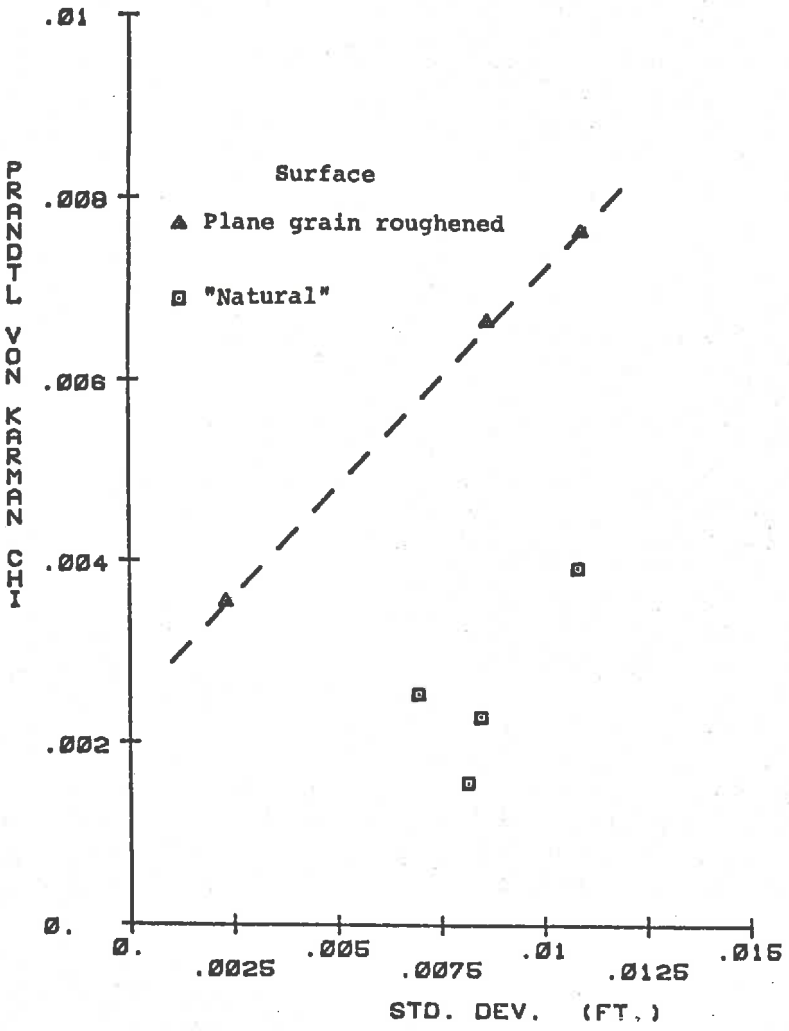

Figure 20. Plot of Prandtl-von Karman χ against standard deviation.

while the Chezy equation gave the following:

$$C = -3.62 + 3859.2\,\sigma \qquad (6.10)$$

Manning's equation gave

$$n = 0.0396 - 1.553\,\sigma \qquad (6.11)$$

for the natural surfaces, which intersects the plane grain roughened surfaces at the point from Bed K1. Despite the few surfaces represented and the limited range of points obtained, and also the physical limitations on Manning's n for natural surfaces, the tendency of rough natural surfaces to tend towards plane grain roughened surfaces for decreasing σ is an encouraging result. Using the equations determined relating Manning's n to σ, predicted values of discharge were calculated and compared to the actual discharge using a scattergram form shown in Figure 21. Using equations (6.7) and (6.11) to obtain Manning's n values for the hydraulic data from all seven surfaces an r^2 of 0.981 and a CV of 16.1% were obtained.

Comparison of Laboratory and "Field" Roughness Coefficients

A distributed parameter watershed model was developed by Huggins (1966). The watershed model used Manning's equation and "optimized" n-values to simulate measured runoff hydrographs for a variety of field situations. Comparisons of laboratory n-values with those required to simulate field measurements are desirable in order to assess the applicability of the laboratory results for predicting field situations.

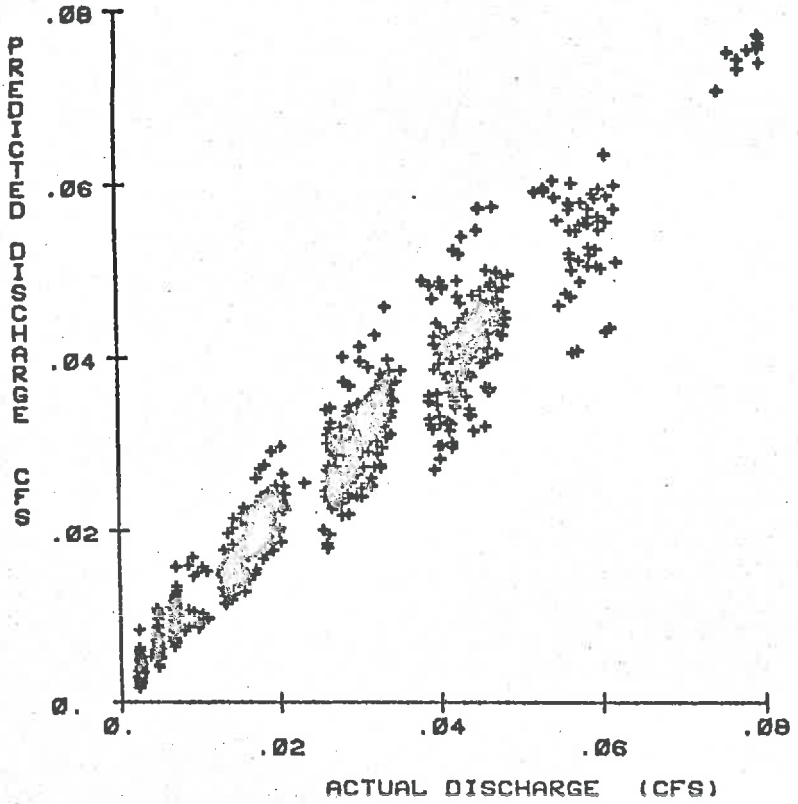

Figure 21. Scattergram of actual discharge against predicted discharge using Manning's n.

In addition, areas requiring further investigation can be determined from such comparisons.

The data for the simulation study were obtained from studies of experimental watersheds located on the Purdue University Throckmorton Farm. Instrumented watersheds gave rainfall and runoff data for a variety of agricultural conditions. Watersheds 4 and 11 had areas of 2.01 and 2.04 acres respectively, and were planted in a corn-soybeans-wheat-meadow rotation. Watershed 4, with a mean slope of 5.1 percent, was farmed using conventional techniques. Watershed 11 was farmed using conservation practices and had a mean slope of 2.2 percent. Both watersheds had silt loam or silty clay loam soils. Optimum roughness parameters were determined, and the results are summarized in Table 16. The roughness coefficient used was Manning's n which was allowed to vary between 0.020 - 0.600 for the purposes of optimization. The purpose of this section is to compare those values obtained for n with those determined in the laboratory and discussed in the previous section.

Considering the laboratory surface Manning's n, as related to standard deviation σ and shown in Figure 18, the values are approximately constant or, if Bed K1 is allowed as a valid point, a linear trend with σ can be discerned. However, the range is small, 0.020-0.0375, since a minimum value for natural surfaces, even if

Table 16: Assumed antecedent watershed conditions for simulation studies (Huggins (1966)).

Date	Infiltration* Rates	Antecedent Soil Moisture (% Saturation)	Infiltration Depth	Crop	% Cover	Potential Interception (in.)	Ave. Retention Depth (in.)	Manning's n
				Watershed #4				
7/19/42	H	55.	11.0	Timothy	90.	.020	.00	.100
6/16/45	L	85.	3.0	Wheat	80.	.010	.00	.055
6/30/45	L	45.	3.5	Wheat	80.	.020	.02	.120
8/14/45	H	60.	8.5	Clover	60.	.010	.02	.230
9/22/45	H	50.	7.0	Clover	85.	.020	.02	.200
6/07/47	L	90.	16.0	New Corn	00.	.000	.14	.070
4/07/48	L	80.	3.0	Corn Stubble	00.	.000	.00	.085
4/07/48	L	90.	3.0	Corn Stubble	00.	.000	.00	.050
7/27/48	L	65.	8.0	Beans	25.	.000	.06	.045
7/19/50	L	70.	7.0	Clover	80.	.020	.01	.140
9/21/50	H	80.	4.0	Clover	80.	.020	.01	.140
6/17/51	L	60.	3.0	Fallow	00.	.000	.00	.020
6/10/53	L	70.	3.0	Wheat	30.	.000	.03	.040
				Watershed #11				
7/19/42	H	55.	9.0	Timothy	80.	.015	.03	.150
6/16/45	L	85.	12.0	Wheat	90.	.015	.06	.250
6/30/45	L	45.	16.0	Wheat	90.	.020	.14	.600
8/14/45	H	60.	12.0	Clover	60.	.010	.12	.600
9/22/45	H	50.	16.0	Clover	95.	.025	.14	.600
6/07/47	L	90.	16.0	New Corn	00.	.000	.12	.300
4/07/48	L	80.	3.0	Corn Stubble	00.	.000	.10	.300
4/07/48	L	90.	3.0	Corn Stubble	00.	.000	.09	.120

*The letter "H" corresponds to the infiltration capacity rates given in Table 5 (Huggins (1966)) and the letter "L" to rates one-half as large, as calculated from

$$\text{Infiltration Rate } f = f_c + A\left[\frac{S-F}{T_p}\right]^P$$

where f_c = steady state infiltration rate, S = storage potential of soil above impeding stratum, F = total volume of water infiltrated, and T_p = total porosity of soil above impeding stratum.

very smooth, is 0.015 (Chow (1959)).

Before further comparing the laboratory and field data, the differences between conditions used to derive the two sets of data should be noted:

(i) The laboratory studies derived the Manning's n-values from regression analysis of the hydraulic test results, while the computer model was used to optimize n for the field conditions.

(ii) The model uses mean slope for each elemental area of the land surface for hydraulic calculations without regard to the actual flow path within each element. The measured slope in the laboratory corresponds much more closely to the slope of the flow path. Slope length also has an effect on the time of overland flow.

The method used in the simulation model to route the overland flow may have some effect on the magnitude of the roughness coefficient determined. The flow is constrained to pass from the original element to either the element below or laterally to the neighboring element depending on the direction of maximum slope for the element. No diagonal movement is permitted by the model.

Watershed 11 is treated with conservation cultivation practices, which have the effect

of increasing surface residue and surface roughness due to cultivation. Infiltration would be increased due to the increased surface roughness effect on retention volume and improved soil structure. In addition, contour cultivation has the effect of reducing the slope and increasing the flow path length for runoff. All of the conditions produced by conservation cultivation have the effect of increasing the surface roughness coefficient in the simulation model. Table 16 shows, for the storm events considered for both watersheds, watershed 11 always gave a higher Manning's n than watershed 4.

(iii) The model lumps any effect of vegetation and surface residue into the roughness coefficient, while the laboratory studies apply to bare soil surfaces.

Vegetation effects were not considered in the laboratory studies. The major effect of vegetation in the watershed model was considered to influence infiltration. Cover provided by plants prevents surface crusts from forming due to raindrop impact on the soil surface. For watershed 4 cover values of 30 percent or less yielded lower roughness coefficients compared with those for higher cover values.

For watershed 11 a similar, but less pronounced, effect is noted. Obstruction to overland flow by vegetation was considered to have a small effect, although it was noted that higher roughness coefficients were obtained for clover crops, which have high stem densities.

(iv) The laboratory studies used measured area/wetted perimeter values to obtain the roughness coefficients, while the simulation study assumed that hydraulic radius equalled mean depth within each element.

Several possible reasons may be hypothesized to explain the large differences between the n-values obtained from the laboratory studies and those required by the simulation model in order for it to yield hydrographs similar to those recorded in the field:

a) The laboratory results do not apply in the field. Considering the laboratory results obtained, the range of Manning's n values correspond to the range recommended by Chow (1959) for non-vegetated surfaces. Hence it was considered that the laboratory results support the validity of the design values for the range of roughness conditions studied.

b) The roughness coefficient in the simulation is an optimized parameter and consequently, becomes a "catch-all" term to make adjustments in the model fitting.

It is difficult or impossible to assess the effect of a particular simulation scheme on an optimized parameter. Since Manning's n has the effect of variable damping on the response hydrograph, the fitting of the calculated to the observed hydrograph by trial and error will introduce spurious effects of unknown magnitude into the coefficient.

c) All or part of the (i) to (iv) reasons given earlier account for the differences between laboratory and simulation study results.

It is difficult to reconcile the difference of more than an order of magnitude between the range of laboratory n-values and those required to provide reasonable agreement between observed and simulated field runoff hydrographs. The quantitative effect of the factors discussed above are generally impossible to assess with the available data. However, point (ii) above is somewhat of an exception in that estimates may be made of "probable" slope ranges in order to evaluate their influence on an n-value for the simulation model.

The watershed model uses elevations of each corner of an element to determine the element slope magnitude and direction. Overland flow is proportioned according to the direction of maximum slope for flow transmission to neighboring elements. The model assumes the flow follows the path of steepest slope, which is acceptable for plane

surfaces, but does not consider the effects of cultivation practices and conservation measures on the flow path. Consideration of the topography of watershed 11 indicates that a contour cultivation system could increase the flow path length by 50% over that expected from a "path of steepest slope" approach. In addition, the slope values change from the mean slope (2.2 percent for watershed 11) due to:

(i) Flow along the contour caused by conservation cultivation practice (at approximately 0.5% slope).

(ii) Flow along established flow paths along which the cumulative effects of erosion have occurred. Soil has been removed from the upper reaches of the channel to reduce the channel slope (for example 1.5% slope for watershed 11).

The above conditions and their effect on Manning's n are considered below.

Assume a uniform flow depth $\bar{y}$ over a watershed at a uniform 2% slope. Using Manning's equation for an assumed n-value of 0.2 and also assuming $R = \bar{y}$, the discharge/ft. width for the "path of steepest flow" approach is:

$$q = \frac{1.49}{n} \bar{y}^{5/3} S^{1/2}$$

and $$f_1(q,\bar{y}) = \frac{S_1^{1/2}}{n_1} = \frac{(0.02)^{1/2}}{0.2}$$

where f_1 indicates a function. To determine the appropriate n value for constant discharge for a contour slope of 0.5%

$$f_1(q,\bar{y}) = \frac{S_1^{1/2}}{n_1} = \frac{S_2^{1/2}}{n_2}$$

After substitution $n_2 = 0.10$.

Similarly for an eroded channel having a slope of 1.5%

$$\frac{S_1^{1/2}}{n_1} = \frac{S_3^{1/2}}{n_3}$$

and $n_3 = 0.173$. Weighting the Manning's n-values in terms of the components, and assuming 33% contour flow and 67% channel flow, the composite Manning's n is

$$n^* = (0.67 \times 0.173) + (0.33 \times 0.1)$$

$$= 0.149$$

Following the calculations a reduction of 25% in an assumed initial Manning's n is achieved. The primary effect is due to the reduced slope components along the flow path. More precise effects would be obtained from inclusion of the above considerations into the watershed model, which would also indicate the effect due to the increased flow path length. It can be seen that micro-topography significantly affects the computed resistance parameter.

CHAPTER VII

CONCLUSION

Summary

Following preliminary analysis of Bed B4 used by Burney (1975), a profile meter was constructed to measure linear height profiles at a spacing of 0.00982 in. over a length of 72.65 in. Profiles were measured across and down the slope on a 2 ft. grid over the surface avoiding end and edge effects. Bed T1 was constructed using a similar resin application process to that used for Bed B4. Bed T1 had a distinct rilling pattern which became more pronounced with distance down the surface. Surface profile readings were recorded as for Bed B4. Hydraulic tests were performed on the surface T1 using two replications of each of 5 slope levels, 4 rainfall levels and 4 upstream inflow levels randomized separately within each replication.

The surface profiles were analyzed to identify the variations within and between surfaces B4 and T1. Spectral analysis was used to investigate the contributions to the total variance across the frequency range. Results obtained showed that linear relationships were obtained for log-log plots of spectral estimate against frequency.

The joint probability distribution of amplitude and frequency was approximated by the amplitude/separation distribution. The two-dimensional array of amplitude and separation occurrences yielded little useful information, although when collapsed into separate amplitude and separation distributions, the amplitude distribution gave qualitative information on the nature of the surfaces. The separation distributions were similar for both surfaces.

The cross-slope profiles were used to develop area/wetted perimeter curves for the surfaces from which flow pattern development could be discerned. Mean area/perimeter curves were obtained for B4 and T1, and also for Burney's (1973) B3 surface, Kundu's (1971) K1, K2 and K3 plane grain roughened surfaces and Foster's (1975) F1 fiber-glas rill replica surface. Hydraulic data were available for all the additional surfaces. Down-slope roughness was characterized by the standard deviation, σ, of detrended heights of points 0.0982 in. apart over a length of 24 in.

Various hydraulic equations were tested using the hydraulic data, the cross-slope roughness being incorporated using area/wetted perimeter relationships. Hydraulic roughness coefficients were optimized for each flow surface using the correlation coefficient (r^2) and coefficient of variation (CV) values. For single parameter equations the hydraulic roughness coefficient was related to the measure of down-slope roughness σ. Separate linear

relationships were obtained for the plane grain roughened surfaces (K1, K2 and K3) and for the "natural" surfaces (B3, B4, T1 and F1).

For the Manning equation the estimated n-values for the two surface categories converged, indicating that the "natural" surfaces tended towards plane grain roughened surfaces for low down-slope roughness values. An attempt was made to relate the laboratory results to field simulation studies performed by Huggins (1966).

Conclusions

From the study of interrelation of surface roughness and hydraulic effects on rough psuedo-natural surfaces in the laboratory the following conclusions were drawn:

(i) Spectra from the surfaces investigated could be adequately described by the equation

$$S(f) = A f^{B}$$

In addition, no characteristic frequency components could be identified for the surface roughness conditions studied in the frequency range 0.027 - 51 cpi.

(ii) The amplitude/frequency distribution was approximated by the amplitude/separation distribution, but little useful information was obtained. After collapsing the joint distributions, the amplitude distribution yielded some quantitative information on surface geometry.

(iii) It was concluded that the area/wetted perimeter relationship gave information on flow pattern development and could be used to characterize cross-slope roughness.

(iv) Using non-linear regression analysis of hydraulic data which included area/wetted perimeter values, the optimized roughness coefficients could be related to down-slope roughness in the form of the standard deviation of heights about mean regression.

(v) Laboratory studies yielded roughness coefficient values which were supported by values in current design use (Chow (1959)).

(vi) Attempts to relate laboratory and field results indicated that further field investigation is necessary.

Recommendations

From the present study the laboratory results yielded roughness coefficients for bare soil surfaces for the range of surface roughness conditions investigated. It is suggested that further information is required from field investigations in order that surface roughness effects on overland flow can be more precisely defined for actual watershed conditions. Specifically the following recommendations are made:

(i) Field information on surface microtopography is necessary to determine the overland flow path characteristics such as direction, slope and path length. The effects introduced by tillage and conservation practices should be included.

(ii) From the flow path characteristics, area/wetted perimeter relationships should be developed to characterize surface roughness perpendicular to the flow direction.

(iii) Surface roughness measurements along the flow path are necessary to further define the flow resistance in the direction of the flow.

(iv) Information on the characteristics of vegetation and crop residues on the soil surface is required to determine the effects of living and dead plant matter on resistance to overland flow. In addition, the effects of vegetal cover on changes in surface roughness due to raindrop impact should be quantified.

BIBLIOGRAPHY

BIBLIOGRAPHY

Akaike, H., 1960. Effect of timing error on the power spectrum of sampled data. Annals of Statistical Math. 11(3):145-165.

Alam, A. M. Z. and J. F. Kennedy, 1969. Friction factors for flow in sand-bed channels. J. Hyd. Div. A.S.C.E. 95(HY6):1973-1992.

Annambhotla, V. S. S., 1969. Statistical properties of bed forms in alluvial channels [illegible] flow resistance. Ph.D. Thesis, Un[illegible]

Ashida, K. and Y. Tanaka, 1967. [illegible] sand waves. Proc. 12th Co[illegible] Hydraulic Res. 2:103-110.

Barron, N. A., 1971. Soil sur[illegible] calculated by geometric m[illegible] University of Illinois.

Becker, L. and W. W-G. Yeh, 1972[illegible] parameters in unsteady open c[illegible]r Resources Res. 8:956-965.

Biery, D. F. and J. W. Delleur, 1961. Discussion of Roughness spacing in rigid open channels by W. W. Sayre and M. L. Albertson. J. Hyd. Div. A.S.C.E. 87(HY5):231-238.

Brakensiek, D. L., 1967. Finite differencing methods. Water Resources Res. 3:847-860.

Brakensiek, D. L. and C. A. Onstad, 1968. The synthesis of distributed inputs for hydrograph prediction. Water Resources Res. 4:79-93.

Brickman, A. D., J. C. Wambold, and J. R. Zimmerman, 1971. An amplitude-frequency description of road roughness. Highway Research Board Special Report 116:53-67.

Burney, J. R., 1973. Hydraulics of shallow flows over stable eroded sand surfaces defined by area spectra. Ph.D. Thesis, Purdue University.

BIBLIOGRAPHY

Akaike, H., 1960. Effect of timing error on the power spectrum of sampled data. Annals of Statistical Math. 11(3):145-165.

Alam, A. M. Z. and J. F. Kennedy, 1969. Friction factors for flow in sand-bed channels. J. Hyd. Div. A.S.C.E. 95(HY6):1973-1992.

Annambhotla, V. S. S., 1969. Statistical properties of bed forms in alluvial channels in relation to flow resistance. Ph.D. Thesis, University of Iowa.

Ashida, K. and Y. Tanaka, 1967. A statistical study of sand waves. Proc. 12th Congress. Inter. Assoc. Hydraulic Res. 2:103-110.

Barron, N. A., 1971. Soil surface depression storage calculated by geometric models. M.S. Thesis, University of Illinois.

Becker, L. and W. W-G. Yeh, 1972. Identification of parameters in unsteady open channel flows. Water Resources Res. 8:956-965.

Biery, D. F. and J. W. Delleur, 1961. Discussion of Roughness spacing in rigid open channels by W. W. Sayre and M. L. Albertson. J. Hyd. Div. A.S.C.E. 87(HY5):231-238.

Brakensiek, D. L., 1967. Finite differencing methods. Water Resources Res. 3:847-860.

Brakensiek, D. L. and C. A. Onstad, 1968. The synthesis of distributed inputs for hydrograph prediction. Water Resources Res. 4:79-93.

Brickman, A. D., J. C. Wambold, and J. R. Zimmerman, 1971. An amplitude-frequency description of road roughness. Highway Research Board Special Report 116:53-67.

Burney, J. R., 1973. Hydraulics of shallow flows over stable eroded sand surfaces defined by area spectra. Ph.D. Thesis, Purdue University.

Burwell, R. E., R. R. Allamaras, and M. Amemiya, 1963. A field measurement of total porosity and surface microrelief of soils. Soil Sci. Soc. Am. Proc. 27:697-700.

Chang, F. F. M., 1970. Ripple concentration and friction factor. J. Hyd. Div. A.S.C.E. 96(HY2):417-430.

Chen, C-L., 1962. An analysis of overland flow. Ph.D. Thesis, Michigan State University.

Chen, C-L. and V. E. Hansen, 1966. Theory and characteristics of overland flow. Trans. A.S.A.E. 9:20-26.

Chow, V. T., 1959. Open Channel Hydraulics. McGraw-Hill Book Co., New York. 680 pp.

Currence, H. D. and W. G. Lovely, 1970. The analysis of soil surface roughness. Trans. A.S.A.E. 13:710-714.

Currence, H. D. and W. G. Lovely, 1971. An automatic soil surface profilometer. Trans. A.S.A.E. 14:69-71.

Curtis, W. R. and W. D. Cole, 1972. Micro-topographic profile gage. Agricultural Engineering 53:17.

Das, K. C., 1970. Laboratory modelling and overland flow analysis. Ph.D. Thesis, Purdue University.

Eagleson, P. S., 1970. Dynamic Hydrology. McGraw-Hill Book Co., New York. 462 pp.

Engelund, F., 1966. Hydraulic resistance of alluvial streams. J. Hyd. Div. A.S.C.E. 92(HY2):315-326.

Foster, G. R., 1968. Analysis of overland flow on short erosion plots. M.S. Thesis, Purdue University.

Foster, G. R., 1971. The overland flow process under natural conditions. Proc. Third International Seminar for Hydrology Professors:173-185.

Foster, G. R., 1975. Hydraulics of a flow in a rill Ph.D. Thesis, Purdue University.

Foster, G. R., L. F. Huggins and L. D. Meyer, 1968. Simulation of overland flow on short field plots. Water Resources Res. 4:1179-1187.

Foster, G. R. and L. D. Meyer, 1972. Efficient processing of microrelief photographs. Paper No. 72-593, A.S.A.E. Winter Meeting, Chicago. 8 pp.

Fread, D. L., 1975. Computation of stage-discharge relationships affected by unsteady flow. Water Resources Bulletin 11:213-228.

Grace, R. A. and P. S. Eagleson, 1966. The modeling of overland flow. Water Resources Res. 2:393-403.

Griffin, W. C., 1971. Introduction to Operations Engineering. Irwin, Homewood, Illinois. 632 pp.

Heerman, D. F., R. J. Wenstrom, and N. A. Evans, 1969. Prediction of flow resistance in furrows from soil roughness. Trans. A.S.A.E. 12:482-485, 489.

Henderson, F. M. and R. A. Wooding, 1964. Overland flow and groundwater flow from a steady rainfall of finite duration. J. Geophys. Res. 69:1531-1540.

Herbich, J. B. and S. Schulitz, 1964. Large scale roughness in open-channel flow. J. Hyd. Div. A.S.C.E. 90(HY6):203-230.

Hill, I. K., 1969. Runoff hydrograph as a function of rainfall excess. Water Resources Res. 5:95-102.

Holman, J. P., 1966. Experimental Methods for Engineers, 2nd Ed., McGraw-Hill Book Co., New York. 423 pp.

Horton, R. E., 1938. The interpretation and application of runoff plat experiments with reference to soil erosion problems. Soil Sci. Soc. Am. Proc. 3:340-349.

Huggins, L. F., 1966. The mathematical simulation of the hydrology of small watersheds. Ph.D. Thesis, Purdue University.

Huggins, L. F. and E. J. Monke, 1966. The mathematical simulation of the hydrology of small watersheds. Purdue University Water Resources Research Center Technical Report No. 1.

Huggins, L. F. and E. J. Monke, 1968. A mathematical model for simulating the hydrologic response of a watershed. Water Resources Res. 4:529-539.

Ishihara, Y., 1964. Hydraulic mechanism of runoff. Proceedings, 1st Australasian Conf. on Hydraulics and Fluid Mechanics, 1962:173-190.

Iwagaki, Y., 1954. On the laws of resistance to turbulent flow in open rough channels. Proc. 4th Japan National Congress for Applied Mechanics:229-233.

Iwagaki, Y., 1955. Fundamental studies on the runoff analysis by characteristics. Disaster Prevention Research Institute, Kyoto University, Bulletin No. 10. 25 pp.

Izzard, C. F., 1942. Runoff from flight strips. Proc. Highway Research Board 22:94-99.

Izzard, C. F., 1946. Hydraulics of runoff from developed surfaces. Proc. Highway Research Board 26:129-146.

Izzard, C. F. and M. T. Augustine, 1943. Preliminary report on analysis of runoff resulting from simulated rainfall on a paved plot. Trans. Am. Geophys. Un. 24:500-511.

Jenkins, G. M. and D. G. Watts, 1968. Spectral Analysis and its Applications. Holden-Day, San Francisco. 525 pp.

Judah, O. M., V. O. Shanholtz, and D. N. Contractor, 1975. Finite element simulation of flood hydrographs. Trans. A.S.A.E. 18:518-522.

Keulegan, G. H., 1938. Laws of turbulent flow in open channels. U.S. National Bureau of Standards. J. of Research 21:707-741.

Keulegan, G. H., 1944. Spatially variable discharge over a sloping plane. Trans. Am. Geophys. Un. 25:956-959.

Kisisel, I. T., A. R. Rao, J. W. Delleur and L. D. Meyer, 1971. Turbulence characteristics of overland flow - the effects of rainfall and boundary roughness. Purdue University Water Resources and Hydromechanics Laboratory Technical Report No. 28.

Kline, S. J. and F. A. McClintock, 1953. Describing uncertainties in single-sampled experiments. Mech. Eng. 75(1):3-8.

Kouwen, N. and T. E. Unny, 1973. Flexible roughness in open channels. J. Hyd. Div. A.S.C.E. 99(HY5):713-728.

Kozin, F., L. J. Cote, and J. L. Bogdanoff, 1963. Statistical studies of stable ground roughness. Tech. Report No. 8391(LL 95). Land Locomotion Lab., U.S. Army Tank Automotive Center, Warren, Michigan.

Kozin, F., L. J. Cote, and J. L. Bogdanoff, 1968. Supplement to the atlas report of the off-road ground roughness. Tech. Report No. 10316(LL130). Land Locomotion Lab., U.S. Army Tank Automotive Center, Warren, Michigan.

Kruse, E. G., C. W. Huntley and A. R. Robinson, 1965. Flow resistance in simulated irrigation boarders and furrows. U.S.D.A.-A.R.S. Conservation Res. Report No. 3. 56 pp.

Kuipers, H., 1957. A reliefmeter for soil cultivation studies. Netherlands J. of Agr. Sci. 5:255-262.

Kundu, P. S., 1971. Mechanics of flow over very rough surfaces. Ph.D. Thesis, Purdue University.

Lambe, T. E. and R. V. Whitman, 1969. Soil Mechanics. John Wiley and Sons, New York. 553 pp.

Langford, K. J., 1971. Overland flow across uneven surfaces. Ph.D. Thesis, University of Melbourne, Australia.

Langford, K. J. and A. K. Turner, 1973. An experimental study of the application of kinematic-wave theory to overland flow. J. Hydrol. 18:125-145.

Liggett, J. A. and D. A. Woolhiser, 1967. Difference solutions of the shallow-water equation. J. Eng. Mech. Div. A.S.C.E. 93(EM):39-71.

Lighthill, M. J. and G. B. Whitman, 1955. On kinematic waves. I. Flood movement in long rivers. Proc. Roy. Soc. Lond. A229:281-316.

Lin, P-N., 1952. Numerical analysis of continuous unsteady flow in open channels. Trans. Am. Geophys. Un. 33:226-234.

Longuet-Higgins, M. S., 1957. The statistical analysis of a random moving surface. Phil. Trans. Roy. Soc. Lond. A249:321-387.

Lovera, F. and J. F. Kennedy, 1969. Friction-factors for flat-bed flows in sand channels. J. Hyd. Div. A.S.C.E. 95(HY4):1227-1234.

Merva, G. E., R. D. Brazee, G. O. Schwab and R. B. Curry, 1970. Theoretical considerations of watershed surface description. Trans. A.S.A.E. 13:462-465.

Mirajgaoker, A. G. and K. L. N. Charlu, 1963. Natural roughness effects in rigid open channels. J. Hyd. Div. A.S.C.E. 88(HY5):29-44.

Mitchell, J. K., 1970. Micro-relief surface depression storage. Ph.D. Thesis, University of Illinois.

Morgali, J. R., 1963. Hydraulic behavior of small drainage basins. Stanford University Civil Engineering Department Technical Report No. 30.

Morgali, J. R. and R. K. Linsley, 1965. Computer analysis of overland flow. J. Hyd. Div. A.S.C.E. 91(HY3):81-100.

Nordin, C. F. and J. H. Algert, 1966. Spectral analysis of sand waves. J. Hyd. Div. A.S.C.E. 92(HY5):95-114.

O'Loughlin, E. M. and E. G. MacDonald, 1964. Some roughness-concentration effects on boundary resistance. La Houille Blanche. Annee 19:773-782.

Overton, D. E., 1971. Mechanics of surface runoff on hillslopes. Proc. Third International Seminar for Hydrology Professors:186-210.

Ragan, R. M., 1965. Synthesis of hydrographs and water surface profiles for unsteady open channel flow. Ph.D. Thesis, Cornell University.

Ranga Raju, K. J. and R. J. Garde, 1970. Resistance to flow over two-dimensional strip roughness. J. Hyd. Div. A.S.C.E. 96(HY3):815-834.

Raudkivi, A. J., 1967. Analysis of resistance in fluvial channels. J. Hyd. Div. A.S.C.E. 93(HY5):73-84.

Roberson, J. A. and C. K. Chen, 1970. Flow in conduits with low roughness concentration. J. Hyd. Div. A.S.C.E. 96(HY4):941-957.

Robinson, A. R. and M. L. Albertson, 1952. Artificial roughness standards for open channels. Trans. Am. Geophys. Un. 33:881-888.

Sayre, W. W. and M. L. Albertson, 1961. Roughness spacing in rigid open channels. J. Hyd. Div. A.S.C.E. 87(HY3):121-150.

Schafer, F. L. and W. G. Lovely, 1967. A recording soil surface profile meter. Agricultural Engineering 48:280-282.

Schlichting, H., 1951. Boundary Layer Theory. McGraw-Hill Book Co., New York. 747 pp.

Schreiber, D. L. and D. L. Bender, 1972. Obtaining overland flow resistance by optimization. J. Hyd. Div. A.S.C.E. 98(HY3):429-446.

Shen, H. W. and R. M. Li, 1973a. Rainfall effects on sheet flow over smooth surface. J. Hyd. Div. A.S.C.E.99(HY5):771-792.

Shen, H. W. and R. M. Li, 1973b. Analysis of resistance over staggered roughness. J. Hyd. Div. A.S.C.E. 99(HY11):2169-2174.

Simons, D. B. and E. V. Richardson, 1961. Forms of bed roughness in alluvial channels. J. Hyd. Div. A.S.C.E. 87(HY3):87-105.

Singh, V. P., 1975. Derivation of surface water lag time for converging overland flow. Water Resources Bulletin 11:505-513.

Smith, K. V. H., 1968. Alluvial channel resistance related to bed form. J. Hyd. Div. A.S.C.E. 94(HY1):59-69.

Squarer, D., 1970. Friction factors and bed forms in fluvial channels. J. Hyd. Div. A.S.C.E. 96(HY4):995-1017.

Strelkoff, T., 1969. One-dimensional equations of open channel flow. J. Hyd. Div. A.S.C.E. 95(HY3):861-876.

Strelkoff, T., 1970. Numerical solutions of the Saint-Venant equations. J. Hyd. Div. A.S.C.E. 96(HY1):223-252.

Task Force Report, 1963. Friction factors in open channels. J. Hyd. Div. A.S.C.E. 89(HY2):97-143.

Task Force Report, 1964. Closure of Friction factors in open channels. J. Hyd. Div. A.S.C.E. 70(HY4):223-227.

Taylor, R. H. and N. H. Brooks, 1961. Discussion of Resistance to flow in alluvial channels by D. B. Simons and E. V. Richardson. J. Hyd. Div. A.S.C.E. 87(HY1):246-257.

Vanoni, V. A. and L-S. Hwang, 1967. Relation between bed forms and friction in streams. J. Hyd. Div. A.S.C.E. 93(HY3):121-144.

Wambold, J. C. and W. H. Park, 1974. Amplitude-frequency description. Instrumentation Technology 22(6):36-40.

Woo, D-C., 1956. Study of overland flow. Ph.D. Thesis, University of Michigan.

Woolhiser, D. A., 1967. Overland flow on a converging surface. Paper No. 67-735. A.S.A.E. Winter Meeting, Detroit. 13 pp.

Woolhiser, D. A. and S. A. Liggett, 1967. Unsteady one-dimensional flow over a plane - the rising hydrograph. Water Resources Res. 3:753-771.

Yen, B. C., 1973. Open channel flow equations revisited. J. Eng. Mech. Div. A.S.C.E. 99(EM5):979-1009.

Yoon, Y. N. and H. G. Wenzel, 1971. Mechanics of sheet flow under simulated rainfall. J. Hyd. Div. A.S.C.E. 97 HY9):1367-1386.

APPENDICES

Appendix A

Profile Meter Operation

Calibration

For each series of profile measurements the linear variable differential transformer (LVDT) was calibrated. The meter was set up on a smooth level surface and levelled with the probe above the surface at its fullest extension. A stepped steel block was used to calibrate the LVDT. The calibration block had 0.050 in. steps, the block step heights having been established to ± 0.0005 in. The profile meter was set up so that the probe rested on the highest step possible, and the meter was started. The cross-carriage advanced the probe down the stepped block, taking approximately 12-15 readings per step. The readings were taken and the probe advanced under computer control, the details of which are given in the next section. When changing from one step to another, partial transition readings sometimes arose, which were rejected by the analysis program, accounting for the variable number of readings at each level.

The calibration readings are given in Tables A1 to A3 for calibrations prior to measurement of Beds B4, T1, and F1 respectively. The points, together with the linear

Table A1: Calibration for LVDT for Bed B4.

Height (in.)	LVDT Reading (MU)	Standard Deviation (MU x 10^{-3})	Standard Deviation (in. x 10^{-3})
1.445	-0.3691	1.808	3.518
1.395	-0.3434	1.784	3.156
1.346	-0.3157	1.335	2.406
1.295	-0.2874	0.842	1.514
1.245	-0.2596	1.460	2.544
1.195	-0.2309	0.884	1.488
1.145	-0.2012	0.699	1.197
1.095	-0.1720	1.538	2.776
1.045	-0.1443	1.688	2.832
0.995	-0.1145	0.845	1.477
0.945	-0.0859	1.430	2.521
0.896	-0.0581	1.010	1.863
0.846	-0.0310	1.019	1.846
0.796	-0.0034	1.556	2.914
0.746	0.0233	0.687	1.274
0.695	0.0508	1.287	2.353
0.646	0.0776	0.735	1.317
0.596	0.1055	0.887	1.628
0.547	0.1322	1.219	2.224
0.497	0.1596	1.129	2.173
0.446	0.1861	1.147	2.187
0.397	0.2118	1.543	3.136
0.347	0.2364	1.476	2.940
0.298	0.2610	1.689	3.519
0.248	0.2850	1.209	2.519

Table A2: Calibration for LVDT for Bed T1.

Height (in.)	LVDT Reading (MU)	Standard Deviation (MU x 10^{-3})	Standard Deviation (in. x 10^{-3})
1.445	-0.4025	0.889	1.684
1.395	-0.3761	0.955	1.654
1.346	-0.3478	0.838	1.494
1.295	-0.3192	1.231	2.305
1.245	-0.2925	0.936	1.608
1.195	-0.2634	1.271	2.222
1.145	-0.2348	0.665	2.602
1.095	-0.2059	1.331	2.303
1.045	-0.1770	0.712	1.223
0.995	-0.1479	0.785	1.397
0.945	-0.1198	1.281	2.202
0.896	-0.0913	0.693	1.246
0.846	-0.0635	1.112	2.044
0.796	-0.0363	1.079	2.013
0.746	-0.0095	0.954	1.822
0.695	0.0172	1.019	1.966
0.646	0.0426	0.936	1.759
0.596	0.0692	0.588	1.104
0.547	0.0953	0.860	1.654
0.497	0.1213	1.046	1.961
0.446	0.1485	1.131	2.182
0.397	0.1739	0.994	1.897
0.347	0.2001	0.807	1.582
0.298	0.2251	1.030	1.988
0.248	0.2510	0.981	1.951
0.199	0.2750	1.024	2.091

Table A3: Calibration for LVDT for Bed F1.

Height (in.)	LVDT Reading (MU)	Standard Deviation (MU x 10^{-3})	Standard Deviation (in. x 10^{-3})
1.746	-0.4007	1.077	1.973
1.696	-0.3734	0.813	1.449
1.647	-0.3459	1.357	2.454
1.596	-0.3177	1.000	1.701
1.546	-0.2883	1.297	2.275
1.496	-0.2598	0.844	1.518
1.445	-0.2313	0.739	1.236
1.395	-0.2014	0.978	1.587
1.346	-0.1712	1.201	2.035
1.295	-0.1411	0.848	1.472
1.245	-0.1123	0.707	1.249
1.195	-0.0840	0.949	1.677
1.145	-0.0557	1.916	3.397
1.095	-0.0275	1.743	3.058
1.045	0.0010	1.668	2.926
0.995	0.0285	0.851	1.553
0.945	0.0559	0.730	1.335
0.896	0.0827	1.195	2.205
0.846	0.1098	0.508	0.927
0.796	0.1372	0.495	0.897
0.746	0.1648	0.979	1.863
0.695	0.1916	0.902	1.637
0.646	0.2186	0.807	1.546
0.596	0.2447	0.786	1.553
0.547	0.2695	0.803	1.247
0.497	0.2942	0.808	1.636

regression calibration equations, are shown in Figure A1. The lack-of-fit standard error was obtained from the summed standard deviations for each calibration: 0.00243 in. for Bed B4, 0.00192 in. for Bed T1 and 0.00186 in. for Bed F1.

The calibration equations from linear regression (ignoring the intercept) are as follows:

For Bed B4,

$$\text{Height (in.)} = -1.8082\,\text{MU} \qquad \text{(A.1)}$$

For Bed T1,

$$\text{Height (in.)} = -1.8270\,\text{MU} \qquad \text{(A.2)}$$

For Bed F1,

$$\text{Height (in.)} = -1.7794\,\text{MU} \qquad \text{(A.3)}$$

Control and Operation

To measure a profile of a surface the profile meter was set up in the desired location. Brass pins mounted in the surface fitted into holes in the center of the lower ends of legs at either end of the profile meter. The profile meter was then levelled parallel to and perpendicular to the direction of the profile, having determined that the probe would pass over the highest points and reach the lowest points of the profile. The cross-carriage was positioned so that the probe was in the initial position at the extreme end of the profile.

The profile meter operated in a fully automatic mode following the initiation of the control program

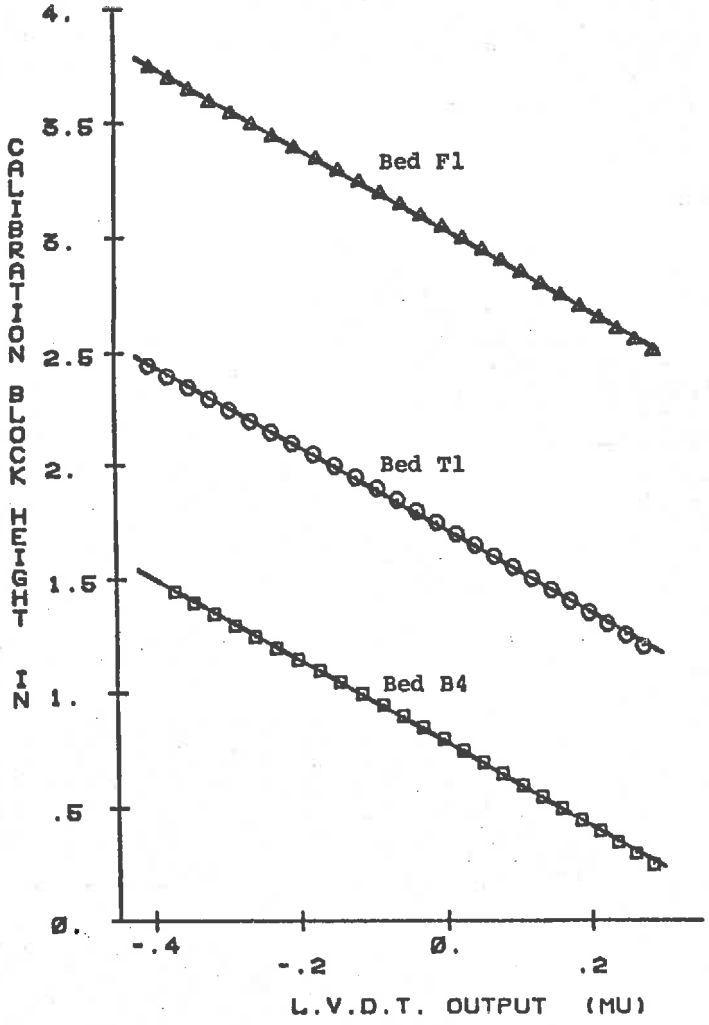

Figure A1. LVDT calibrations showing data, regression lines and 95% confidence limits. Calibrations are displaced vertically since intercept is arbitrary.

on the TR-48/DES-30. The meter was controlled using the logic system of the DES-30 computer which is given in Figure A2, aided by on-line analysis of the LVDT signal by the TR-48 computer as indicated in Figure A3.

The LVDT detects the position of an iron core mounted on a probe by inductive coupling of a high frequency ac voltage to two secondary coils. The amplitude and the phase difference between the induced ac voltages in the secondary coils is converted to a linear dc current output by a demodulator unit. The output current is passed through a resistor and a low pass filter to attenuate high frequency noise from the primary coil and produce a voltage output related to probe position. The LVDT signal is transmitted to the analog computer via low noise instrumentation lines. The signal is filtered to remove the majority of the 60 Hz noise picked up in transmission and is passed to multiplexer channel MPX 14 for recording on magnetic tape.

In addition, the LVDT signal is compared to a fixed voltage level by means of electronic comparator 1, and the comparator output is fed to the logic circuit via analog-to-digital (A/D) line 20. The voltage level used is set by potentiometer 55 so that the LVDT output will exceed the preset voltage at the top of the probe travel. Comparator 1 output is used to check that the probe has been lifted above the preset level.

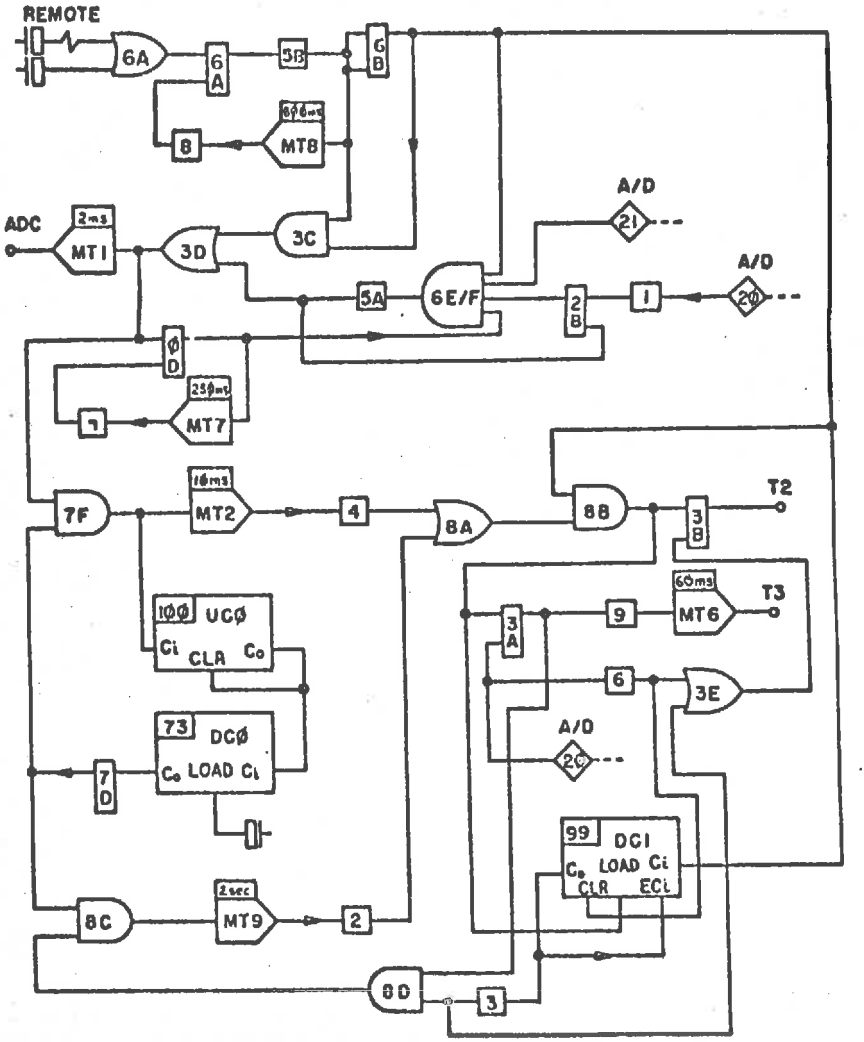

Figure A2. Profile meter control circuit.

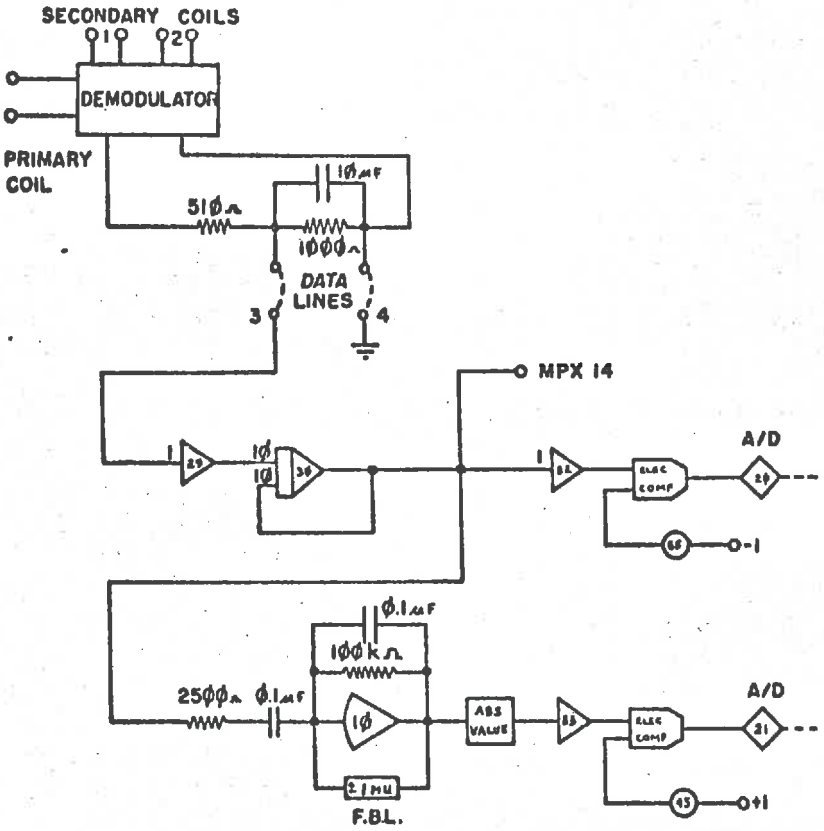

Figure A3. Profile meter LVDT signal analysis circuit.

The LVDT signal is also passed through a differentiator circuit with ± 1 MU feedback limitation, and an absolute value circuit to obtain an approximate derivative of the signal. The derivative is compared, by electronic comparator 2, to a threshold value set on potentiometer 45. Comparator 2 indicates when the LVDT signal derivative falls below the threshold value, which signifies that the probe is in contact with the surface and that the LVDT signal is stable. The output of comparator 2 is available to the DES-30 via A/D line 21.

The profile meter logic circuit, together with the inputs from the TR-48 analog computer, is shown in Figure A2. The control circuit operated at a clock frequency of 1 kHz. The cross-carriage was positioned so that the probe was in contact with the bed surface at the beginning of the profile. The DES-30 was enabled and down-counter DCØ was loaded manually. The profile measurement sequence was initiated by activating either the remote push-button or one on the DES-30. To eliminate contact "bounce" effects flip-flop 6A was set and monotimer MT 8 prevented further signals for 800 ms. Flip-flop 6B was set, which enabled further operations, and a 2 ms pulse was sent to the analog-to-digital conversion (ADC) request for MPX 14. The PDP-11/20 computer handled the ADC request and recording of the readings on magnetic tape. The ADC was registered on up-counter UCØ, and, following

a 10 ms delay (MT 2), the probe lift signal on Trunk T2 was initiated by flip-flop 3B. The logic signal was transmitted to the profile meter circuit which passed current to the probe lift solenoid. The initiate probe lift signal was also passed to the load of DC1, which provided a maximum lift pulse duration of 100 ms. When comparator 1 indicated that the probe had lifted completely, the probe lift signal was terminated, DC1 was cleared, and a 60 ms pulse (MT 6) was sent to the cross-carriage stepper motor via Trunk T3. The cross-carriage was then advanced one step (0.00982 in.).

As the probe descended comparator 1 indicated when the probe had fallen below the preset level and the next ADC was enabled by setting flip-flop 2B. Comparator 2 (via A/D 21) indicated that the LVDT signal was stable, and if all conditions of multiple input and-gate 6 E/F were satisfied, the next ADC was requested. Monotimer MT 7 controlled the maximum rate of operation by delaying the reset of flip-flop ØD for 250 ms, giving a maximum operation rate of approximately 3 readings per second.

If the probe failed to rise above the level detected by comparator 1 following the 100 ms lift pulse controlled by DC1, a delay cycle of 2 sec. (MT 9) was initiated. The time delay allowed the power transistors in the control circuit to cool before a second lift pulse was applied. The profile meter operation could be terminated by a second activation of either push-button which toggled flip-flop 6B.

The sequence could be restarted using either push-button without loss of registration of the probe position.

Normal termination occurred when the required number of readings (7400) had been recorded. The ADC's were counted on UCØ and after 100 readings a blip was sent to DCØ and UCØ was cleared. DCØ counted 74 blocks of 100 readings and then set flip-flop 7D which terminated the operation sequence.

Appendix B

Rainfall Simulator Operation

Calibration

Prior to operation of the rainfall simulator for hydraulic testing on Bed T1, three calibrations were performed. The analog signal analysis circuit for the TR-48 shown in Figure B4 was used in conjunction with a PDP-11/20 digital computer program to sample multiplexed outputs for the signals. Each calibration was performed separately. For each level of a variable the computer program took 50 readings in a random fashion, having a range of delays between readings of 100 ms to 500 ms. The time taken to acquire the 50 readings varied between 14.9 and 19.9 seconds. Readings were recorded in Machine Units (MU), 1 MU equalling 10 volts.

Bed Weight Calibration

Before calibrating the bed weight, a 52 lbf weight was hung directly below each of the four strain-gauged supporting rods in turn and the bed weight measured. Also the same weight was hung underneath the bed in various positions along the centerline of the bed section used. The readings obtained from the sampled bed weight signal (Amplifier 34 in the track mode), which consisted

of the summed outputs of the four strain-gauge sets, were closely grouped. The readings had a mean of 0.1260 MU and a standard deviation of 0.0018 MU, compared to a single reading standard deviation of 0.0020 MU. It was concluded that load response was independent of load position. For calibration, the weights were added along the centerline of the bed section used.

The set of calibration readings for bed weight was obtained from an increasing and a decreasing load sequence, which yielded 100 data values per bed load point. The readings were used to determine a regression line relating bed load in pounds force (lbf) to the sampled output of track/hold amplifier A34. The results are presented in Figure B1. The regression equation is presented as:

$$\text{Bed load (lbf)} = 347.9\ \text{MU} \qquad \text{(B.1)}$$

since the intercept is unimportant. The mean standard error is 0.0024 MU, which corresponds to 95% confidence limits of ± 1.6 lbf. The bed surface area was 13.85 ft. by 6.87 ft. equalling 95.14 ft^2, which yields 95% confidence limits of ± 0.0033 in. for average value depth measurements over the surface.

Mass Runoff Calibration

A similar procedure to that given above was used to calibrate the weighing tank at the lower end of the flow surface, which is used to collect runoff during

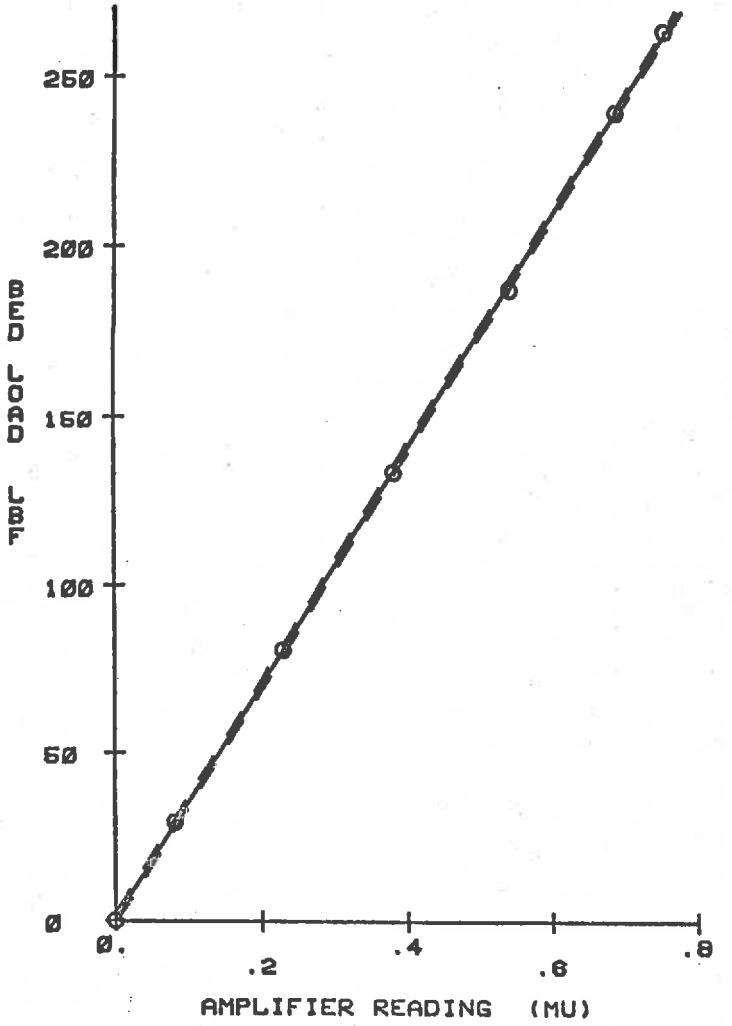

Figure B1. Bed weight calibration showing data, regression line and 95% confidence limits.

the course of a test. The output signal obtained from Track/Hold amplifier A26 (shown in Figure B4) was derived from the summed output of the strain-gauge pairs mounted in the two cantilever beams supporting the weighing tank.

The regression line obtained from calibration is presented as:

$$\text{Weight (lbf)} = 503.0\,\text{MU} \qquad \text{(B.2)}$$

The calibration data and the regression line are shown in Figure B2. The mean standard error is 0.0013 MU, which corresponds to 95% confidence limits of ±1.19 lbf, or ±0.0026 in. for average water depth measurements from the surface.

Runoff Rate Calibration

The derivative circuit shown in Figure B4 for amplifier AØ6 produces a runoff rate signal at Track/Hold amplifier A35 by differentiation of the weighing tank signal. The derivative circuit was calibrated using a preset voltage as input to an integrator, which yielded a ramp input whose slope was proportional to the initial voltage. To calibrate the derivative circuit, the ramp slope and the derivative circuit output were separately sampled as given earlier. Four voltage levels were used, and the linear regression equation is given as

$$\text{Ramp slope (MU/sec)} = 0.0275\ \text{(Differentiator output) (MU)} \qquad \text{(B.3)}$$

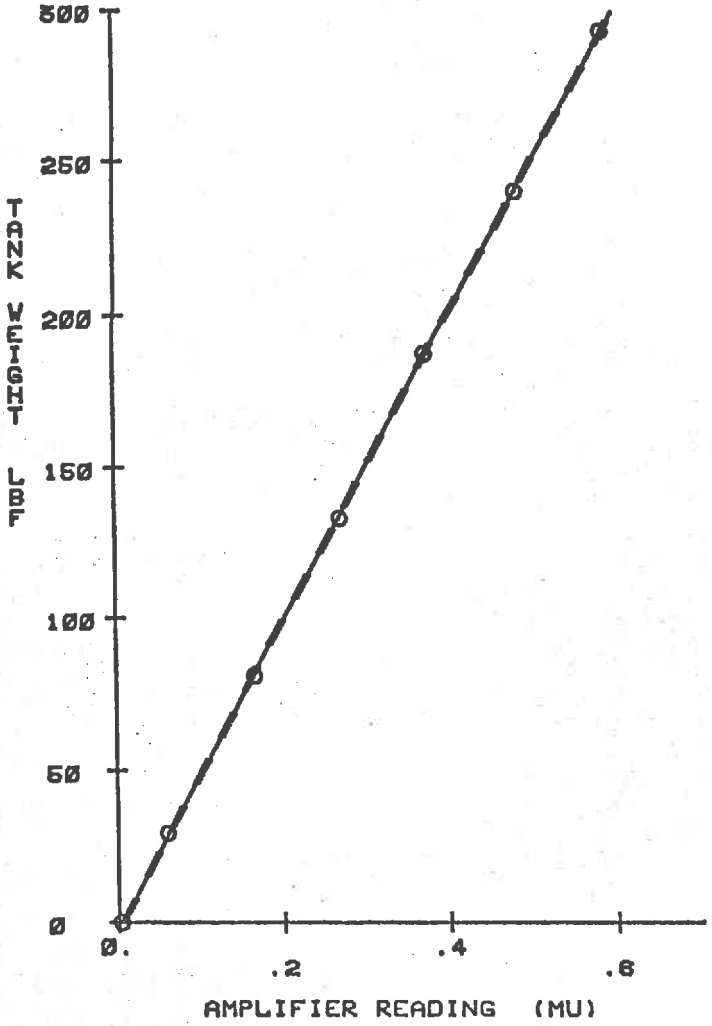

Figure B2. Mass runoff calibration showing data, regression line and 95% confidence limits.

having a mean standard error of 3.30×10^{-5} MU. The calibration curve is shown in Figure B3. In conjunction with equation (B.2), the runoff rate in in./hr. units,

$$\text{Runoff rate} = \frac{0.0275 \times 503.0 \times 43200}{95.14 \times 62.4}$$

$$= 100.66 \text{ (in./hr.)/MU} \qquad \text{(B.4)}$$

The 95% confidence limits for the runoff rate on ± 0.34 in./hr. using the mean standard errors from the mass runoff and differentiator calibrations.

Control and Operation

The DES-30 logic control program and the TR-48 analysis program are shown in conjunction in Figure B4. The DES-30 logic program was designed to operate at a clock frequency of 1 kHz. The rainfall simulator was set up with the required bed slope, rainfall rate and upstream inflow rate using the laboratory local controls. The bed was allowed to drain until the drip rate was small. A plug was placed in the weighing tank outlet, so the weighing tank signal would indicate cumulative runoff over the test. The chart recorder in the laboratory was adjusted for range and zeroed.

The test was usually initiated with the laboratory push button and the chart recorder started. The push button produced a blip from differentiator 5A which set flip-flop 3A, and started a series of 1 Hz pulses to

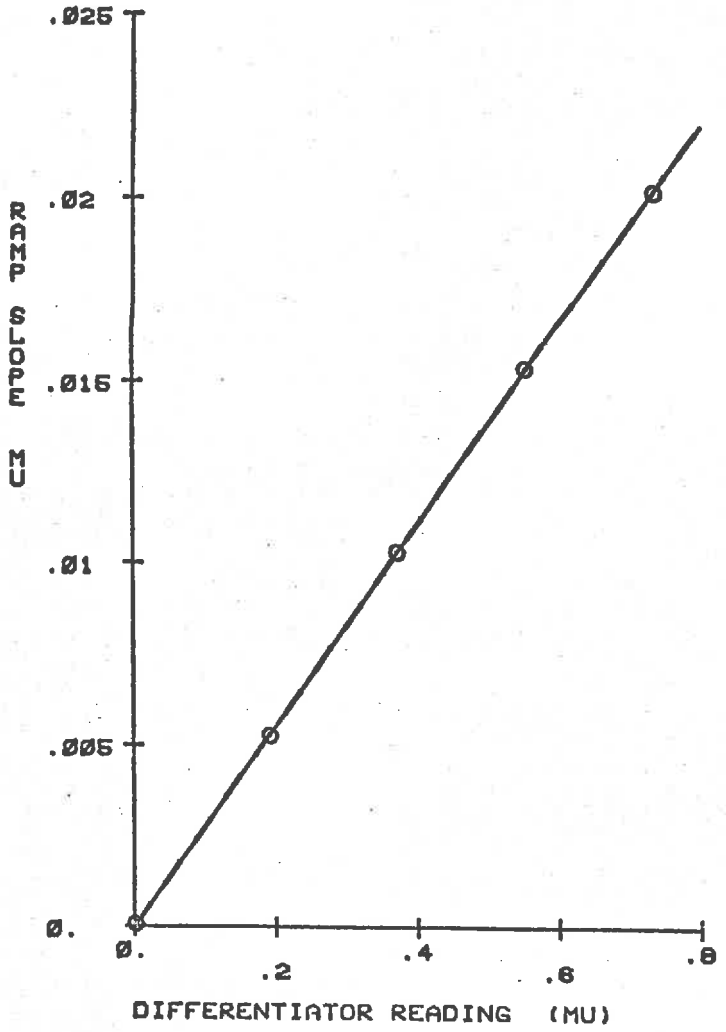

Figure B3. Differentiator calibration showing data, regression line and 95% confidence limits.

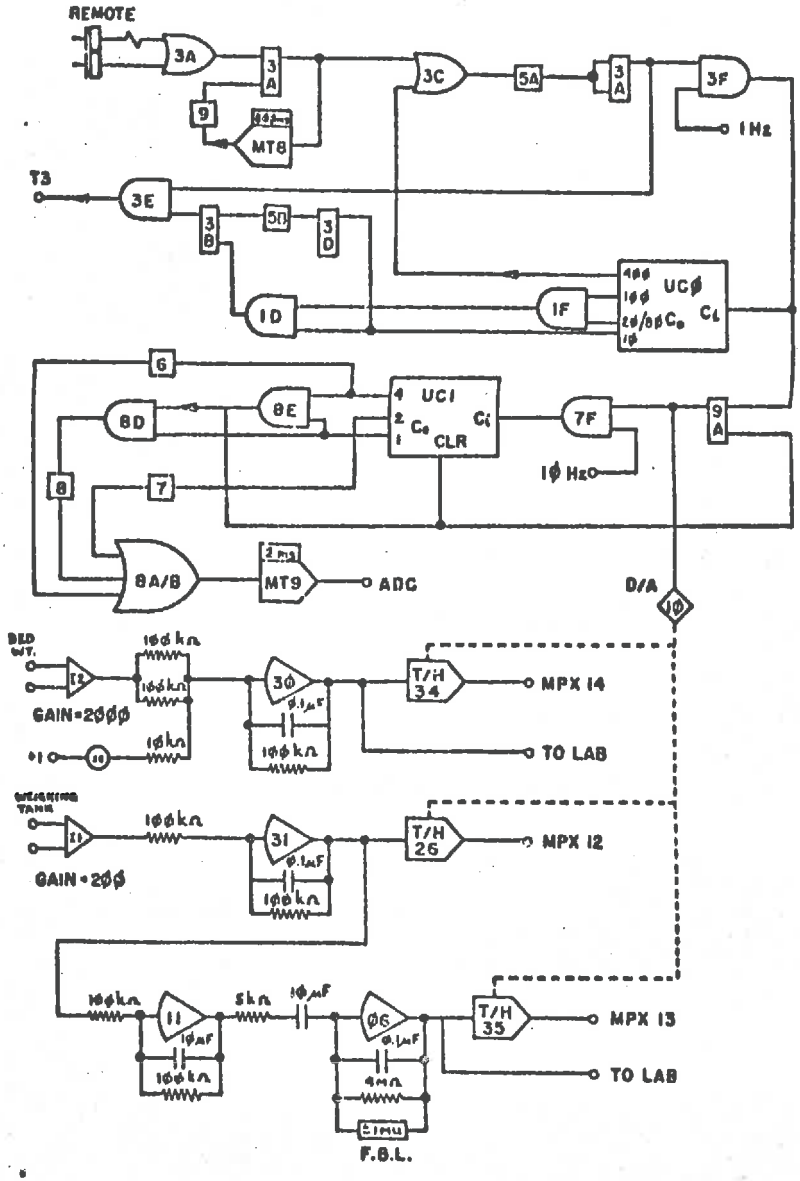

Figure B4. Rainfall simulator control and analysis circuits.

up-counter UCØ which times the operations of the test. In addition the pulses set flip-flop 9A, which set the Track/Hold amplifiers A26, A34 and A35 to "hold" via D/A 10. Flip-flop 9A also initiated a series of 10 Hz pulses to UC1 which caused a series of four 2 ms pulses to be sent to the ADC request channel at 100 ms intervals. The ADC requests were transmitted to the multiplexer channels 12, 13, and 14, which corresponded to the weighing tank, runoff rate and bed load signals respectively. Thus four values of each of the three signals were recorded each second on magnetic tape using the PDP-11/20 data handling structure. 100 ms after the last ADC, UC1 was cleared and flip-flop 9A was reset, causing the Track /Hold amplifiers to return to the "track" mode.

For the first 10 seconds of the test, datum values were stored, after which flip-flop 3B was set. A low (+3.6v) signal was then sent to the rainfall simulator control by Track T3 which started the rainfall and/or upstream inflow previously selected. The test application time was set prior to the test on UCØ as 120 seconds for upstream inflows of 12 in./hr. or greater, and 180 seconds otherwise. After the application time had elapsed, flip-flop 3B was reset, which caused the rainfall/upstream inflow to shut off due to a high (Ov) signal sent to T3.

If both rainfall and upstream inflow were applied initially, the local override controls were used to apply a second rainfall application. A second equilibrium

condition for rainfall only was obtained, which allowed the rainfall and upstream inflow components to be separated during analysis.

Under normal operations UCØ toggled flip-flop 3A after the duration of the test (400 sec.). If necessary either push button could be used to abort the test, which also shut off the rainfall/upstream inflow if required.

Appendix C

Uncertainty Analysis

Profile Measurements

The calibration standard errors determined for the profile meter are given in Appendix A, and have an overall mean value of 0.0020 in. The primary cause for the error from measurement was electrical noise in the system. In operation the errors in height readings arose primarily from probe placement, with some affect due to electrical noise "spikes". From the design of the cross-carriage and probe support (see Figure 5) the drive was considered to provide precise location of the cross carriage. The incremental steps were measured using a dial indicator gauge calibrated in increments of 0.0001 in. and each step was 0.00982 in. to within the accuracy of the gauge. The maximum cumulative position error along a 72 in. traverse was ± 0.005 in.

The primary cause of error in height readings was caused by errors in probe location due to deflection. The probe was carried in Teflon bearings having 0.005 in. clearance and the probe descent was damped to reduce impact. The lateral deflection of the probe was checked using a ground steel wedge having a face 15 degrees from vertical and a mean horizontal deflection of 0.00267 in.

was obtained, which corresponded to a maximum vertical uncertainty of 0.00936 in. A mean value for uncertainty in height measurement was estimated to be 0.005 in. This value is considered to be a "worst typical case" condition for step sided grains. For larger wedge angles the horizontal deflection was greatly reduced.

Spectral Analysis

Akaike (1950) determined that the estimated spectrum S(f) can be expressed as

$$S(f) = \phi^2\lambda(f) + \Delta s \int_{-\infty}^{\infty} (1 - \phi^2)\lambda(f)df \qquad (C.1)$$

where $\lambda(f)$ is the true spectrum, ϕ^2 is a function introduced by aliasing or folding back of frequency components higher than the Nyquist frequency, and Δs is the data spacing. Equation (C.1) applies for data sampling for random non-cumulative errors, which is the case in the present study since the carriage location errors are negligibly small, and probe deflection depends on the surface micro-geometry. The implied assumption is that the micro-geometry is randomly distributed.

The integral expression in equation (C.1) is a white noise component which is additive across the frequency band. The components outside the frequency band are included in the aliasing term. The white noise due to calibration errors was estimated by distributing the variance across the frequency band of 0 to 50 cpi. From

a mean standard error of 0.0020 in. the spectral estimate due to calibration error is 8.0×10^{-8} in.^{3}.

To investigate the white noise component introduced by probe placement errors, profile 5.5 down-slope was selected at random following the profile measurements on Bed T1. The profile meter was relocated on the profile and the measurements replicated. A difference spectrum was determined from differences in height measurements. The difference spectrum had a mean value of 2.5×10^{-7} in.^{3}, and is shown in Figure C1. Bed T1 profile 5.5 was rougher than the other two down-slope profiles, and could be compared to profile 9 across the slope in respect to elevation differences. The difference spectrum obtained represents a demanding test, especially when considering Bed B4 spectra which had lower elevation variations. The difference spectrum compares favorable to the spectral estimate derived from calibration (2.5×10^{-7}in.^{3} against 8.0×10^{-8} in.^{3}), the difference being attributed to placement errors of the probe after relocation of the profile meter.

Amplitude/Separation Distribution

Amplitude was determined after clustering of the data, which provided an average elevation for a group of 10 points. The uncertainty in measurement of individual height values was estimated to be ±0.005 in. The uncertainty of the mean of 10 height values is also 0.005 in. by the uncertainty analysis of Kline and McClintock (1953). Since

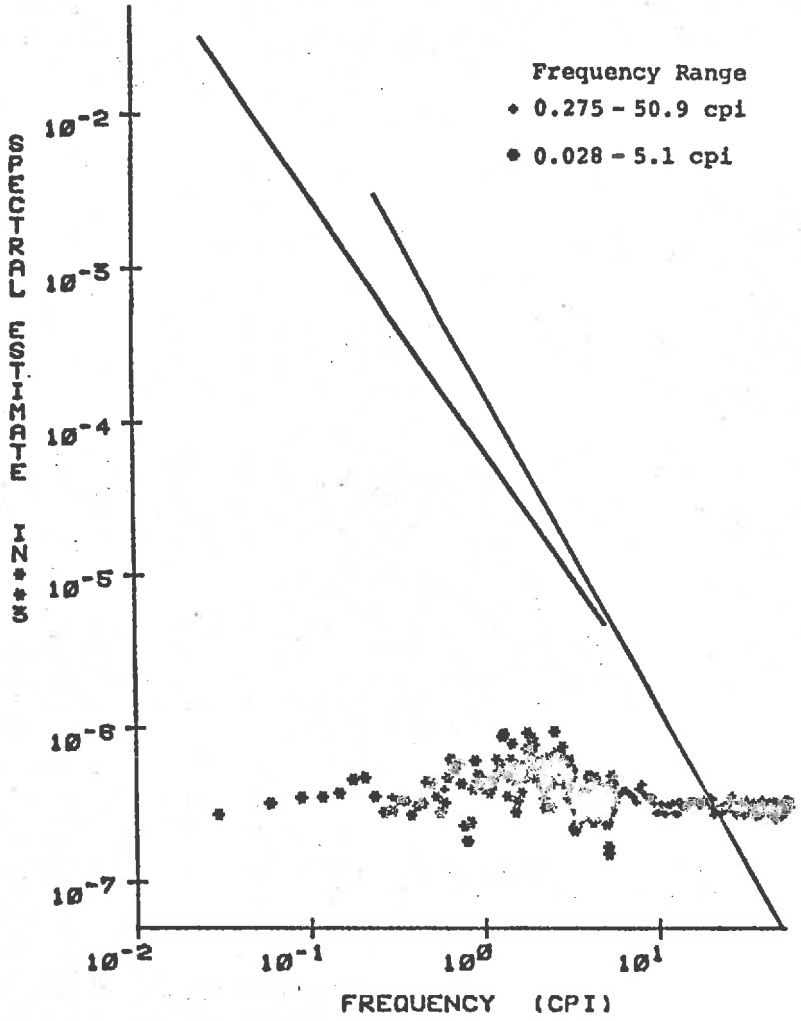

Figure C1. Difference spectrum obtained from Bed T1 profile 5.5. Regression equations are given for the Bed B4 profile 7 spectra.

the amplitudes are classified in bands having bandwidths of 0.025 in. for Bed B4 and 0.075 in. for Bed T1, the overall effect of the amplitude uncertainty on the event counts is small.

Due to the discretization of the profile, which is a continuous process, separation is computed in increments of 0.0982 in. The uncertainty in the separation estimation is one or at most two increments. The effect of separation uncertainty on event counts is considered to be small since separation is classified in bands having bandwidths of 2.0 in.

Area/Wetted Perimeter Analysis

The flow cross-sectional area is determined from a detrended profile by calculating the area between the profile and a horizontal line of given elevation. Since the original data is clustered before computing the flow area, the maximum number of areal increments is 740. (The wetted perimeter is calculated for a given flow area by calculating the length of the profile below the horizontal line.) The maximum uncertainty in each increment is 4.9×10^{-4} in.^{2} and for the maximum area the uncertainty is 0.013 in.^{2}

The wetted perimeter is calculated for a given flow area, defined by the profile and the horizontal line, by calculating the length of the profile below the line. The maximum uncertainty of the perimeter of each increment

is 0.01 in. and for the maximum wetted perimeter the uncertainty is 0.27 in.

For a flow surface an average area/wetted perimeter relationship was calculated from the results obtained from five profiles. The uncertainties in the area/wetted perimeter determinations were considered to be small.

Hydraulic Analysis

Since precise relationships between the hydraulic variables are not available, the hydraulic analysis uncertainty is expressed in terms of the uncertainties of each hydraulic variable.

The flow cross-sectional area is determined from the detention depth and the bed width. From calibration of the bed load (Appendix B) the 95% confidence limits for detention are ± 0.0033 in. For actual experimental values, the steady-state detention is determined from 20 values which are subjected to Chauvenet's criterion (Holman (1966)) to reject spurious high or low values (See computer program, HYDAN, Appendix D). The number of rejected points is not known, but is considered to be a maximum of 2. The 95% confidence limits are considered to provide a reasonable estimate of uncertainty for the detention. An uncertainty value for bed width variation is estimated to be ± 0.25 in. Using the analysis of Kline and McClintock (1953), the uncertainty in flow area is estimated to be 0.25 $in.^2$.

To obtain an estimate of wetted perimeter the flow cross-sectional area is used in the area/wetted perimeter relationship. Consequently, uncertainty in the wetted perimeter depends on the uncertainty in the flow area and the gradient of the area/wetted perimeter curve. Assuming a minimum gradient of 10 percent for the area/wetted perimeter curve, the flow area uncertainty gives a maximum wetted perimeter uncertainty of ± 2.5 in.

The calibration error for discharge gave 95% confidence limits of ± 0.34 in./hr. (Appendix B), which is considered to be a satisfactory estimate of discharge uncertainty.

The slope of the flow surface could be set at the desired inclination with an uncertainty of ± 0.1 in. at a radius of 14 ft. The uncertainty in slope measurement was estimated to be ± 0.06% at a 1 percent slope, which was considered to be negligible.

The uncertainties in the hydraulic variables are small or negligible, with the possible exception of the discharge uncertainty for low discharge values.

Appendix D

Computer Programs

SPEC

```
      PROGRAM SPEC(INPUT,OUTPUT,TAPE5=INPUT,TAPE6=OUTPUT,TAPE8,
     *TAPE1)
C ------------------------------------------------------------------
C
C                      VARIABLE  DEFINITION
C                      --------------------
C
C        Z(I) = ELEVATION (I) IN PROFILE
C           N = NUMBER OF POINTS IN PROFILE
C         LAG = MAXIMUM NUMBER OF LAGS
C         NIC = NUMBER OF POINTS IN CLUSTER
C       RZ(I) = AUTOCOVARIANCE (I)
C      RAW(I) = RAW SPECTRAL ESTIMATE (I)
C       SP(I) = SMOOTHED SPECTRAL ESTIMATE (I)
C     FREQ(I) = FREQUENCY (I)
C        DELS = INTERVAL BETWEEN ELEVATION VALUES
C        ZBAR = MEAN ELEATION OF PROFILE
C         VAR = VARIANCE OF ELEVATIONS ABOUT MEAN
C        GRAD = GRADIENT OF LINEAR REGRESSION OF PROFILE
C        CEPT = INTERCEPT OF LINEAR REGRESSION OF PROFILE
C
C ------------------------------------------------------------------
      DIMENSION Z(8000),RZ(500),SP(500),HD(14)
      DIMENSION FREQ(500)
      COMMON DELS,LAG,LLAG,Q,PMD,CONST
      N=7400
      LAG=185
      NIC=1
      IWRITE=1
      DELS=0.009817
      NIR=480
      PI=3.14159265358979
      FLAG=FLOAT(LAG)
      Q=PI/FLAG
      LLAG=LAG+1
      NOR=INT(FLOAT(N)/FLOAT(NIR))
      READ(8) HD
      WRITE(6,101) (HD(I),I=5,14)
  101 FORMAT(1H1,5X,'SPECTRAL ANALYSIS',/,5X,'-------- --------',
     *3/,5X,'DATA IDENTIFICATION',2/,5(5X,2A10,/))
      DO 10 J=1,NOR
      IS=(J-1)*NIR+1
      IF=J*NIR
      READ(8) (Z(I),I=IS,IF)
   10 CONTINUE
      NCK=NOR*NIR
      IF(NCK.EQ.N) GO TO 15
      IS=NOR*NIR+1
      READ(8) (Z(I),I=IS,N)
   15 CONTINUE
      IF(NIC.EQ.1) GO TO 50
      NOC=N/NIC
      DO 30 J=1,NOC
      CLUST=0.
      DO 20 K=1,NIC
      KC=(J-1)*NIC+K
      CLUST=CLUST+Z(KC)
   20 CONTINUE
      Z(J)=CLUST/NIC
   30 CONTINUE
```

```
      N=NOC
      DELS=DELS*NIC
   50 CONTINUE
      CONST=2.*DELS/PI
      PMD=0.5/(FLAG*DELS)
      WRITE(6,102) N,NIC,DELS,LAG
  102 FORMAT(5X,I6,' DATA POINTS - EACH AS CLUSTER OF',I5,/,
     *5X,'EQUIVALENT SPACING =',F6.4,' INCHES',/,
     *5X,'NO. OF LAGS =',I5,/)
      CALL MEAN(N,Z,ZBAR,VAR)
      CALL POWER(N,Z,ZBAR,RZ,SP,FREQ)
      IF(IWRITE.EQ.0) STOP
      HD(3)=8HSPECTRAL
      HD(4)=9HESTIMATES
      WRITE(1) (HD(J),J=3,14)
      WRITE(1) (FREQ(I),I=1,LLAG),(SP(I),I=1,LLAG)
      END
C
C
      SUBROUTINE MEAN(N,Z,ZBAR,VAR)
      DIMENSION Z(8000),X(8000)
      COMMON DELS,LAG,LLAG,Q,PMD,CONST
      SUM=Z(1)
      SUMSQ=Z(1)*Z(1)
      X(1)=0.
      DO 310 I=2,N
      SUM=SUM+Z(I)
      SUMSQ=SUMSQ+Z(I)*Z(I)
      X(I)=X(I-1)+DELS
  310 CONTINUE
      XBAR=0.5*(N-1)*DELS
      ZBAR=SUM/N
      VAR=(SUMSQ-(N*ZBAR*ZBAR))/(N-1)
      SUMX=0.
      SUMZ=0.
      SUMXZ=0.
      DO 320 I=1,N
      ZDEV=Z(I)-ZBAR
      XDEV=X(I)-XBAR
      SUMZ=SUMZ+ZDEV*ZDEV
      SUMX=SUMX+XDEV*XDEV
      SUMXZ=SUMXZ+ZDEV*XDEV
  320 CONTINUE
      GRAD=SUMXZ/SUMX
      CEPT=ZBAR-GRAD*XBAR
      DO 330 I=1,N
      Z(I)=Z(I)-(CEPT+GRAD*X(I))
  330 CONTINUE
      WRITE(6,301) N,ZBAR,VAR,GRAD,CEPT
  301 FORMAT(3/,5X,'SUBROUTINE MEAN',/,5X,'MEAN OF',I6,
     *' POINTS =',F6.4,/,5X,'VARIANCE      =',E15.6,2/,5X,
     *'LINEAR REGRESSION LINE FITTED TO DATA',/,5X,'GRADIENT  =',
     *E15.6,/,5X,'INTERCEPT  =',E15.6,//,5X,'ANALYSIS PROCEEDS ',
     *'WITH DATA MODIFIED TO DEVIATIONS FROM REGRESSION LINE')
      RETURN
      END
C
C
      SUBROUTINE POWER(N,Z,ZBAR,RZ,SP,FREQ)
      DIMENSION Z(8000),RZ(500),SP(500),RAW(500)
      DIMENSION FREQ(500)
      COMMON DELS,LAG,LLAG,Q,PMD,CONST
C      AUTOCOVARIANCE CALCULATION
      DO 520 I=1,LLAG
```

```
      ...
      CUMZ=0.
      M=I-1
      NZ=N-M
      FNZ=FLOAT(NZ)
      DO 510 J=1,NZ
      K=M+J
      CUMZ=CUMZ+Z(J)*Z(K)
  510 CONTINUE
      RZ(I)=CUMZ/FNZ
  520 CONTINUE
      SLAG=LAG*DELS
      WRITE(6,501) SLAG
  501 FORMAT(3/,5X,'AUTOCOVARIANCE CALCULATION',/,5X,
     *'LAG RANGE = 0.0 TO ',F7.4,' INCHES',/,
     *10X,'LAG (INCHES)',5X,'AUTOCOVARIANCE',/)
      DIST=-DELS
      DO 530 I=1,LLAG
      DIST=DIST+DELS
      WRITE(6,502) DIST,RZ(I)
  502 FORMAT(12X,F7.4,10X,E15.6)
  530 CONTINUE
C      SPECTRUM CALCULATION
      SZERO=RZ(1)
      RZ(1)=.5*RZ(1)
      RZ(LLAG)=.5*RZ(LLAG)
      SA=-Q
      DO 620 IH=1,LLAG
      SA=SA+Q
      S=-SA
      DO 610 JP=1,LLAG
      S=S+SA
      RAW(IH)=RAW(IH)+RZ(JP)*COS(S)
  610 CONTINUE
      RAW(IH)=RAW(IH)*CONST
  620 CONTINUE
      SP(1)=0.54*RAW(1)+0.46*RAW(2)
      SP(LLAG)=0.54*RAW(LLAG)+0.46*RAW(LAG)
      DO 630 J=2,LAG
      SP(J)=0.54*RAW(J)+0.23*(RAW(J-1)+RAW(J+1))
  630 CONTINUE
      FMAX=LAG*PMD
      WRITE(6,601) FMAX
  601 FORMAT(5/,5X,'SMOOTHED SPECTRAL ESTIMATES',2/,
     *8X,'NYQUIST FREQUENCY =',F8.4,' CYCLES/INCH',3/,
     *10X,'FREQUENCY',6X,'SPECTRAL ESTIMATE',/)
      FREQ(1)=0.
      DO 640 I=1,LLAG
      IF(I.EQ.1) GOTO 639
      FREQ(I)=FREQ(I-1)+PMD
  639 CONTINUE
      WRITE(6,602) FREQ(I),SP(I)
  602 FORMAT(10X,F8.4,7X,E15.6)
  640 CONTINUE
      CKSUM=0.5*(SP(1)+SP(LLAG))
      DO 650 J=2,LAG
      CKSUM=CKSUM+SP(J)
  650 CONTINUE
      CKSUM=CKSUM*Q/DELS
      DIFF=CKSUM-SZERO
      WRITE(6,603) CKSUM,SZERO,DIFF
  603 FORMAT(3/,5X,'CHECK SUM OF SPECTRAL ESTIMATES =',E15.6,/,
     *5X,'AND SHOULD BE ',E15.6,/,5X,'THE DIFFERENCE IS',E15.6)
      RETURN
      END
```

AMSEP

```
      PROGRAM AMSEP(INPUT,OUTPUT,TAPE5=INPUT,TAPE6=OUTPUT,TAPE8,
     *TAPE1)
C ------------------------------------------------------------------
C
C                        VARIABLE DEFINITION
C                        -------------------
C
C         Z(I) = ELEVATION (I) IN PROFILE
C            N = NUMBER OF POINTS IN PROFILE
C          NIC = NUMBER OF POINTS IN CLUSTER
C         S(I) = SEPARATION (I)
C     MAT(I,J) = AMPLITUDE/SEPARATION MATRIX (I,J)
C         DELS = INTERVAL BETWEEN ELEVATION VALUES
C         ZBAR = MEAN ELEVATION OF PROFILE
C          VAR = VARIANCE OF ELEVATIONS ABOUT MEAN
C         GRAD = GRADIENT OF LINEAR REGRESSION OF PROFILE
C         CEPT = INTERCEPT OF LINEAR REGRESSION OF PROFILE
C          RUP = UPPER LIMIT OF AMPLITUDE
C          RLO = LOWER LIMIT OF AMPLITUDE
C         SRNG = MAXIMUM SEPARATION
C
C ------------------------------------------------------------------
      DIMENSION Z(8000),HD(14),S(600),MAT(20,20),SDV(20)
      COMMON DELS
      N=7400
      NIC=10
      IWRITE=1
      DELS=0.009817
      NIR=480
      NOR=INT(FLOAT(N)/FLOAT(NIR))
      READ(8) HD
      WRITE(6,101) (HD(I),I=5,14)
  101 FORMAT(1H1,5X,'AMPLITUDE/SEPARATION ANALYSIS',/,6X,
     *'---------- ---------- --------',
     *3/,5X,'DATA IDENTIFICATION',2/,5(5X,2A10,/))
      DO 10 J=1,NOR
      IS=(J-1)*NIR+1
      IF=J*NIR
      READ(8) (Z(I),I=IS,IF)
   10 CONTINUE
      NCK=NOR*NIR
      IF(NCK.EQ.N) GO TO 15
      IS=NOR*NIR+1
      READ(8) (Z(I),I=IS,N)
   15 CONTINUE
      IF(NIC.EQ.1) GO TO 50
      NOC=N/NIC
      DO 30 J=1,NOC
      CLUST=0.
      DO 20 K=1,NIC
      KC=(J-1)*NIC+K
      CLUST=CLUST+Z(KC)
   20 CONTINUE
      Z(J)=CLUST/NIC
   30 CONTINUE
      N=NOC
      DELS=DELS*NIC
   50 CONTINUE
      WRITE(6,102) N,NIC,DELS
  102 FORMAT(5X,I6,' DATA POINTS - EACH AS CLUSTER OF',I5,/,
```

```
     *5X,'EQUIVALENT SPACING =',F6.4,' INCHES',/)
      CALL MEAN(N,Z,ZBAR,VAR,ZMAX)
      NHI=0
      SDIV=2.
      NDIV=20
      RUP=0.75
      RLO=-0.75
      SRNG=40.
      NSEC=N-1
      DO 150 I=1,NSEC
      S(I)=0.
  150 CONTINUE
      SMAX=0.
      DO 200 I=1,NSEC
      IF(Z(I).LT.Z(I+1)) GOTO 200
      IF(Z(I).GT.Z(I+1)) GO TO 170
      S(I)=DELS
      GO TO 200
  170 CONTINUE
      I2=I+2
      N2=NSEC-1
      DO 180 J=I2,N2
      IF(Z(J).LT.Z(I)) GO TO 180
      S(I)=(J-I)*DELS
      IF(S(I).GT.SMAX) SMAX=S(I)
      GO TO 200
  180 CONTINUE
      IF(S(I).NE.0.) GO TO 200
      NHI=NHI+1
      WRITE(6,201) I,Z(I)
  201 FORMAT(5X,'POINT ',I4,' IS HIGH POINT - ELEVATION =',F8.4)
  200 CONTINUE
      WRITE(6,202) NHI
  202 FORMAT(2/,5X,'TOTAL OF HIGH POINTS =',I4,3/)
      DO 220 K=1,NDIV
      DO 210 L=1,NDIV
      MAT(K,L)=0
  210 CONTINUE
  220 CONTINUE
      RDIV=(RUP-RLO)/NDIV
      DO 250 I=1,NSEC
      IF(S(I).EQ.0) GO TO 250
      IF(Z(I).GT.RUP) GO TO 240
      IF(Z(I).LT.RLO) GO TO 245
      K=INT((RUP-Z(I))/RDIV)+1
      L=INT(S(I)/SDIV)+1
      MAT(K,L)=MAT(K,L)+1
      GO TO 250
  240 CONTINUE
      WRITE(6,203) I,Z(I),S(I)
  203 FORMAT(5X,'ABOVE UPPER LIMIT, POINT',I3,' - ELEVATION =',
     *F8.4,3X,'SEPARATION =',F8.4)
      GO TO 250
  245 CONTINUE
      WRITE(6,204) I,Z(I),S(I)
  204 FORMAT(8X,'BELOW LOWER LIMIT, POINT',I3,' - ELEVATION =',
     *F8.4,3X,'SEPARATION =',F8.4)
  250 CONTINUE
      DO 270 I=1,NSEC
      IF(S(I).LE.SRNG) GO TO 270
      WRITE(6,208) I,S(I)
  208 FORMAT(5X,'POINT',I3,' OUT OF RANGE - SEPARATION =',F8.4)
  270 CONTINUE
      WRITE(6,205)
```

```
  205 FORMAT(1H1,3/,5X,'AMPLITUDE/SEPARATION TABLE',/,
     *5X,'---------- ---------- -----',2/)
      DO 300 K=1,NDIV
      RNG=RUP-((K-1)*RDIV)
      WRITE(6,209) RNG
  209 FORMAT(2X,F6.4)
      WRITE(6,206) (MAT(K,L),L=1,NDIV)
  206 FORMAT(10X,20(I3,3X))
  300 CONTINUE
      WRITE(6,209) RLO
      DO 310 I=1,NDIV
      SDV(I)=(I-1)*SDIV
  310 CONTINUE
      WRITE(6,211) (SDV(I),I=1,NDIV),SRNG
  211 FORMAT(/,7X,21(F4.1,2X))
      SRNG2=SRNG/2
      WRITE(6,212) SRNG2
  212 FORMAT(1H1,3/,5X,'POINTS WITH SEPARATION .GT.  ',F8.4,2/,
     *5X,'POINT',9X,'ELEVATION',9X,'SEPARATION',/)
      DO 350 I=1,NSEC
      IF(S(I).LT.SRNG2) GO TO 350
      WRITE(6,213) I,Z(I),S(I)
  213 FORMAT(5X,I4,10X,F8.4,10X,F8.4)
  350 CONTINUE
      END
C
C
      SUBROUTINE MEAN(N,Z,ZBAR,VAR,ZMAX)
      DIMENSION Z(8000),X(8000)
      COMMON DELS
      SUM=Z(1)
      SUMSQ=Z(1)*Z(1)
      X(1)=0.
      DO 310 I=2,N
      SUM=SUM+Z(I)
      SUMSQ=SUMSQ+Z(I)*Z(I)
      X(I)=X(I-1)+DELS
  310 CONTINUE
      XBAR=0.5*(N-1)*DELS
      ZBAR=SUM/N
      VAR=(SUMSQ-(N*ZBAR*ZBAR))/(N-1)
      SUMX=0.
      SUMZ=0.
      SUMXZ=0.
      DO 320 I=1,N
      ZDEV=Z(I)-ZBAR
      XDEV=X(I)-XBAR
      SUMZ=SUMZ+ZDEV*ZDEV
      SUMX=SUMX+XDEV*XDEV
      SUMXZ=SUMXZ+ZDEV*XDEV
  320 CONTINUE
      GRAD=SUMXZ/SUMX
      CEPT=ZBAR-GRAD*XBAR
      DO 330 I=1,N
      Z(I)=Z(I)-(CEPT+GRAD*X(I))
  330 CONTINUE
      WRITE(6,301) N,ZBAR,VAR,GRAD,CEPT
  301 FORMAT(3/,5X,'SUBROUTINE MEAN',/,5X,'MEAN OF',I6,
     *' POINTS =',F6.4,/,5X,'VARIANCE      =',E15.6,2/,5X,
     *'LINEAR REGRESSION LINE FITTED TO DATA',/,5X,'GRADIENT  =',
     *E15.6,/,5X,'INTERCEPT  =',E15.6,//,5X,'ANALYSIS PROCEEDS ',
     *'WITH DATA MODIFIED TO DEVIATIONS FROM REGRESSION LINE')
      ZMAX=Z(1)
      ZMIN=Z(1)
```

```
      DO 340 I=2,N
      IF(Z(I).GT.ZMAX) ZMAX=Z(I)
      IF(Z(I).LT.ZMIN) ZMIN=Z(I)
340   CONTINUE
      DIFF=ZMAX-ZMIN
      WRITE(6,302) ZMAX,ZMIN,DIFF
302   FORMAT(2/,5X,'MAXIMUM HEIGHT =',F8.4,5X,'MINIMUM HEIGHT =',F8.4,
     *//,5X,'DIFFERENCE IN ELEVATION =',E11.4)
      RETURN
      END
```

ARPE

```
      PROGRAM ARPE(INPUT,OUTPUT,PUNCH,TAPE5=INPUT,TAPE6=OUTPUT
     *,TAPE7=PUNCH,TAPE8,TAPE1)
C ------------------------------------------------------------------
C
C                        VARIABLE DEFINITION
C                        -------------------
C
C        Z(I) = ELEVATION (I) IN PROFILE
C           N = NUMBER OF POINTS IN PROFILE
C         NIC = NUMBER OF POINTS IN CLUSTER
C     AREA(I) = AREA (I) OF SECTION BETWEEN SUCCESSIVE ELEVATION
C               VALUES
C    PERIM(I) = PERIMETER (I) OF SECTION BETWEEN SUCCESSIVE
C               ELEVATION VALUES
C       ISW(I) = SWITCH INDICATING CONTIBUTING/NON-CONTRIBUTING
C               SECTION
C     ATOT(I) = TOTAL AREA (I) OF CROSS-SECTION
C     PTOT(I) = PERIMETER (I) FOR ATOT(I)
C     ACHK(I) = AREA CHECK (I) FOR ATOT(I)
C      KSW(I) = NUMBER OF SECTIONS CONTRIBUTING TO ATOT(I)
C        X(I) = MEAN HEIGHT (I) OF SECTION BETWEEN SUCCESSIVE
C               ELEVATION VALUES
C        ZMAX = MAXIMUM ELEVATION OF PROFILE
C        DELS = INTERVAL BETWEEN ELEVATION VALUES
C         VAR = VARIANCE OF ELEVATIONS ABOUT MEAN
C        GRAD = GRADIENT OF LINEAR REGRESSION OF PROFILE
C        CEPT = INTERCEPT OF LINEAR REGRESSION OF PROFILE
C
C ------------------------------------------------------------------
      DIMENSION Z(8000),HD(14),AREA(800),PERIM(800),ISW(800)
      DIMENSION ATOT(100),PTOT(100),ACHK(100)
      DIMENSION KSW(100),X(800)
      COMMON DELS
      N=7400
      NIC=10
      IWRITE=1
      IPUNCH=0
      ISTOR=1
      DELS=0.009817
      NIR=480
      NOR=INT(FLOAT(N)/FLOAT(NIR))
      READ(8) HD
      WRITE(6,101) (HD(I),I=5,14)
  101 FORMAT(1H1,5X,'AREA/PERIMETER ANALYSIS',/,6X,
     *'----- --------- --------'
     *3/,5X,'DATA IDENTIFICATION',2/,5(5X,2A10,/))
      DO 10 J=1,NOR
      IS=(J-1)*NIR+1
      IF=J*NIR
      READ(8) (Z(I),I=IS,IF)
   10 CONTINUE
      NCK=NOR*NIR
      IF(NCK.EQ.N) GO TO 15
      IS=NOR*NIR+1
      READ(8) (Z(I),I=IS,N)
   15 CONTINUE
      IF(NIC.EQ.1) GO TO 50
      NOC=N/NIC
      DO 30 J=1,NOC
      CLUST=0.
```

```
      DO 20 K=1,NIC
      KC=(J-1)*NIC+K
      CLUST=CLUST+Z(KC)
   20 CONTINUE
      Z(J)=CLUST/NIC
   30 CONTINUE
      N=NOC
      DELS=DELS*NIC
   50 CONTINUE
      WRITE(6,102) N,NIC,DELS
  102 FORMAT(5X,I6,' DATA POINTS - EACH AS CLUSTER OF',I5,/,
     *5X,'EQUIVALENT SPACING =',F6.4,' INCHES',/)
      CALL MEAN(N,Z,ZBAR,VAR,ZMAX)
C     INCREMENT ADDED TO AVOID SIGN CHANGE  *******
      DO 70 I=1,N
      Z(I)=Z(I)+5.
   70 CONTINUE
      ZMAX=ZMAX+5.
      ASUM=0.
      PSUM=0.
      NSEC=N-1
      DO 210 I=1,NSEC
      X(I)=ZMAX-(Z(I)+Z(I+1))/2.
      AREA(I)=X(I)*DELS
      ASUM=ASUM+AREA(I)
      PERIM(I)=SQRT((Z(I)-Z(I+1))*(Z(I)-Z(I+1))+DELS*DELS)
      PSUM=PSUM+PERIM(I)
      ISW(I)=1
  210 CONTINUE
      WRITE(6,201) ASUM,PSUM
  201 FORMAT(2/,5X,'TOTAL FLOW AREA BELOW ZMAX =',F8.4,
     */,5X,'TOTAL CORRESPONDING PERIMETER =',F8.4)
      NDIV=100
      DELA=ASUM/(NDIV-1)
      CONT=0.
      DO 220 I=1,NDIV
      PTOT(I)=0.
      ACHK(I)=0.
  220 CONTINUE
      ATOT(0)=ASUM+DELA
      KSW(0)=NSEC
      DO 250 I=1,NDIV
      ATOT(I)=ATOT(I-1)-DELA
      KSW(I)=KSW(I-1)
      DO 230 J=1,NSEC
      IF(ISW(J).EQ.0) GO TO 230
      PTOT(I)=PTOT(I)+PERIM(J)
      ACHK(I)=ACHK(I)+(X(J)-CONT)*DELS
  230 CONTINUE
      DELX=DELA/(KSW(I-1)*DELS)
      CONT=CONT+DELX
      DO 240 J=1,NSEC
      IF(ISW(J).EQ.0) GO TO 240
      IF(X(J).GT.CONT) GO TO 240
      ISW(J)=0
      KSW(I)=KSW(I)-1
  240 CONTINUE
  250 CONTINUE
      DO 260 I=1,NDIV
      WRITE(6,209) ATOT(I),ACHK(I),PTOT(I),KSW(I)
  209 FORMAT(5X,3(F10.4,5X,),I5)
  260 CONTINUE
      IF(IPUNCH.EQ.0) GO TO 280
      DO 270 I=1,NDIV
```

```
      IF(ATOT(I).LT.0.) ATOT(I)=0.
      WRITE(7,199) ATOT(I),PTOT(I)
  199 FORMAT(2F10.4)
  270 CONTINUE
  280 CONTINUE
      IF(ISTOR.EQ.0) GO TO 300
      DO 290 I=1,NDIV
      IF(ATOT(I).LT.0.) ATOT(I)=0.
      WRITE(1,199) ATOT(I),PTOT(I)
  290 CONTINUE
  300 CONTINUE
      END
C
C
      SUBROUTINE MEAN(N,Z,ZBAR,VAR,ZMAX)
      DIMENSION Z(8000),X(8000)
      COMMON DELS
      SUM=Z(1)
      SUMSQ=Z(1)*Z(1)
      X(1)=0.
      DO 310 I=2,N
      SUM=SUM+Z(I)
      SUMSQ=SUMSQ+Z(I)*Z(I)
      X(I)=X(I-1)+DELS
  310 CONTINUE
      XBAR=0.5*(N-1)*DELS
      ZBAR=SUM/N
      VAR=(SUMSQ-(N*ZBAR*ZBAR))/(N-1)
      SUMX=0.
      SUMZ=0.
      SUMXZ=0.
      DO 320 I=1,N
      ZDEV=Z(I)-ZBAR
      XDEV=X(I)-XBAR
      SUMZ=SUMZ+ZDEV*ZDEV
      SUMX=SUMX+XDEV*XDEV
      SUMXZ=SUMXZ+ZDEV*XDEV
  320 CONTINUE
      GRAD=SUMXZ/SUMX
      CEPT=ZBAR-GRAD*XBAR
      DO 330 I=1,N
      Z(I)=Z(I)-(CEPT+GRAD*X(I))
  330 CONTINUE
      WRITE(6,301) N,ZBAR,VAR,GRAD,CEPT
  301 FORMAT(3/,5X,'SUBROUTINE MEAN',/,5X,'MEAN OF',I6,
     *' POINTS =',F6.4,/,5X,'VARIANCE      =',E15.6,2/,5X,
     *'LINEAR REGRESSION LINE FITTED TO DATA',/,5X,'GRADIENT  =',
     *E15.6,/,5X,'INTERCEPT  =',E15.6,//,5X,'ANALYSIS PROCEEDS ',
     *'WITH DATA MODIFIED TO DEVIATIONS FROM REGRESSION LINE')
      ZMAX=Z(1)
      ZMIN=Z(1)
      DO 340 I=2,N
      IF(Z(I).GT.ZMAX) ZMAX=Z(I)
      IF(Z(I).LT.ZMIN) ZMIN=Z(I)
  340 CONTINUE
      DIFF=ZMAX-ZMIN
      WRITE(6,302) ZMAX,ZMIN,DIFF
  302 FORMAT(2/,5X,'MAXIMUM HEIGHT =',F8.4,5X,'MINIMUM HEIGHT =',F8.4,
     */,5X,'DIFFERENCE IN ELEVATION =',E11.4)
      RETURN
      END
```

POIS

```
      PROGRAM POIS(INPUT,OUTPUT,TAPE5=INPUT,TAPE6=OUTPUT,TAPE1,TAPE2)
C ------------------------------------------------------------------
C
C                        VARIABLE DEFINITION
C                        ===================
C
C        X(I) = DISTANCE (I) ALONG PROFILE
C     PLOC(I) = LOCATION OF PARTICLE (I)
C      OFF(I) = OFFSET OF PARTICLE (I)
C      DIA(I) = DIAMETER OF PARTICLE (I)
C        DBAR = MEAN PARTICLE DIAMETER
C        DMIN = MINIMUM PARTICLE DIAMETER
C        DMAX = MAXIMUM PARTICLE DIAMETER
C        PLAM = PARTICLE DENSITY
C       PSEED = SEED FOR PARTICLE LOCATION RANDOM NUMBER STRING
C       OSEED = SEED FOR PARTICLE OFFSET RANDOM NUMBER STRING
C       DSEED = SEED FOR PARICLE DIAMETER RANDOM NUMBER STRING
C        DELS = INTERVAL BETWEEN ELEVATION VALUES
C        NPTS = NUMBER OF POINTS IN PROFILE
C
C ------------------------------------------------------------------
      DIMENSION X(8000),PLOC(5000),OFF(5000),DIA(5000)
C     PROFILE K3 -------- DBAR=0.3126 IN.    ******************
      DBAR=0.312598
      DMAX=0.375
      DMIN=0.25
      PLAM=2.415
      PLIN=PLAM*DBAR
      PSEED=35620601744334767B
      OSEED=5742427225444611 5B
      DSEED=422063375714533718
      NPTS=7400
      DELS=0.009817
      P=RANF(PSEED)
      PLOC(0)=0.
      READ(1) (X(I),I=1,NPTS)
      DO 10 I=1,5000
      P=RANF(0)
      PLOC(I)=PLOC(I-1)+ALOG(1-P)/(-PLIN)
      IF(PLOC(I).GT.76.) GO TO 20
   10 CONTINUE
   20 CONTINUE
      NPART=I-1
      D=RANF(DSEED)
      DO 30 I=1,NPART
      D=RANF(0)
      DIA(I)=DMIN+D*(DMAX-DMIN)
   30 CONTINUE
      O=RANF(OSEED)
      DO 40 I=1,NPART
      O=RANF(0)
      OFF(I)=DBAR*(O-0.5)
   40 CONTINUE
      DO 100 I=1,NPTS
      DIST=I*DELS
      DO 60 J=1,NPART
      IF(DIST.LT.PLOC(J)) GO TO 70
   60 CONTINUE
   70 CONTINUE
      PLACE=PLOC(J)
```

```
      DIAM=DIA(J)
      OSET=OFF(J)
      CALL HEIGHT(DIST, PLACE, DIAM, OSET, HT)
      HFOR=HT
      PLACE=PLOC(J-1)
      DIAM=DIA(J-1)
      OSET=OFF(J-1)
      CALL HEIGHT(DIST, PLACE, DIAM, OSET, HT)
      HBAC=HT
      IF(HBAC. GT. HFOR) GO TO 90
      X(I)=X(I)+HFOR
      GO TO 100
   90 CONTINUE
      X(I)=X(I)+HBAC
  100 CONTINUE
      WRITE(6, 199)
  199 FORMAT(1H1, 2/, 4X, 'I', 9X, 'X(I)', 8X, 'PLOC', 8X, 'OFF',
     *10X, 'DIA', 8X, 'NPART', /)
      DO 200 J=1, NPART
      I=INT(PLOC(J)/DELS)
      WRITE(6, 201) I, X(I), PLOC(J), OFF(J), DIA(J), J
  201 FORMAT(2X, I5, 4(5X, F8. 4), 5X, I5)
  200 CONTINUE
      WRITE(2) (X(I), I=1, NPTS)
      ENDFILE 2
      STOP
      END
C
C
      SUBROUTINE HEIGHT(DIST, PLACE, DIAM, OSET, HT)
      RAD=DIAM/2.
      OSET=ABS(OSET)
      IF(OSET. GT. RAD) GO TO 100
      CHORD=SQRT((RAD*RAD)-(OSET*OSET))
      DIFF=ABS(PLACE-DIST)
      IF(CHORD. LE. DIFF) GO TO 100
      HT=RAD+SQRT((CHORD*CHORD)-(DIFF*DIFF))
      RETURN
  100 CONTINUE
      HT=0. 0
      RETURN
      END
```

HYDAN

```
      PROGRAM HYD (TAPE1, INPUT, OUTPUT, PUNCH, TAPE5=INPUT, TAPE6=OUTPUT, TAP
     *E7=PUNCH)
C
C          ANALYSIS OF HYDRAULIC TEST DATA
C ------------------------------------------------------------------
C
C     DATA REPRESENTING MASS RUNOFF, RUNOFF RATE AND BED WEIGHT ARE
C     RECORDED IN MACHINE UNITS (1 M.U. = 10 VOLTS) CODED IN BCD FORM ON
C     MAGNETIC TAPE.  EACH SET OF 3 VALUES REPRESENT ON-THE-SECOND
C     RECORDINGS WITH ONE SET PER PRU.  THIS PROGRAM CONVERTS THE DATA
C     TO INCH HOUR UNITS AND INCORPORATES CHECKS ON THE CALIBRATION
C     COEFFICIENTS AND OPERATION OF THE EQUIPMENT.
C
C                                          (AFTER BURNEY (1973))
C
C ------------------------------------------------------------------
C
C                        VARIABLE DEFINITION
C                        ===================
C
C
C       W(I) = BED WEIGHT (I)
C       W(I) = WEIGHING TANK LOAD (I)
C      DW(I) = DERIVATIVE OF WEIGHING TANK LOAD (I)
C       B(I) = BED WEIGHT (I)
C      SLOPE = BED SLOPE
C          N = TOTAL TIME OF TEST
C         N1 = TIME OF INITIAL FLOW APPLICATION
C         N2 = TIME OF CESSATION OF INITIAL FLOW APPLICATION
C         N3 = TIME OF CESSATION OF SECOND FLOW APPLICATION
C         TN = TEST NUMBER
C
C ------------------------------------------------------------------
      DIMENSION W(402), DW(402), B(402), REJ(20), HD(14)
      INTEGER T(10), PUN, SLOPE
   50 READ(5,100) N, N1, N2, N3, SLOPE, TN, LFC, IT, PUN, NL
      WRITE(6,101) TN
C     .....READ IN RAW DATA.....
      IF(IT.EQ.0) GO TO 8
      READ(1) (HD(I),I=1,14)
      READ(1) (W(I), I=1,400)
      READ(1) (DW(I), I=1,400)
      READ(1) (B(I), I=1,400)
      GO TO 9
    8 DO 10 I=1,N
   10 READ(1,102) W(I), DW(I), B(I)
C     .....CHECK INITIALISATION DATA.....
    9 CONTINUE
      WRITE(6,129) HD
  129 FORMAT(7(10X,2A10,/))
      CALL CHAV(W,1,N1,1,NP)
      CALL CHAV(DW,1,N1,2,NP)
      CALL CHAV(B,1,N1,3,NP)
C     .....CONVERT MACHINE UNIT READINGS TO INCH, HOUR UNITS.....
      AREA = 95.135
      WW = 62.4
      M = N + 1
      DO 11 I=1,M
      W(I) = (W(I) - W(401))*502.996*12./(WW*AREA)
      DW(I) = DW(I)*0.027442*502.996*43200/(AREA*WW)
   11 B(I) = (B(I) - B(401))*347.866*12./(WW*AREA)
```

```
      WRITE(6,103) DW(401)
C     .....WRITE OUT TEST DATA IN INCH-HOUR UNITS WITH TIME ZERO AS
C          START OF RAINFALL AND OVERLAND FLOW.....
      M = (N - N1)/10 + 1
      DO 12 I=1,M
C     CHANGE IN PRINT OUT ROUTINE  ********************
      K=I*10-1
      J = K - 9
      IF(K.GT.N) GO TO 15
      L1 = J - N1
      DO 13 L=1,10
      T(L) = L1
   13 L1 = L1 + 1
      L1 = K - J + 1
      WRITE(6,104) (T(L), L=1,L1)
      WRITE(6,105) (W(L), L=J,K)
      WRITE(6,106) (DW(L), L=J,K)
   12 WRITE(6,107) (B(L), L=J,K)
C     .....PUNCH DATA IF REQUIRED.....
   15 IF(PUN.EQ.0) GO TO 14
      WRITE(7,108) (W(I), I=N1,N)
      WRITE(7,108) (DW(I), I=N1,N)
      WRITE(7,108) (B(I), I=N1,N)
C     .....STEADY STATE VALUES.....
   14 N5 = N2 - 19
      N9 = N2-N1
      N6 = 0
      CALL CHAV(DW,N5,N2,4,JP)
      DAV = DW(401)
      DSE = DW(402)
      WRITE(6,109) SLOPE
      CALL CHAV(B,N5,N2,5,NP)
      IF(N3) 16,17,18
   16 WRITE(6,110) N6, N9
      GO TO 19
   17 WRITE(6,111) N6, N9
   19 WRITE(6,112) DW(401), DW(402), B(401), B(402)
      GO TO 20
   18 WRITE(6,113) N6, N9
      GO TO 19
   20 IF(N3) 22,22,21
   21 N6 = N3 - 19
      CALL CHAV(DW,N6,N3,6,KP)
      AA = FLOAT(JP-2)
      BB = FLOAT(KP-2)
      SED = (AA*DSE*DSE+BB*DW(402)*DW(402))/(AA+BB)
      CALL CHAV(B,N6,N3,7,NP)
      N6 = N6 - N1
      N9 = N3 - N1
      N3 = -N3
      IF(LFC) 16,45,17
   22 IF(LFC) 33,29,34
   33 RAIN = DAV - DW(401)
      WRITE(6,120) RAIN, SED
      GO TO 29
   34 FLOW = DAV - DW(401)
      WRITE(6,114) FLOW, SED
C     .....APPLICATION RATES FROM SLOPE OF MASS FLOW AT STEADY STATE.....
   29 L1 = N5
      L2 = N2
      N6 = 0
      N9 = N2-N1
   26 DO 24 I=L1,L2
      J = I - L1 + 1
```

```
   24 REJ(J) = W(I)
      CALL LREQ(REJ,L1,L2,C,SEC)
      IF(LFC.EQ.0.OR.N3.GT.0) GO TO 25
      CC = C
      SED =SEC
      N3 = -N3
      L1 = N3-19
      L2 = N3
      GO TO 26
   25 WRITE(6,115)
      IF(N3) 27,28,31
   31 WRITE(6,116) N6, N9, CC, SED
      N6 = L1 - N1
      N9 = N3 - N1
      IF(LFC) 27,45,28
   27 WRITE(6,117) N6, N9, C, SEC
      IF(N3.LT.0) GO TO 30
   35 C = CC - C
      AA = FLOAT(N2-N5-1)
      BB = FLOAT(N3-N6-1+N1)
      SEC = SQRT((AA*SED*SED+BB*SEC*SEC)/(AA+BB))
      IF(LFC) 37,45,36
   36 WRITE(6,114) C, SEC
      GO TO 38
   37 WRITE(6,120) C, SEC
   38 N6 = 0
      N9 = N2-N1
      C = CC
      GO TO 30
   28 WRITE(6,118) N6, N9, C, SEC
      IF(LFC) 45,30,35
C     .....MASS BALANCE.....
   30 N7 = N2 - 1
      DS = 0.
      DO 32 I=N1,N7
   32 DS = DS + (DW(I)+DW(I+1))/7200.
      TA =   C*FLOAT(N2-N1)/3600.
      WDET = TA - W(N2)
      DDET = TA - DS
      WRITE(6,119)
      WRITE(6,121) N6, N9, TA, DS, DDET, W(N2), WDET
      N7 = N-11
      DO 40 I=N2,N7
   40 DS = DS+(DW(I)+DW(I+1))/7200.
      N6 = N-10
      N7 = N6-N1
      WRITE(6,122) N7, W(N6), DS
      IF(N3.GT.0) GO TO 45
      BD = B(N6)-B(N1)
      EW = TA-W(N6)-BD
      WRITE(6,123) N7, EW
   45 IF(NL.NE.0) GO TO 50
  100 FORMAT(5I5,A8,4I2)
  101 FORMAT(1H1,40X,'HYDRAULIC ANALYSIS OF TEST ',A8//)
  102 FORMAT(3F6.4)
  103 FORMAT(5X,'AVERAGE RATE OF DRIP PRIOR TO TEST WAS ',F8.4,' IN./HR.
     *'//20X,'TEST DATA FOLLOWS'/)
  104 FORMAT(//2X,'TIME (SEC.)',10X,10(7X,I3))
  105 FORMAT(2X,'MASS RUNOFF (INS.)',3X,10F10.4)
  106 FORMAT(2X,'RUNOFF RATE (IN./HR.)',10F10.4)
  107 FORMAT(2X,'DETENTION (IN.)',6X,10F10.4)
  108 FORMAT(10F8.4)
  109 FORMAT(//20X,'STEADY STATE RUNOFF VALUES ON A SLOPE OF',I3,
     *' PERCENT ARE AS BELOW'/)
```

```
  110 FORMAT(5X,'OVERLAND FLOW ONLY DURING PERIOD',I4,' TO',I4,' SEC. ')
  111 FORMAT(5X,'RAINFALL ONLY DURING PERIOD',I4,' TO',I4,' SEC. ')
  112 FORMAT(5X,'FROM STEADY STATE RUNOFF RATE,RATE OF APPLICATION =',
     *F8.4,' IN./HR.  WITH RECORDED STD. ERROR OF',F8.4,' IN./HR.'/
     *5X,'FROM STEADY STATE DED WEIGHT STEADY STATE DETENTION =',F8.4,
     *' IN.  WITH RECORDED STD. ERROR OF',F8.4,' IN.'/)
  113 FORMAT(5X,'RAINFALL AND OVERLAND FLOW APPLIED DURING PERIOD',I4,
     *' TO',I4,' SEC. ')
  114 FORMAT(5X,'RATE OF OVERLAND FLOW BY SUBTRACTION =',F8.4,
     *' IN./HR.  WITH STD. ERROR OF',F8.4,' IN./HR.')
  115 FORMAT(//10X,'APPLICATION RATES FROM MASS FLOW RECORDING AT'
     *' STEADY STATE'/)
  116 FORMAT(5X,'RATE OF APPLICATION DURING PERIOD',I4,' TO',I4,
     *' SEC.  FROM SLOPE OF MASS FLOW =',F8.4,' IN./HR.  WITH STD. ERROR OF'
     *,F8.4,' IN./HR.')
  117 FORMAT(5X,'RATE OF OVERLAND FLOW DURING PERIOD',I4,' TO',I4,
     *' SEC.  FROM SLOPE OF MASS FLOW =',F8.4,' IN./HR.  WITH STD.  ',
     *'ERROR OF',F8.4,' IN./HR.')
  118 FORMAT(5X,'RATE OF RAINFALL DURING PERIOD',I4,' TO',I4,' SEC.  '
     * 'FROM SLOPE OF MASS FLOW =',F8.4,' IN./HR.  WITH STD. ERROR OF',
     *F8.4,' IN./HR.')
  119 FORMAT(/10X,'MASS BALANCE')
  120 FORMAT(5X,'RATE OF RAINFALL BY SUBTRACTION =',F8.4,' IN./HR.  WITH
     * STD.  ERROR OF',F8.4,' IN./HR.')
  121 FORMAT(5X,'DURING PERIOD',I4,' TO',I4,' SEC.  APPLICATION WAS',
     *F8.4,' IN.  (FROM SLOPE OF STEADY STATE MASS FLOW)'/5X,
     *'INTEGRATED RUNOFF RATE =',F8.4,'IN.  AND DETENTION BY SUBTRACTION
     *=',F8.4,' IN.'/5X,'RECORDED MASS RUNOFF =',F8.4,' IN.  AND '
     *'DETENTION BY SUBTRACTION =',F8.4,' IN.')
  122 FORMAT(5X,'RECORDED MASS RUNOFF FOR',I4,' SEC.  WAS',F8.4,
     .*' IN.  FROM MASS RECORDING AND',F8.4,' IN.  FROM INTEGRATED RUNOFF'
     *' RATE')
  123 FORMAT(5X,'EXCESS INFLOW OVER OUTFLOW AT TIME',I4,' SEC.  WAS',
     *F8.4,' IN.')
      END
C
C
      SUBROUTINE CHAV(A,N1,N2,IS,NN)
      DIMENSION A(402), J(5), X(5), P(20)
      DATA(P(I), I=1,20) /6*0.,1.80,1.86,1.91,1.96,2.00,2.04,2.07,2.10,
     *2.13,2.16,2.18,2.20,2.22,2.24/
      L = 1
      DO 32 I=1,4
   32 J(I) = 0
      NN = N2 - N1 + 1
   12 SUM = 0.
      SS = 0.
      DO 10 I=N1,N2
      SUM = SUM + A(I)
   10 SS = SS + A(I)*A(I)
      A(401) = SUM/FLOAT(NN)
      A(402) = SQRT((SS-SUM*A(401))/FLOAT(NN))
      XUL = A(401) + A(402)*P(NN)
      XLL = A(401) - A(402)*P(NN)
      IF(L.NE.1) GO TO 14
      DO 11 I=N1,N2
      IF(A(I).GT.XLL.AND.A(I).LT.XUL) GO TO 11
      J(L) = I
      X(L) = A(I)
      A(I) = 0.
      NN = NN - 1
      L = L + 1
      IF(L.GE.5) GO TO 20
   11 CONTINUE
```

```
      IF(L.EQ.1) RETURN
      GO TO 12
   14 L = L - 1
      DO 15 M=1,L
      K = J(M)
   15 A(K) = X(M)
      RETURN
   20 WRITE(6,101) IS
      NN = NN + L - 1
      GO TO 14
  101 FORMAT(/2X,'EXCESSIVE INSTABILITY IN DATA SET ',I3/)
      END
C
C
      SUBROUTINE LREG(X,K1,K2,B,SEB)
      DIMENSION X(20), T(20)
      DO 10 I=K1,K2
      J = I - K1 + 1
   10 T(J) = FLOAT(I)/3600.
      SX = 0.
      ST = 0.
      SXT = 0.
      ST2 = 0.
      SX2 = 0.
      J = K2 - K1 + 1
      DO 11 I = 1,J
      SX = SX + X(I)
      ST = ST + T(I)
      SXT = SXT + X(I)*T(I)
      SX2 = SX2 + X(I)*X(I)
   11 ST2 = ST2 + T(I)*T(I)
      XJ = FLOAT(J)
      SP = SXT-SX*ST/XJ
      CST = ST2-ST*ST/XJ
      B = SP/CST
      RB = SP*B
      CSX = SX2-SX*SX/XJ
      SEB = SQRT((CSX-RB)/(XJ-2.))
      RETURN
      END
```

VITA

VITA

Born: Terence Hugh Podmore, Chester, England, July 16, 1943.

Parents: Arthur and Alethea Podmore.

Married: Carol Ann Lipscomb, September 6, 1968.

Children: Alethea Ann and Jonathan Lockhart.

Education:
Wirral Grammar School, Bebington, England, 1962.
Imperial College, London University, 1962-1964.
National College of Agricultural Engineering, Silsoe, Bedford, England, A.N.C.A.E., July 1967.
Michigan State University, M.S. in Ag. Eng., June 1969.
Purdue University, Ph.D., December 1975.

Professional Experience:
Graduate Assistant, Michigan State University, 1967-1969.
Lecturer in Agricultural Engineering, Darling Downs Institute of Advanced Education, Queensland, Australia, 1970-1972.
Graduate Instructor, Purdue University, 1972-1975.

Professional Societies:
Institution of Agricultural Engineers (U.K.).
American Society of Agricultural Engineers.

Honorary: Alpha Epsilon.